Identification and targeting of microbial putrescine acetylation in bloodstream infections

Author List:

Jared R. Mayers[1,2,3], Jack Varon[1,2], Ruixuan R. Zhou[4], Martin Daniel-Ivad[3,5], Courtney Beaulieu[5], Amrisha Bholse[5,6], Nathaniel R. Glasser[3], Franziska M. Lichtenauer[3], Julie Ng[1,2], Mayra Pinilla Vera[1], Curtis Huttenhower[5,6,7], Mark A. Perrella[1,2], Clary B. Clish[5], Sihai D. Zhao[4,8], Rebecca M. Baron[1,2]*, Emily P. Balskus[3,9]*

Affiliations:

[1] Division of Pulmonary and Critical Care Medicine, Department of Medicine, Brigham and Women's Hospital, Boston, MA, USA 02115

[2] Harvard Medical School, Boston, MA, USA 02115

[3] Department of Chemistry and Chemical Biology, Harvard University, Cambridge, MA, USA 02138

[4] Department of Statistics, University of Illinois at Urbana Champaign, Champaign, IL, USA 61820

[5] Broad Institute of MIT and Harvard, Cambridge, MA, USA 02142

[6] Department of Biostatistics, Harvard T.H. Chan School of Public Health, Boston, MA, USA 02115

[7] Department of Immunology and Infectious Diseases, Harvard T.H. Chan School of Public Health, Boston, MA, USA

[8] Carl R. Woese Institute for Genomic Biology, University of Illinois at Urbana Champaign, Champaign, IL, USA 61820

[9] Howard Hughes Medical Institute, Harvard University, Cambridge, MA, USA 02138

*Correspondence: balskus@chemistry.harvard.edu and rbaron@bwh.harvard.edu

SUMMARY

The growth of antimicrobial resistance (AMR) has highlighted an urgent need to identify bacterial pathogenic functions that may be targets for clinical intervention. Although severe bacterial infections profoundly alter host metabolism, prior studies have largely ignored alterations in microbial metabolism in this context. Performing metabolomics on patient and mouse plasma samples, we identify elevated levels of bacterially-derived *N*-acetylputrescine during gram-negative bloodstream infections (BSI), with higher levels associated with worse clinical outcomes. We discover that SpeG is the bacterial enzyme responsible for acetylating putrescine and show that blocking its activity reduces bacterial proliferation and slows pathogenesis. Reduction of SpeG activity enhances bacterial membrane permeability and results in increased intracellular accumulation of antibiotics, allowing us to overcome AMR of clinical isolates both in culture and *in vivo.* This study highlights how studying pathogen metabolism in the natural context of infection can reveal new therapeutic strategies for addressing challenging infections.

Keywords:

Metabolomics, polyamines, *N*-acetylputrescine, sepsis, antibiotic resistance, polyamine/diamine acetyltransferase

INTRODUCTION

Antimicrobial-resistant (AMR) bacterial infections represent an escalating global public health crisis directly responsible for 1.27 million deaths in 2019[1], a number predicted to rise to 10 million by 2050[2]. Widespread antibiotic administration during the COVID-19 pandemic only accelerated this trend by selecting for the development of resistance in bacterial infections[3-6]. US deaths from AMR infections rose 15% between 2019 to 2020 alone with 40% of these infections acquired in the hospital[7].

Bloodstream infection (BSI) is a top cause of mortality attributable to AMR[1]. It is present in the majority of patients with septic shock[8-10], the most severe form of sepsis associated with low blood pressure and organ damage in response to infection. Septic shock has a morality rate over 40%[11,12]. BSIs are most commonly caused by gram-negative bacteria such as *Escherichia coli*, *Klebsiella pneumoniae,* and *Pseudomonas aeruginosa*[13]. These microbes are members of the World Health Organization Priority 1 group of pathogens, recognized as primary drivers of AMR-associated mortality[1] and priority targets for antibiotic development. Treatment options for BSI and AMR-infections more broadly remain limited both by a narrow repertoire of targets and challenges in drug development that have slowed the pipeline of new antimicrobial agents[14-16].

Exploiting disease-associated metabolism for clinical benefit has proven promising in contexts such as cancer[17] and Mendelian disorders[18], but this paradigm is underutilized in bacterial infections. While prior studies in the context of BSI have focused on how severe bacterial infections alter host metabolism predominantly as a marker of clinical outcomes[19-23], these studies have largely ignored microbial metabolic activities. Identifying alterations in bacterial metabolism specifically in the context of infection could highlight previously underappreciated processes that play causal roles in disease and are thus more likely to be targets of effective therapies.

In this study, we analyze samples from gram-negative BSIs in patients and animal models to characterize microbial metabolism in the natural context of infection, hypothesizing this would prioritize microbial metabolic processes involved in pathogenesis for further investigation and define new targets for efforts to combat AMR-associated infections. Using an iterative, comparative metabolomics pipeline, we identify acetylation of

putrescine as a prominent microbial metabolic activity in BSIs. Characterizing and inhibiting the bacterial acetyltransferase responsible for this activity revealed a direct impact of this metabolism on bacterial fitness in culture and *in vivo*. Finally, this discovery demonstrated that treatment with an acetyltransferase inhibitor could resensitize multi-drug resistant (MDR) bacteria to existing clinical antibiotics. Overall, we have defined a generalizable workflow for identifying, investigating, and exploiting metabolic vulnerabilities in bacterial pathogens.

RESULTS

Comparative metabolomics highlights *N*-acetylputrescine as a probable bacterial-derived metabolite in bloodstream infections.

To identify bacterial metabolites elevated in human plasma during infection, we first examined an existing cohort of patient plasma samples and identified a small subset from patients admitted to the intensive care unit (ICU) with culture positive gram-negative BSIs (*Escherichia coli, Klebsiella* spp.*, Pseudomonas* spp.) who had banked blood samples drawn contemporaneously or near-contemporaneously with their positive blood cultures as well from controls admitted to the ICU for other reasons (**Figure S1A-B** and **Table S1**)[23]. Targeted liquid chromatography–mass spectrometry (LC–MS)-based metabolomics revealed significant differences in 62 metabolites (with an FDR<0.05) between the two groups (**Figure 1A** and **Table S2**). To prioritize metabolites for further investigation, we determined the extent to which these 62 metabolites were correlated with clinical outcomes as measured by APACHE II scores[24,25] and found that elevated levels of eight metabolites were associated with increased mortality (**Figure 1A-B** and **Figure S1C**). Of these eight, elevations in *N*-acetylputrescine were the most significantly different between cases and controls (**Figure 1A**). Both *N*-acetylputrescine and a second elevated metabolite, 4-acetamidobutanoate, arise from acetylation of the polyamine putrescine (**Figure 1A-B**)[26,27]. We did not observe elevations in another mono-acetylated polyamine, *N1*-acetylspermidine. We viewed this unexpected increase in levels of metabolites from a specific pathway, putrescine metabolism (**Figure 1C**) as potentially indicating an important role for this pathway during BSI and prioritized these metabolites for further investigation. Incidentally, our cohort reproduced previously reported significant decreases of multiple lysophosphatidyl choline species in sepsis (**Figure S1D**)[28,29], although these alterations were not associated with clinical outcomes.

To further investigate whether putrescine and/or lysophosphatidyl choline metabolites were bacterially-derived, we compared plasma metabolomics profiles of sterile injury and live infection in mouse models of sepsis/BSI, hypothesizing that levels of microbial products would change only in the presence of live bacteria. Using the cecal-slurry (CS) model[30], we compared an intraperitoneal (IP) injection of PBS, heat-killed CS (HK CS), and live CS and observed significant elevations in both *N*-acetylputrescine and 4-acetamidobutanoate only in those

mice receiving live CS (**Figure 1D** and **Figure S2A-B**). By contrast, lysophosphatidyl cholines decreased in both HK and live CS (**Figure S2C**), consistent with a host-derived metabolic response to an inflammatory stimulus. Elevations in *N*-acetylputrescine and 4-acetamidobutanoate were also seen in the cecal ligation and puncture (CLP) model[31] in the context of live infection, but not when utilizing *E. coli* lipopolysaccharide (LPS) as a sterile, inflammatory insult (**Figure S2D**). Thus in both models, plasma *N*-acetylputrescine and 4-acetamidobutanoate increases required a live infection, consistent with bacterial production of these metabolites. As both models involve polymicrobial infections, we also investigated whether these putrescine metabolites were altered in the context of single organism infections. Production of putrescine metabolites in HK CS was rescued by the addition of live *E. coli* (**Figure 1E**). A separate *Klebsiella pneumoniae* pneumonia[32,33] model produced increased levels of putrescine metabolites (**Figure 1F-G** and **Figure S3**).

To confirm the microbial origin of putrescine-derived metabolites identified in our human and mouse studies, we cultured a panel of multidrug resistant (MDR) clinical isolates of *E. coli, K. pneumoniae,* and *P. aeruginosa* in minimal medium supplemented with putrescine and measured production of *N*-acetylputrescine and 4-acetamidobutanoate in culture supernatants. All strains tested produced *N*-acetylputrescine, while *P. aeruginosa* also produced the downstream metabolite 4-acetamidobutanoate (**Figure 1H** and **Figure S4A-B**)[26]. To assess production of these metabolites by mammalian hosts, we performed IP injections of putrescine in mice and measured plasma levels of *N*-acetylputrescine and 4-acetamidobutanoate (**Figure 1H** and **Figure S4A-E**). This demonstrated minimal generation of plasma putrescine metabolites in mammals, which is consistent with the previously reported restriction of mammalian *N*-acetylputrescine production to the brain, likely as a precursor for GABA synthesis[27,34]. Interestingly, only mice and *P. aeruginosa* produced 4-acetamidobutanoate from *N*-acetylputrescine whereas the remaining bacteria did not (**Figure S4F-H)**[34], suggesting cooperative metabolism may explain some of the observed plasma metabolite alterations in both patients and mice with certain infections. Overall, these data highlight putrescine acetylation as a prominent microbial metabolic activity detectable in gram-negative BSI.

SpeG homologs produce *N*-acetylputrescine in gram-negative pathogens

As a first step in investigating the importance of putrescine acetylation during BSI, we sought to identify the bacterial enzyme(s) responsible for this activity. Putrescine acetylation by *E. coli* has been reported previously[26], but the responsible enzyme has not been identified. Polyamine/diamine *N*-acetyltransferases (EC: 2.3.1.57) quickly emerged as likely candidates. These enzymes are structurally diverse, and their activity has been biochemically validated across kingdoms[35]. *E. coli* and *K. pneumoniae* strains universally encode one member of this family, SpeG (sharing >89% amino acid ID), which is annotated as the putative putrescine *N*-acetyltransferase. However, its acetylation activity *in vitro* and in culture has only been demonstrated experimentally toward the longer chain polyamines spermidine and spermine, with acetylation of putrescine explicitly not observed *in vitro* or missed in culture[35-37], possibly because the physiologically relevant substrate concentrations were not studied. This has led to the perception that spermidine is the substrate for SpeG despite it being found at 5-to-10-fold lower intracellular concentrations than putrescine in these microbes (1–5 mM compared with 20–30 mM). Spermine is not present in these bacteria[38-41].

We investigated whether SpeG was responsible for putrescine acetylation in *E. coli*. By examining an *E. coli* BW25113 *speG* mutant previously generated as part of the KEIO collection[42], we confirmed that deletion of *speG* resulted in a loss of *N*-acetylputrescine production in culture (**Figure 2A**). Complementation with a plasmid encoding *speG* rescued *N*-acetylputrescine production (**Figure 2A**), and incubation of purified enzyme with putrescine and acetyl-CoA established that SpeG catalyzes this reaction (**Figure 2B** and **Figures S5A**). We next sought to determine the kinetic parameters of SpeG toward putrescine to gain insight into why this activity had been missed previously. SpeG displayed activity toward putrescine at the high end of physiologic intracellular putrescine levels in *E. coli* (K_{half} = 51.0 ± 5.4 mM) (**Figure 2C**)[38,40,43]. Although physiologic, the putrescine concentrations we used are higher than those previously examined, indicating how this activity could have escaped detection. As a control, we confirmed SpeG could acetylate spermidine and observed kinetic parameters similar to those published previously (**Figure S5B**)[35]. The K_{half} (590.1 ± 30.8 μM) towards spermidine was well below the intracellular concentrations (1–5 mM)[38,40], indicating that SpeG already operates near or at maximum velocity on spermidine under physiologic conditions. Consistent with SpeG's dodecameric

quarternary structure and allosteric binding sites, we observed cooperative kinetics with both putrescine and spermidine (**Figure 2C** and **Figure S5B**)[35,44]. This combination of kinetic parameters that reflect metabolite concentrations and cooperative kinetics suggests a previously overlooked role for SpeG as particularly responsive modulator of intracellular putrescine levels, enabling a rapid increase in activity when high concentrations are reached.

Although patients with *P. aeruginosa* infection were included in our original cohort demonstrating an association between *N*-acetylputrescine and BSI, and we observed *P. aeruginosa* production of *N*-acetylputrescine in culture, *Pseudomonas* spp. lack a biochemically validated polyamine *N*-acetyltransferase. To begin identifying the *P. aeruginosa* enzyme(s) responsible for this metabolism, we searched the list of all putative polyamine/diamine *N*-acetyltransferases in the UniProt database, which are designated by EC 2.3.1.57[45,46]. This list included a single enzyme from *P. aeruginosa* PAO1, PA4114, which is annotated as a spermidine acetyltransferase sharing homology to the experimentally validated *Bacillus subtilis* BltD enzyme[47,48]. Additionally, we conducted a BLAST search using the *E. coli* SpeG amino acid sequence as a query and identified two additional candidate uncharacterized *P. aeruginosa* PAO1 enzymes, PA1377 and PA1472, which display low sequence identities to SpeG (26% amino acid ID each). We condensed the list of sequences from EC 2.3.1.57 into representative sequences sharing >80% amino acid sequence ID (i.e. RepNode80) and then performed a MUSCLE alignment[49] with these sequences and the candidate *P. aeruginosa* sequences, followed by a maximum likelihood phylogenetic analysis. Strikingly, each of the three candidate *P. aeruginosa* enzymes clustered in clades containing a structurally distinct, validated polyamine acetyltransferase (**Figure 2D**)[50,51].

To experimentally determine whether any of these candidate *P. aeruginosa* enzymes could acetylate putrescine, we complemented the *E. coli* BW25113 *speG* mutant[42] with plasmids encoding *PA4114, PA1472*, and *PA1377.* This approach demonstrated that PA1472, but not PA4114 and PA1377, could rescue putrescine acetylation (**Figure 2E** and **Figure S5D**). Incubation of purified enzymes with putrescine and acetyl-CoA further established PA1472 as the likely *P. aeruginosa* SpeG homolog (**Figure 2F** and **Figure S5A**). We next determined the kinetic properties of PA1472 toward putrescine and confirmed that like SpeG, it is most active at the high end of

intracellular putrescine concentrations (K_m = 30.7 ± 9.9 mM) (**Figure 2G**)[41]. Consistent with PA1472 possessing putrescine *N*-acetyltransferase activity, its dimer AlphaFold2 predicted structure resembled the crystal structure of SpeG (3WR7, RMSD 1.891), despite the low % amino acid ID shared between the primary sequences (**Figure 2H**)[44]. Together, these data implicate PA1472, and not the annotated PA4114, as the likely putrescine *N*-acetyltransferase in *P. aeruginosa*. This finding highlights both the diversity of the enzymes capable of carrying out this chemistry and emphasizes the importance of experimental validation of computation hits when assigning enzyme functions.

Our initial sequential metabolomics studies on human samples, mouse models, and bacterial cultures highlighted putrescine acetylation as a microbially-mediated transformation detectable in BSI. To further confirm our assignment of *N*-acetylputrescine as bacterial in origin, we determined the kinetic parameters of the human homolog of SpeG, spermidine/spermine acetyltransferase 1 (SAT1), against putrescine. This revealed that SAT1 had a K_m (8.70 ± 2.43 mM) well above reported intracellular putrescine concentrations in eukaryotic cells (sub-mM range). This is consistent with our mouse experiment (**Figure 1H**) indicating SAT1 contributes minimally to putrescine acetylation under physiologic conditions (**Figure S5A** and **Figure S5C**)[38]. As a control, we confirmed SAT1's robust activity toward spermidine (V/K = 2.1 x 10^6 M^{-1} min^{-1}) (**Figure S5A** and **Figure S5D**)[52]. There was also little predicted structural similarity of either SpeG or PA1472 to SAT1 (2B5G, RMSD 11.454 and 12.187 respectively) (**Figure S5E**)[53]. Overall, these data confirmed the ability of SpeG to acetylate putrescine in *E. coli*, identified a likely *P. aeruginosa* putrescine acetyltransferase, and further suggested that bacterial enzymes are responsible for the increases in plasma *N*-acetylputrescine seen in BSI.

Loss of SpeG activity impairs *E. coli* fitness in culture and *in vivo*

Across kingdoms, polyamines play diverse roles in the regulation of gene expression and protein translation and are implicated in the maintenance of cell membrane homeostasis and protection from oxidative stress[54]. As high levels of these polycationic molecules can be toxic[37], intracellular concentrations must be tightly regulated, with charge neutralization through acetylation by SpeG thought to play a key role in bacteria[55]. *SpeG* deletion has been reported to hinder intracellular proliferation of *Salmonella*[56] and to impair the resistance of

the methicillin-resistant *Staphylococcus aureus* (MRSA) USA300 strain to extracellular host polyamines[57,58]. The importance of *speG* for pathogenesis may not be universal, however, as *Shigella* spp. have silenced *speG* expression to promote spermidine accumulation [59]. Nevertheless, the increased levels of acetylated putrescine metabolites we observed in patient plasma suggests this activity may be important for the pathogens studied here, especially during the metabolically stressful process of BSI[15].

To examine whether *speG* deletion is similarly important in *E. coli*, we compared growth of wildtype, *ΔspeG* and complemented BW25113 strains, which revealed no difference in proliferation (**Figure S6A**). To see if this response was strain-specific, we attempted to delete *speG* from two clinical *E. coli* isolates (M 1/5 and E23), but were unsuccessful, raising the possibility that *speG* might be essential in some strains and/or that BW25113 *ΔspeG* possessed an unappreciated compensatory change. To avoid both of these potential issues, we turned to an inducible CRISPRi system[60], which resulted in ~50% repression of *speG* transcription with a guide RNA targeting *speG* compared with a control guide targeting *RFP* in BW25113 (**Figure S6B**). This transcriptional repression resulted in a specific, dramatic suppression of *E. coli* proliferation in BW25113 (**Figure S6C**), calling into question the reliability of this deletion strain to elucidate secondary phenotypes related to *speG* loss. To address this concern, we then applied this system to the clinical *E. coli* isolates described above and observed closer to 70% repression of *speG* transcription (**Figure 3A** and **Figure S6D**). Consistent with a role in putrescine acetylation, *speG* repression resulted in significant decreases in extracellular *N*-acetylputrescine production (**Figure 3B** and **Figure S6E**), as well as significantly increased intracellular putrescine accumulation with a concomitant decrease in *N*-acetylputrescine (**Figure 3C** and **Figure S6F**). Reducing *speG* expression in these clinical isolates also recapitulated the growth defect observed with CRISPRi in *E. coli* BW25113 (**Figure 3D** and **Figure S6G-H**). Supplementation of the culture media with *N*-acetylputrescine did not rescue the proliferation defect, suggesting that SpeG's regulation of polyamines, rather than the acetylated products themselves, conferred the proliferative advantage (**Figure S6I**). Finally, we sought to determine the consequences of reduction of *speG* expression *in vivo*. Using a modification of the rescue experiment from **Figure 1E,** we found that repression of *speG* transcription using inducible CRISPRi in *E. coli* E23 resulted in a significant delay in mortality compared with controls (**Figure 3E**). Combined with our earlier data, these findings support the

hypothesis that increases in plasma *N*-acetylputrescine during bacterial infection arise from bacterial metabolism and that this highlights a metabolic process, polyamine acetylation, that plays an important role in pathogen physiology.

Diminazene inhibits SpeG and reduces bacterial proliferation

Given these observations, we sought a chemical method of inhibiting bacterial polyamine acetylation. While small molecule inhibitors of SpeG have not been reported, inhibitors of the human polyamine *N*-acetyltransferase SAT1 have been developed and studied as potential anti-cancer therapies[61,62]. It has also been previously shown that diminazene, a structural mimic of spermidine used a veterinary antitrypanosomal agent (**Figure 4A**), is an inhibitor of SAT1 with a K_i of 2.4 μM[44,55,63]. Indirect evidence has suggested diminazene may inhibit the SpeG homolog from MRSA USA300, although it has not been tested against this enzyme directly[64]. To test if diminazene inhibits putrescine acetyltransferase activity of *E. coli* SpeG we determined IC_{50}s for this drug *in vitro* using both putrescine and spermidine as substrates (**Figure 4B** and **Figure S7A**). Diminazene's IC_{50} against SpeG with putrescine as a substrate (26.2 ± 3.7 μM) was similar to our measurement of its IC_{50} for SAT1 with spermidine (21.0 ± 0.6 μM) (**Figure S7B**), consistent with this drug being a broad-spectrum polyamine acetyltransferase inhibitor. In agreement with our CRISPRi experiments, diminazene treatment with doses similar to those used against MRSA USA300[64] significantly decreased extracellular levels of *N*-acetylputrescine (**Figure 4C** and **Figure S7C**) and significantly increased intracellular putrescine accumulation while decreasing *N*-acetylputrescine levels (**Figure 4D** and **Figure S7D**) in clinical isolates. Diminazene treatment also inhibited growth in a dose-dependent manner (**Figure 4E** and **Figure S7E**) and increased sensitivity to drug treatment was observed during growth in minimal medium (**Figure S7E-G**).

Given its structure and the pleiotropic roles of polyamines in cells, we wanted to test whether the growth suppression phenotype of diminazene in *E. coli* was SpeG-dependent or due to off-target effects. Prior work has suggested that diminazene may disrupt the proton motive force in *E. coli,* in addition to its known ability to bind nucleic acids[65]. There is also some evidence it could be broadly effective in *S. aureus* strains, including those likely lacking SpeG, albeit at higher doses[66]. Nevertheless, using our inducible CRISPRi system, we found

that reducing *speG* expression rendered *E. coli* resistant to the growth inhibitory effects of 10 μM diminazene (**Figure 4F** and **Figure S7H**) indicating that at least at this modest dose, diminazene's effects on bacterial growth are mediated through SpeG activity. Finally, we sought to determine MIC_{90}s of diminazene across the previously studied MDR clinical isolates. Consistent with previous reports, diminazene sensitivity can vary across strains, with *E. coli* often more sensitive than *Klebsiella* spp. (**Figure S7I-J**)[66]. Together, these data suggest that we could leverage diminazene as a tool to further investigate the importance of polyamine acetylation across Gram-negative pathogens.

Inhibiting polyamine acetylation increases bacterial membrane permeability and synergizes with clinical antibiotics

Several of the cellular processes regulated by polyamines[54], which may be vulnerable to perturbations of polyamine metabolism, are also targets of antibiotics, with examples including DNA replication/transcription (quinolones), translation (macrolides and tetracyclines), and the cell membrane (beta-lactams and vancomycin)[15]. To elucidate which of these processes may be involved in the growth limitation phenotype observed upon repression of SpeG activity, we conducted drug synergy testing in the *E. coli* clinical isolates[67,68] with diminazene and the antibiotics ciprofloxacin, erythromycin, tetracycline, and vancomycin. Using a checkerboard assay format, we found that diminazene synergized with vancomycin, a drug used exclusively to treat gram-positive infections (**Figure 5A** and **Figure S8A**), reducing the vancomycin MIC_{90} from above the limit of our assay (>128 μg/mL) to 32-64 μg/mL depending on the dose of diminazene. These findings suggest that SpeG inhibition by diminazene may be increasing permeability of the outer membrane, allowing this large glycopeptide drug, which would not normally permeate the outer membrane, to reach its target in the periplasm[69]. Importantly, inducible CRISPRi of *speG* produced a similar result, resulting in a clear reduction of the vancomycin MIC_{90} (**Figure 5B** and **Figure S8B-C)**.

We then directly assessed SpeG's effect on bacterial inner and outer membrane permeability using a previously published fluorescence-based assay[70,71]. Inducible CRISPRi of *speG* increased permeability of both the outer and inner plasma membrane (**Figure 5C** and **Figure S8B**). Diminazene treatment for 6 hours phenocopied these

observations in a dose-dependent manner (**Figure 5D** and **Figure S8E**), including at the dose at which we see SpeG-dependent growth inhibition (10 μM). Diminizene-mediated increases membrane permeability were greatly diminished with a shorter 3-hour treatment (**Figure S8F**), which is also consistent with SpeG inhibition driving this phenotype, rather than a direct effect on the outer membrane[69,72]. These data demonstrate that inhibiting the intracellular metabolic enzyme target SpeG can impact a membrane phenotype, creating a vulnerability that increases susceptibility to antibiotic treatment.

Two primary mechanisms of antibiotic resistance are limiting antibiotic entry into bacterial cells and efflux of antibiotics[73]. Given the effects of SpeG inhibition on membrane permeability, we hypothesized that diminazene treatment could perhaps re-sensitize MDR pathogens to existing antibiotics. Examining our panel of MDR patient isolates (**Figure 1H**), we specifically tested for synergy between diminazene and antibiotics to which these isolates were resistant. We found synergy between diminazene and tetracycline and/or ciprofloxacin in almost all these strains, in some cases re-achieving MIC_{90}s at or below clinically relevant breakpoints (**Figure 6A** and **Figure S9A**). These findings were consistent with a recent report focused on repurposing old antimicrobials similar to pentamidine[69,72], which found synergy between diminazene and streptomycin or chloramphenicol in some strains of drug resistant *E. coli*, *K. pnuemoniae*, and *S. aureus*, although the mechanism underlying this observation was not elucidated[66]. In our MDR strains, synergistic interactions were directly associated with increased intracellular accumulation of antibiotics (**Figure 6B** and **Figure S9B**) suggesting that diminazene treatment was improving cellular access of these drugs[74,75].

Finally, we sought to test whether this synergy is observed *in vivo*. We focused on the tetracycline-resistant *E. coli* E1 strain, one of the strains for which diminazene treatment shifts the MIC_{90} back into the clinically sensitive range (**Figure 6A**). We performed a rescue of HK CS using the *E. coli* E1 line at a previously determined $LD_{80\text{-}90}$ dose of bacteria. One hour after infection, we initiated treatment with clinically relevant doses of either vehicle, diminazene alone (7 mg/kg daily), tetracycline alone (25 mg/kg every 12 hours), or a combination of diminazene and tetracycline[76-80]. In vehicle and monotherapy groups, the expected mortality was observed by 48 hours, while combination therapy increased median and overall survival (**Figure 6C**). Tetracycline treatment alone

improved median survival, but did not change the overall proportion of survivors (**Figure 6C**). This may indicate that peak concentrations of tetracycline after dosing could briefly overcome the resistance mechanism(s) utilized by E1, slowing but ultimately failing to clear the infection. Together, these data suggest that targeting SpeG activity therapeutically could provide opportunities to revisit our existing antibiotic arsenal and create new avenues for intervention in challenging to treat infections.

DISCUSSION

Due to the rising rates of infections and deaths attributed to AMR pathogens, new and creative strategies are needed to replenish our dwindling pipeline of antibiotics[81]. Metabolism represents the biochemical manifestation of genetic, epigenetic, transcriptomic, and proteomic inputs which most accurately reflects an organism's phenotype[82]. To this end, deciphering the metabolic activities of pathogens *in vivo* during infection is likely to highlight microbial pathways which support infection and could implicate new targets for intervention[83]. In this study, guided by our observation that *N*-acetylputrescine is elevated during BSI, we identify putrescine acetylation as a prominent microbial metabolic activity during infection and demonstrate that blocking this activity impairs pathogen fitness. This susceptibility occurred in part through increasing membrane permeability, which created an opportunity for synergy with existing clinical antibiotics. This strategy directly circumvents multiple modes of antibiotic resistance utilized by pathogens to limit intracellular access of drugs[73,81]. Thus, our workflow enables the identification of metabolic activities important for infection in patient samples. Characterizing the mechanism responsible for the observed changes and exploring its impact on pathogenesis ultimately allows us to leverage this understanding to identify new potential avenues for treatment.

The elevation of pathogen-derived *N*-acetylputrescine in human and mouse plasma during infection and its association with poor outcomes raises the possibility that this metabolite could be used clinically as marker of infections involving pathogens encoding SpeG homologs. Pathogen identification currently involves direct testing or culturing of biomaterial, which frequently requires several days[84] and often misses a large proportion of BSIs[9]. The rapid identification of unique bacterial metabolites in patient biofluids could diagnose infection with a particular pathogen or group of pathogens possessing particular metabolic enzyme(s) independent of culture while simultaneously providing the guidance needed to specifically target the active metabolic pathways therapeutically. The presence or absence of bacterial metabolites could also be used to help guide antibiotic stewardship and limit unnecessary use of antibiotics, a known contributor to the development of AMR[4,85]. Supporting the potential of this approach, we found elevation of *N*-acetylputrescine in a parallel independent cohort of patients with septic shock compared with outpatient controls (R Rogers, *submitted*). Interestingly, this

metabolite also distinguished patients between patients with septic shock and those with non-infectious, cardiogenic shock. Moving forward, larger validation cohorts are needed to determine formal characteristics and potential clinical utility of such a test.

Polyamines are ubiquitous across all life forms although the predominant intracellular polyamine molecules can vary widely across and within kingdoms[38,86]. They impinge on a multitude of cellular processes including the regulation of gene expression and protein translation, protection from oxidative stress, cell membrane function, cell growth, and pH tolerance[38,43,54,61,87-89]. At a chemical level, the amine groups of polyamines are protonated and positively charged at physiologic pH, while the alkyl backbones linking these amines enable hydrophobic interactions and impart flexibility[90,91], such that the polycationic polyamines can bind to negatively charged macromolecules including DNA, RNA, membrane lipids, and proteins[38,40,43,90,91]. Given these promiscuous interactions, high concentrations of polyamines can be toxic[37] and their levels are tightly regulated through a combination of synthesis, import/export, and metabolism[54]. Charge neutralization via acetylation of the terminal amines of the longer chain polyamines, spermidine and spermine, is thought to be a key metabolic mechanism of regulation, particularly under stressful conditions. In eukaryotic cells this reaction is performed by SAT1 while bacteria employ various acetyltransferases, including SpeG[55,92]. *SpeG* deletion has been reported to hinder intracellular proliferation of *Salmonella*[56] and impair the resistance of the MRSA USA300 strain to host polyamines[57,58], directly tying its activity to pathogen fitness. Nevertheless, the mechanism by which the loss of polyamine acetylation could impair fitness remained unclear.

Our identification of *N*-acetylputrescine as a bacterial metabolite elevated in BSI, and not *N*-acetylspermidine, was initially puzzling given previous reports of SpeG activity. To our knowledge, until this study there were no experimental data demonstrating SpeG's activity toward putrescine. This is striking, as putrescine is the most abundant polyamine in the bacterial pathogens investigated here, while spermidine is present at about 5-to-10-fold lower concentrations[38-41]. Notably, under physiologic conditions, intracellular spermidine concentrations (1-5 mM) can be an order of magnitude greater than the corresponding K_{half} for SpeG (~600 μM), indicating that SpeG already operates on this substrate at or near its V_{max} and perturbations in spermidine concentration are

likely to have little impact on the rate of *N*-acetylspermidine production. Putrescine concentrations, in contrast, sit just below the measured K_{half} (~50 mM), indicating that SpeG likely plays a critical role in managing putrescine levels if they shift outside of tolerable ranges. To this end, SpeG's cooperative kinetics[35,44] enable a rapid and robust increase in activity under these conditions. Together, these observations indicate that, in addition to responding to spermidine and other exogenous polyamines, a major previously unrecognized role of SpeG and its homologs in the bacterial pathogens studied here is likely the management of intracellular putrescine levels.

Because polyamines interact with numerous cellular processes, we leveraged both genetic and chemical biology approaches to interrogate the impact of SpeG inhibition and prioritize pathways for further study. Our results highlighted membrane integrity as an SpeG-dependent property that may be exploited therapeutically, allowing us to significantly increase antibiotics' access to cells and efficacy[93]. Our focus on membrane permeability, however, does not exclude the possibility that SpeG inhibition impacts other pathways within the cell. Further characterization of additional mechanism(s) by which SpeG inhibition impairs bacterial fitness are needed as disruptions of other pathways could provide important insight into SpeG's role in enabling pathogenesis while also defining additional opportunities for intervention.

Due to the important role SpeG plays in the fitness of the gram-negative clinical isolates examined here, SpeG and its homologs represent an intriguing target across a broader range of AMR-associated pathogens. The remaining members of the top six AMR-associated pathogens[1], *Acinetobacter baumannii*, *Streptococcus pneumoniae*, and *Staphyloccocus aureus*, all possess genes annotated as polyamine *N*-acetyltransferases (**Figure 2D**). The MRSA USA300 *speG* homolog is part of the Arginine Catabolic Mobile Element that has contributed to the clinical success of this strain and has been partially characterized with spermidine and spermine as substrates[57,58,64]. This homolog clusters with the *E. coli* and *K. pneumoniae* homologs in our phylogenetic analysis, confirming prior analyses showing a high degree of sequence similarity between these proteins[35]. Like *P. aeruginosa* PA1472, candidate homologs in *A. baumannii* and *S. pneumoniae* cluster separately, but map to the microbial side of the phylogenetic tree, distinct from eukaryotic homologs. Interestingly, a distinct polyamine acetyltransferase more similar to the mammalian SAT1 enzyme and not

included in our phylogenetic analysis, was recently described in *A. baumannii,* with a narrow substrate scope predominantly limited to short chain 1,3-diaminopropane[94]. The *A. baumannii* candidate enzyme included in our phylogenetic analysis was not studied and its role in polyamine metabolism is unknown. Thus, while these initial leads are promising, further experimentation is needed to determine the functional roles of these candidate polyamine *N*-acetyltransferases and their potential contributions to pathogenesis.

While there were no demonstrated inhibitors of SpeG at the start of this study, we show that diminazene, a livestock antitrypanosomal drug and known inhibitor of SAT1, can also inhibit SpeG with similar potency[63,64]. Diminazene is not licensed for humans because of numerous toxicities in animals including convulsions, frequent urination and defecation, kidney and liver injury[95]. Despite being similarly susceptible to diminazene, the crystal structures of *E. coli* and *Vibrio cholerae* SpeG and *H. sapiens* SAT1 highlight several key structural distinctions, specifically a homo-dodecamer quaternary structure and the aforementioned allosteric polyamine binding site in the microbial enzyme compared with the simpler homodimer and single substrate binding site per subunit of the human enzyme[35,44,52]. These structural differences could provide an opportunity for the development of a microbial-specific polyamine acetyltransferase inhibitor, which could potentially target additional AMR-associated SpeG homologs. Interestingly, the recent solving of the MRSA USA300 SpeG homolog's quaternary structure[96] demonstrates marked overall similarity with the *E. coli* and *V. choerae* enzymes. Additionally, our AlphaFold2 prediction of PA1472 closely resembles *E. coli* SpeG, raising the possibility of a similar quaternary structure for this enzyme. Whether this is also true for the candidate *A. baumannii* and *S. pneumoniae* homologs and whether these structural predictions are experimentally supported will require further studies.

Overall, this study demonstrates the power of leveraging the natural, *in vivo* context of an infection to prioritize characterization of underappreciated aspects of microbial metabolism that contribute to disease. As our investigations of putrescine acetylation demonstrate, the resulting follow-up experiments can both inform our perspective on the key biological functions of specific microbial enzymes, identify new biomarkers that can guide therapy, and highlight potential vulnerabilities for therapeutic intervention. Thus, we anticipate that this

study represents a starting point in developing a blueprint to investigate metabolism not only in gram-negative BSIs, but other infectious syndromes and clinically-relevant pathogens *in vivo*, with the ultimate goal of providing new tools to combat AMR.

ACKNOWLEDGEMENTS

J.R.M., J.V., J.N. were supported by NHLBI T32 grant 5T32HL007633. M.D.I. was supported by a Canadian Institutes of Health Research Postdoctoral Fellowship (MFE-176575). N.R.G. was supported by an NSF Postdoctoral Research Fellowship in Biology under grant 1907240. R.M.B. was supported by R01 HL142093-01. E.P.B. was supported by the NSF Alan T. Waterman Award (CHE-20380529). E.P.B is a Howard Hughes Medical Institute Investigator.

AUTHOR CONTRIBUTIONS

Conceptualization, J.R.M., R.M.B., and E.P.B.; Methodology, J.R.M., J.V., R.R.Z, M.D.I., A.B., N.R.G., J.N., C.H., M.A.P, C.B.C., S.D.Z., R.M.B., and E.P.B.; Investigation, J.R.M., J.V., R.R.Z., M.D.I., C.B., N.R.G., F.M.L, J.N, M.P.V., M.A.P., C.B.C., S.D.Z., R.M.B., and E.P.B.; Writing – Original Draft, J.R.M., R.M.B., and E.P.B; Funding Acquisition, R.M.B. and E.P.B.; Supervision, C.H., M.A.P. S.D.Z., R.M.B., and E.P.B.

DECLARATION OF INTERESTS

The authors declare no competing interests.

Figure 1. Putrescine metabolites are elevated in humans with gram-negative septic shock and mouse models of sepsis and are produced by bacteria

(A) Volcano plot highlighting significant elevations in *N*-acetylputrescine and 4-acetamidobutanoate in humans with gram-negative septic shock

(B) *N*-acetylpturescine and 4-acetomidobutanoate levels correlate with worse clinical outcomes as measured by APACHE II scores

(C) Putrescine metabolic pathway outlining production of *N*-acetylputrescine and 4-acetamidobutanoate

(D) Putrescine metabolites are elevated in the mouse cecal slurry model of septic shock/BSI; HK = heat killed, CS = cecal slurry; n = 8 PBS, n = 7 HK CS, n = 4 Live CS; p-values were determined by One-way ANOVA followed by Tukey's multiple comparisons test

(E) Septic shock/BSI with heat-killed cecal slurry rescued with *E. coli* BW25113 results in increased plasma putrescine metabolite levels; n = 5 HK CS, n = 9 HK CS + *E. coli* BW25113; Two-tailed p-values were determined by unpaired t test

(F) *Klebsiella pneumoniae* pneumonia results in increased bronchial alveolar lavage (BAL) fluid levels of *N*-acetylputrescine; n = 4 PBS, n = 6 *K. pneumoniae* (KP9); Two-tailed p-values were determined by Mann Whitney test to include the outlier.

(G) *Klebsiella pneumoniae* pneumonia results in increased plasma levels of *N*-acetylputrescine; n = 4 PBS, n = 6 *K. pneumoniae* (KP9); Two-tailed p-values were determined by Mann Whitney test to include the outlier.

(H) Bacterial and mouse production of *N*-acetylputrescine + 4-acetamidobutanoate from putrescine; n = 3 for bacteria, representative data from 1-3 independent repeats; n = 6 mice; Blue = *E. coli*, Green = *K. pneumoniae*, Red = *P. aeruginosa*

For all panels, data presented are means ± SEM; *p < 0.05; **p < 0.01; ***p < 0.001; ****p<0.0001

Figure 2. SpeG homologs are responsible for production of *N*-acetylputrescine in gram-negative pathogens

(A) Complementation in *E. coli* BW25113 demonstrates SpeG can produce *N*-acetylputrescine; n = 3 per condition, representative data from 3 independent experiments

(B) 1 hour production of *N*-acetylputrescine from putrescine by recombinant purified enzymes; n = 3 per condition, representative data from 3 independent experiments; NE = no enzyme, GFP = green fluorescent protein

(C) Kinetics of putrescine acetylation by SpeG is consistent with previously demonstrated cooperative mechanism on spermidine, n = 2-3 per substrate concentration, representative data from 4 independent experiments; summary parameters includes all experiments

(D) Maximum-likelihood phylogenetic tree of a representative member of each group of protein sequences sharing >80% amino acid ID (RepNode80); Blue = *E. coli* SpeG clade, Purple = mammalian SAT1 clade, Turquoise = *B. subtilis* BltD clade

(E) Complementation in *E. coli* BW25113 demonstrates PA1472 can produce *N*-acetylputrescine; n = 3 per condition, representative data from 2-3 independent experiments

(F) 1 hour production of *N*-acetylputrescine from putrescine by recombinant purified enzymes; n = 3 per condition, representative data from 2-3 independent experiments; NE = no enzyme, GFP = green fluorescent protein

(G) Kinetics of PA1472 on putrescine; n = 2 per concentration, representative data from 3 independent experiments; summary parameters includes all experiments

(H) SpeG (PDB: 3WR7) and PA1472 (AlphaFold2) dimers

For all panels, data presented are means ± SEM

Figure 3. Suppression of *speG* expression impacts proliferation

(A) Suppression of *speG* expression with inducible CRISPRi in *E. coli* patient bloodstream isolate E23; n = 3 per condition, representative data from 2 independent experiments

(B) Decreased levels of extracellular *N*-acetylputrescine with inducible CRISPRi of *speG* in E23, concentrations normalized to OD_{600} = 1.0 ; n = 3 per condition, representative data from 2 independent experiments

(C) Increased relative intracellular putrescine levels (concentrations normalized to OD_{600} = 1.0 and then normalized to concentration of control condition) and decreased ratio of *N*-acetylputrescine/putrescine

with inducible CRISPRi of *speG* in E23; n = 3 per condition, representative data from 2 independent experiments

(D) Inducible CRISPRi of *speG* suppresses E23 growth in culture; n = 3 per condition, representative data from 3 independent experiments

(E) Inducible CRISPRi of *speG* delays mortality in a cecal slurry model of sepsis with E23; n = 10 mice per group for all groups except n = 9 for *RFP* – aTC; p-value determined by Log-rank (Mantel-Cox) test

For panels A-D, data presented are means ± SEM; Two-tailed p-values were determined by unpaired t test; *p < 0.05; **p < 0.01; ***p < 0.001; ****p<0.0001

aTC = anhydrotetracycline

Figure 4. Diminazene inhibits SpeG and phenocopies inducible CRISPRi

(A) Structures of spermidine and diminazene

(B) Determination of *in vitro* IC_{50} of diminazene against speG with putrescine substrate; n = 2 per inhibitor concentration, representative data from 3 independent experiments; summary data includes all experiments

(C) Diminazene treatment reduces extracellular levels of *N*-acetylputrescine in E23, concentrations normalized to OD_{600} = 1.0; n = 3 per condition, representative data from 3 independent experiments; p-values were determined by One-way ANOVA followed by Dunnett's multiple comparisons test with all comparisons made against no drug control

(D) Diminazene treatment increases relative intracellular putrescine levels (concentrations normalized to OD_{600} = 1.0 and then normalized to concentration of control, 0 μM) condition) and decreases the ratio of *N*-acetylputrescine in E23; n = 3 per condition, p-values were determined by One-way ANOVA followed by Dunnett's multiple comparisons test with all comparisons made against no drug control

(E) MIC_{90} of diminazene treated E23, M 1/5, and BW25113 in LB; n = 3 per condition, representative data from 3 independent experiments; summary data includes all experiments

(F) Inducible CRISPRi of *speG* blocks growth inhibition by diminazene in E23; n = 3 per condition, representative data from 2 independent experiments; Two-tailed p-values were determined by unpaired t test

For all panels, data presented are means ± SEM; *p < 0.05; **p < 0.01; ***p < 0.001; ****p<0.0001

aTC = anhydrotetracycline

Figure 5. Reducing SpeG activity enhances membrane permeability.

(A) Checkerboard assays demonstrate synergy between diminazene and vancomycin in *E. coli* E23; representative data from 3 independent experiments

(B) Inducible CRISPRi of *speG* reduces MIC of vancomycin in *E. coli* E23; mean growth of n = 3 per condition, representative data from 3 independent experiments

(C) Inducible CRISPRi of *speG* enhances membrane permeability in E23; n = 3 per condition, representative data from 2 independent experiments; Two-tailed p-values were determined by unpaired t test

(D) Diminazene treatment for 6 hours enhances membrane permeability in *E. coli* E23; n = 3 per condition, representative data from 2 independent experiments; p-values were determined by One-way ANOVA followed by Dunnett's multiple comparisons test with all comparisons made against no drug control

For panels B-D, data presented are means ± SEM; *p < 0.05; **p < 0.01; ***p < 0.001; ****p<0.0001

aTC = anhydrotetracycline

Figure 6. Blocking SpeG synergizes with existing clinical antibiotics in resistant bacteria in culture and *in vivo*

(A) Checkerboard assays demonstrate synergy between diminazene and antibiotics to which the assayed MDR strains are clinically resistant; representative data from 3-4 independent experiments per strain

(B) Diminazene treatment enhances uptake of antibiotics to which MDR strains are resistant; n = 3 per condition, representative data from 1-3 independent experiments; Two-tailed p-values were determined by unpaired t test

(C) Combination of diminazene and tetracycline treatment reduces mortality in a cecal slurry model of sepsis with the tetracycline resistant clinical isolate *E. coli* E1; n = 10 mice per group; p-value determined by Log-rank (Mantel-Cox) test

For panels B, data presented are means ± SEM; *p < 0.05; **p < 0.01; ***p < 0.001; ****p<0.0001

aTC = anhydrotetracycline

Figure S1. Putrescine metabolites are elevated in humans with gram-negative septic shock

(A) Patient characteristics

(B) APACHE II distribution by organism; Blue = *E. coli*, Green = *K. pneumoniae*, Red = *P. aeruginosa*

(C) Correlation plots for the other 6 metabolites of significance that also showed significant correlations with APACHE II; DMGV = dimethylguanidino valerate

(D) Volcano plot with highlighting significant decreases in numerous lysophosphatidylcholine species

Figure S2. Putrescine metabolites are elevated in mouse models of septic shock

(A) Time course of putrescine metabolite changes in cecal slurry model; HK = heat killed, CS = cecal slurry; n = 8 PBS, n = 7 HK CS, n = 4 Live CS; p-values were determined by Two-way ANOVA followed by Tukey's multiple comparisons test

(B) Putrescine metabolites are elevated in the mouse cecal slurry model of septic shock in female mice; HK = heat killed, CS = cecal slurry; n = 6 PBS, n = 6 HK CS, n = 12 Live CS; p-values were determined by One-way ANOVA followed by Tukey's multiple comparisons test

(C) Time course of representative lysophosphatidylcholine (lysoPC) changes in cecal slurry model; HK = heat killed, CS = cecal slurry; n = 8 PBS, n = 7 HK CS, n = 4 Live CS; p-values were determined by Two-way ANOVA followed by Tukey's multiple comparisons test

(D) Cecal ligation and puncture 24 hour time point demonstrates similar elevations in putrescine metabolites; n = 4 PBS, n = 3 lipopolysaccaride (LPS), n = 3 cecal ligation and puncture (CLP). p-values were determined by One-way ANOVA followed by Tukey's multiple comparisons test

For all panels, data presented are means ± SEM; *p < 0.05; **p < 0.01; ***p < 0.001; ****p<0.0001

Figure S3. *Klebsiela pneumoniae* pneumonia levels of 4-acetamidobutanoate

(A) *Klebsiella pneumoniae* pneumonia results in increased bronchial alveolar lavage (BAL) fluid levels of 4-acetamidobutanoate; n = 4 PBS, n = 6 *K. pneumoniae* (KP9); Two-tailed p-values were determined by Mann Whitney test to include outlier.

(B) *Klebsiella pneumoniae* pneumonia results in trend towards increased plasma levels of 4-acetamidobutanoate; n = 4 PBS, n = 6 *K. pneumoniae* (KP9); Two-tailed p-values were determined by Mann Whitney test to include outlier.

For all panels, data presented are means ± SEM

Figure S4. Putrescine metabolite production by bacteria and mice

(A) Production of *N*-acetylputrescine from putrescine by bacteria and mice; n = 3 for bacteria, representative data from 1-3 independent repeats; n = 6 mice

(B) Production of 4-acetamidobutanoate from putrescine by bacteria and mice; n = 3 for bacteria, representative data from 1-3 independent repeats; n = 6 mice

(C) Time course of putrescine levels in mouse plasma after IP injection; n = 6 mice for each treatment

(D) Time course of *N*-acetylputrescine plasma levels in mice after IP injection with 100 mg/kg of putrescine; n = 6 mice for each treatment

(E) Time course of 4-acetamidobutanoate plasma levels in mice after IP injection with 100 mg/kg of putrescine; n = 6 mice for each treatment

(F) Production of 4-acetamidobutanoate from *N*-acetylputrescine by bacteria and mice; n = 3 for bacteria, representative data from 1-3 independent repeats; n = 3 mice

(G) Time course of *N*-acetylputrescine plasma levels in mice after IP injection with 50 mg/kg of *N*-acetylputrescine; n = 4 PBS, n = 3 *N*-acetylputrescine

(H) Time course of 4-acetamidobutanoate plasma levels in mice after IP injection with 50 mg/kg of *N*-acetylputrescine; n = 4 PBS, n = 3 *N*-acetylputrescine

For all panels, data presented are means ± SEM

Figure S5. SpeG homologs are responsible for production of *N*-acetylputrescine in bacteria and are distinct from mammals

(A) Uncropped protein gel of purified proteins

(B) Kinetics of SpeG on spermidine; n = 3 per concentration, representative data from 3 independent experiments; summary parameters includes all experiments

(C) Kinetics of SAT1 on putrescine; n = 3 per concentration, representative data from 4 independent experiments; summary parameters includes all experiments

(D) Kinetics of SAT1 on spermidine; n = 3 per concentration, representative data from 3 independent experiments; summary parameters includes all experiments

(E) SpeG (PDB: 3WR7), PA1472 (AlphaFold2), SAT1 (PDB: 2B5G) dimers

For all panels, data presented are means ± SEM

Figures S6. Suppresion of SpeG expression impacts proliferation

(A) *E. coli* BW25113 parental strain growth compared with KEIO collection *ΔspeG* suggests no clear effect on proliferation; n = 3 per cell line; representative data from 3 independent experiments

(B) Suppression of *speG* expression with inducible CRISPRi in BW25113; n = 3 per condition, representative data from 2 independent experiments

(C) Inducible CRISPRi of *speG* in BW25113 demonstrates suppression of *speG* expression impairs proliferation; n = 3 per condition, representative data from 2 independent experiments

(D) Suppression of *speG* expression with inducible CRISPRi in M 1/5; n = 3 per condition, representative data from 3 independent experiments

(E) Decreased levels of extracellular *N*-acetylputrescine with inducible CRISPRi of *speG* in M 1/5, concentrations normalized to OD_{600} = 1.0; n = 3 per condition, representative data from 2 independent experiments

(F) Inducible CRISPRi of *speG* blocks putrescine to *N*-acetylputrescine conversion intracellularly in M 1/5; n = 3 per condition

(G) Raw growth curves for inducible CRISPRi in M 1/5 and E23 (Figure 3D and Figure S6H)

(H) Inducible CRISPRi of *speG* suppress growth in *E. coli* isolate M 1/5; n = 3 per condition, representative data from 2 independent experiments

(I) Supplementation of inducible CRISPRi cultures of *speG* with 1mM *N*-acetylputrescine does not rescue proliferation defect; n = 3 per condition, representative data from 3 independent experiments

For all panels data presented are means ± SEM; Two-tailed p-values were determined by unpaired t test; *p < 0.05; **p < 0.01; ***p < 0.001; ****p<0.0001

aTC = anhydrotetracycline

Figure S7. Diminazene inhibits SpeG and phenocopies inducible CRISPRi

(A) Determination of *in vitro* IC_{50} of diminazene against SpeG with spermidine substrate; n = 2 per inhibitor concentration, representative data from 3 independent experiments; summary parameter includes all experiments

(B) Determination of *in vitro* IC_{50} of diminazene against SAT1 with spermidine substrate; n = 2 per inhibitor concentration, representative data from 3 independent experiments; summary parameter includes all experiments

(C) Diminazene treatment reduces extracellular levels of *N*-acetylputrescine in M 1/5, concentrations normalized to OD_{600} = 1.0; n = 3 per condition, representative data from 3 independent experiments; p-values were determined by One-way ANOVA followed by Dunnett's multiple comparisons test with all comparisons made against no drug control

(D) Diminazene treatment increases relative intracellular putrescine levels and decreases the ratio of *N*-acetylputrescine in M 1/5 ; n = 3 per condition; normalized to OD_{600} = 1.0, then normalized to the concentration of the control, 0 μM, condition; p-values were determined by One-way ANOVA followed by Dunnett's multiple comparisons test with all comparisons made against no drug control

(E) Growth curves for diminazene treatment MIC_{90}s of E23, M 1/5, and BW25113 in LB; n = 3 per condition

(F) MIC_{90} of E23 and M 1/5 in M9 minimal media with 0.4% glucose and 0.2% Cas-AA; n = 3 per condition, representative data from 2 independent experiments; summary MIC_{90}s combine all experiments

(G) Representative growth curves for diminazene treatment MIC_{90}s of E23 and M 1/5 in M9 minimal media with 0.4% glucose and 0.2% Cas-AA (Figure S7F); n = 3 per condition

(H) Inducible CRISPRi of *speG* blocks growth inhibition by diminazene in M 1/5; n = 3 per condition, presentative data from 3 independent experiments

(I) MIC curves of MDR clinical isolates of *E. coli, K. pneumonia*, *P. aeruginosa* in LB; n = 3 per condition, representative data from 3 independent experiments

(J) Calculated MIC_{90} values for MDR patient isolates in LB (Figure S7I)

For all panels data presented are means ± SEM; *p < 0.05; **p < 0.01; ***p < 0.001; ****p<0.0001

aTC = anhydrotetracycline

Figure S8. Reducing SpeG activity enhances membrane permeability

(A) Checkerboard assays demonstrate synergy between diminazene and vancomycin in M 1/5; representative data from 4 independent experiments

(B) Growth relative to no vancomycin of inducible CRISPRi of *speG* in E23 in LB with vancomycin gradient; n = 3 per condition, representative data from 3 independent experiments (graphical summary of data in **Figure 5B**).

(C) Inducible CRISPRi of *speG* reduces MIC of vancomycin in M 1/5 and corresponding growth curves relative to no vancomycin; mean of n = 3 per condition, representative data from 3 independent experiments

(D) Inducible CRISPRi of *speG* enhances membrane permeability of M 1/5; n = 3 per condition, representative data from 2 independent experiments; Two-tailed p-values were determined by unpaired t test

(E) Diminazene treatment for 6 hours enhances membrane permeability in M1/5; n = 3 per condition, representative data from 2 independent experiments; p-values were determined by One-way ANOVA followed by Dunnett's multiple comparisons test with all comparisons made against no drug control

(F) Diminazene treatment for 3 hours has minimal to no effect on membrane permeability in E23 and M 1/5; n = 3 per condition; p-values were determined by One-way ANOVA followed by Dunnett's multiple comparisons test with all comparisons made against no drug control

For B-F, data presented are means ± SEM; *p < 0.05; **p < 0.01; ***p < 0.001; ****p<0.0001

aTC = anhydrotetracycline

Figure S9. Blocking SpeG synergizes with existing clinical antibiotics in resistant bacteria

(A) Checkerboard assays demonstrate synergy between diminazene and antibiotics to which the assayed MDR strains are clinically resistant; representative data from 1-3 independent experiments per cell line

(B) Diminazene treatment enhances uptake of antibiotics to which MDR strains are resistant; n = 3 per condition, representative data from 2 independent experiments; Two-tailed p-values were determined by unpaired t test

For panel B, data presented are means ± SEM; *p < 0.05; **p < 0.01; ***p < 0.001; ****p<0.0001

aTC = anhydrotetracycline

Table S1. Individual patient characteristics

Table S2. Targeted metabolomics results

Table S3. Codon optimized gene sequences for *E. coli* expression (5’ -> 3’)

Table S4. Primers used for complementation cloning

Table S5. qRT-PCR primers

Table S6. Primers used for complementation cloning

Table S7. Multiple reaction monitoring (MRM) transitions

MATERIALS AND METHODS

Human Metabolomics

Patient Samples

Patient samples were selected from the pre-existing Registry of Critical Illness (RoCI) cohort, housed at Brigham and Women's Hospital (BWH) in Boston, MA, USA[97]. RoCI is approved by the Partners/Mass General Brigham Human Research Committee. Informed consent was obtained for blood collection. Curation of the database identified 21 patients with positive blood cultures growing either *Escherichia coli, Klebsiella pneumoniae,* or *Pseudomonas aeruginosa* with contemporaneous or near contemporaneous plasma samples banked and available for metabolomic analysis. Twenty-two controls admitted to the intensive care unit for reasons other than septic shock were identified for use as controls.

Metabolomics

Metabolomic measurements were made using 3 complementary liquid chromatography–tandem mass spectroscopy (LC-MS) methods. For each method, pooled plasma reference samples were included every 20 samples, and results were standardized using the ratio of the value of the sample to the value of the nearest pooled reference multiplied by the median of all reference values for the metabolite.

HILIC analyses of water-soluble metabolites in the positive ionization mode (HILIC-pos) were conducted using an LC-MS system composed of a Shimadzu Nexera X2 U-HPLC (Shimadzu Corp) coupled to a Q Exactive hybrid quadrupole orbitrap mass spectrometer (Thermo Fisher Scientific). Plasma samples (10 µL) were prepared via protein precipitation with the addition of 9 volumes of 74.9:24.9:0.2 v/v/v acetonitrile/methanol/formic acid containing stable isotope-labeled internal standards (valine-d_8, Sigma-Aldrich; and phenylalanine-d_8, Cambridge Isotope Laboratories). The samples were centrifuged (10 minutes, 9000*g*, 4 °C), and the supernatants were injected directly onto a 150×2 mm, 3-µm Atlantis HILIC column (Waters). The column was eluted isocratically at a flow rate of 250 µL/min with 5% mobile phase A (10 mmol/L ammonium formate and 0.1% formic acid in water) for 0.5 minute followed by a linear gradient to 40% mobile phase B (acetonitrile with 0.1% formic acid) over 10 minutes. Mass spectroscopic (MS) analyses were

performed by using electrospray ionization in the positive ion mode using full scan analysis over 70 to 800 *m/z* at 70000 resolution and 3 Hz data acquisition rate. Other MS settings were as follows: sheath gas 40, sweep gas 2, spray voltage 3.5 kV, capillary temperature 350 °C, S-lens RF 40, heater temperature 300 °C, microscans 1, automatic gain control target 1e6, and maximum ion time 250 ms.

HILIC analyses of water-soluble metabolites in the negative ionization mode (HILIC-neg) were conducted by using an LC-MS system composed of an AQUITY UPLC system (Waters and a 5500 QTRAP mass spectrometer [SCIEX]). Plasma samples (30 µL) were prepared via protein precipitation with the addition of 4 volumes of 80% methanol containing inosine-^{15}N4, thymine-d_4, and glycocholate-d_4 internal standards (Cambridge Isotope Laboratories). The samples were centrifuged (10 minutes, 9000*g*, 4 °C), and the supernatants were injected directly onto a 150×2.0 mm Luna NH2 column (Phenomenex). The column was eluted at a flow rate of 400 µL/min with initial conditions of 10% mobile phase A (20 mmol/L ammonium acetate and 20 mmol/L ammonium hydroxide in water) and 90% mobile phase B (10 mmol/L ammonium hydroxide in 75:25 v/v acetonitrile/methanol) followed by a 10-minute linear gradient to 100% mobile phase A. MS analyses were performed using electrospray ionization and selective multiple reaction monitoring scans in the negative ion mode. To create the method, declustering potentials and collision energies were optimized for each metabolite by infusion of reference standards. The ion spray voltage was –4.5 kV and the source temperature was 500 °C.

Positive ion mode analyses of polar and nonpolar plasma lipids (C8-pos) were conducted using an LC-MS system composed of a Shimadzu Nexera X2 U-HPLC (Shimadzu Corp) coupled to a Exactive Plus orbitrap mass spectrometer (Thermo Fisher Scientific). Plasma samples (10 µL) were extracted for lipid analyses using 190 µL of isopropanol containing 1,2-didodecanoyl-*sn*-glycero-3-phosphocholine (Avanti Polar Lipids). After centrifugation, supernatants were injected directly onto a 100×2.1 mm, 1.7-µm ACQUITY BEH C8 column (Waters). The column was eluted isocratically with 80% mobile phase A (95:5:0.1 v/v/v 10 mmol/L ammonium acetate/methanol/formic acid) for 1 minute followed by a linear gradient to 80% mobile phase B (99.9:0.1 v/v methanol/formic acid) over 2 minutes, a linear gradient to 100% mobile phase B over 7 minutes, then 3 minutes at 100% mobile phase B. MS analyses were performed using electrospray ionization in the positive ion mode

using full scan analysis over 200 to 1000 *m/z* at 70000 resolution and 3 Hz data acquisition rate. Other MS settings were as follows: sheath gas 50, in source collision-induced dissociation 5 eV, sweep gas 5, spray voltage 3 kV, capillary temperature 300 °C, S-lens RF 60, heater temperature 300 °C, microscans 1, automatic gain control target 1e6, and maximum ion time 100 ms. Lipid identities were determined based on comparison with reference plasma extracts and were denoted by the total number of carbons in the lipid acyl chain(s) and total number of double bonds in the lipid acyl chain(s).

Raw data from Q Exactive/Exactive Plus instruments were processed using TraceFinder software (ThermoFisher Scientific) and Progenesis QI (Nonlinear Dynamics), whereas MultiQuant (SCIEX) was used to process 5500 QTRAP data. For each method, metabolite identities were confirmed using authentic reference standards or reference samples.

Statistical Analyses

Targeted metabolomics analyses. To normalize and standardize the LC–MS data, measurements from the internal standards were first corrected by removing the technical variation associated with injection order. This technical variation was characterized by regressing the internal standards readings on injection order using a local degree-two polynomial regression with an alpha parameter of 5, implemented using the R function loess. To correct for technical variation, internal standards were converted to ratios relative to the fitted readings from the regression. These ratios were then averaged across all internal standards used. The same procedure was used to correct for technical variation from each of the profiled metabolites. Finally, normalized metabolite readings were calculated by subtracting natural log-transformed average corrected standard from natural log-transformed corrected metabolite readings. Only metabolites that had less than 10% missing data in each of the two patient groups (septic shock and control patients) were considered.

To identify candidate metabolites, each metabolite was tested using a Wilcoxon to test to determine whether it was present at different levels between the two patient groups. Metabolites with false discovery rate-adjusted p-values less than 0.05 were deemed significantly differentially abundant. Each metabolite was also tested for

association with APACHE II scores among all patients using Spearman's correlation, and with mortality among all patients using a Wilcoxon test. A false discovery rate cutoff of 0.05 was used to identify statistically significant metabolites.

Mouse Models

Models of Infection

All mouse experiments were conducted in accordance with protocols approved by the BWH Institutional Animal Care and Use Committee (IACUC). For most experiments, we used C57BL/6N SPF[98] male mice 10-12 weeks of age purchased from Charles River Laboratories. The cecal slurry studies were also conducted in a cohort of C57BL/6N SPF female mice 10-12 weeks of age purchased from Charles River Laboratories. All mice were allowed to acclimate for more than one week prior to use.

Cecal Ligation and Puncture (CLP). CLP was performed as previously described[99]. Briefly, after induction of anesthesia and analgesia with ketamine (85 mg/kg) and xylazine (34 mg/kg), mice were anesthetized, and a midline laparotomy was performed. The cecum was externalized, ligated, and punctured, after which a small amount of cecal contents were extruded from the puncture holes. The cecum was then replaced in the abdomen, and the abdominal incision was closed in layers. The mice were resuscitated with 1 mL of phosphate-buffered saline (PBS) and placed in a warmed cage for postoperative recovery. As our study was focused on identifying bacterial metabolites in plasma, the mice did not receive antibiotics to avoid reducing the sensitivity of our analyses. Mice were sacrificed at 24 hours. Original groups were n = 4 mice in PBS and CLP, n = 3 for LPS. One CLP mouse did not survive the full 24 hours and was excluded from analysis.

Cecal Slurry. Cecal slurry was performed as previously described[30]. Briefly, 10-14 week old C57B/6 mice from Charles River were sacrificed and whole cecum dissected. The entire cecal contents were collected with sterile forceps, spatula, and culture dishes. Collected contents were pooled and weighed before mixing 0.5 mL sterile water per 100 mg cecal contents. After resuspension, the cecal slurry was filtered through 100 μm sterile mesh filters (Falcon). The filtered cecal slurry was then mixed with an equal volume of sterile 30% glycerol in PBS.

This final solution was aliquoted and stored at –80 ºC until use.

Heat killed cecal slurry was produced by heating room temperature cecal slurry at 72 ºC for 15 min. After cooling to 37 ºC, an undiluted aliquot was plated on LB Lennox agar (VWR) to confirm the absence of culturable bacteria. For male mice, sepsis was induced with a 200 µL intraperitoneal injection of thawed live cecal slurry (live bacteria confirmed by plating). As controls, 200 µL of heat killed cecal slurry and 200 µL of 15% glycerol in sterile PBS were used. Mice were sacrificed at 24 hours. Original groups were n = 8, mice that did not survive the full 24 hours were excluded from analysis. For the smaller female mice, sepsis was induced with a 150 µL intraperitoneal injection of thawed live cecal slurry (live bacteria confirmed by plating). As controls, 150 µL of heat killed cecal slurry and 150 µL of 15% glycerol in sterile PBS were used. Female mice were sacrificed at 20 hours. Original groups were n = 6 each for PBS and heat-killed cecal slurry and n = 12 for live cecal slurry.

For the *E. coli* BW25113 HK CS rescue experiment, *E. coli* were grown overnight to stationary phase in LB Lenox Broth (VWR) before cells were washed 2x with PBS and OD_{600} determined by NanoDrop 2000c (Thermo Scientific). Cultures were spun down and resuspended to a calculated 1 x 10^8 CFU/mL (www.agilent.com/store/biocalculators/calcODBacterial.jsp) in heat killed cecal slurry prior to administration. Actual CFU was determined to be ~4 x 10^7 CFU/mL by plating serial dilutions. 200 µL of this resuspension was injected into the peritoneal space of each mouse and mice were sacrificed at 24 hours. Groups were n = 5 heat-killed cecal slurry and n = 9 heat-killed cecal slurry + *E. coli* BW25113

For the CRISPRi experiment HK CS rescue experiment, mice received 3 days of 20 µm filter-sterilized drinking water ± 250 mg/L anhydrotetracycline (Cayman Chemicals) in red-tinted bottles (Ancare) to inhibit degradation by light. This was continued after administration of bacteria until the completion of the experiment. *E. coli* (E23) CRISPRi cell lines (details below) were grown overnight to stationary phase in LB Lenox Broth (VWR) before dilution 1:50 into fresh media in the morning ± 2 µM anhydrotetracycline. After 5 hours of culture, cells were washed 2x with PBS and OD_{600} determined by NanoDrop 2000c (Thermo Scientific). Cultures were spun down and resuspended to a calculated 5.0 x 10^7 CFU/mL

(www.agilent.com/store/biocalculators/calcODBacterial.jsp) in heat killed cecal slurry (± 2 μM anhydrotetracycline) prior to administration. Actual CFU was determined to be ~2 x 10^7 CFU/mL by plating serial dilutions. 200 μL of this resuspension was injected into the peritoneal space of each mouse and survival monitored over the proceeding 20 hours. Originally planned as n = 10 mice per group. One mouse planned for the *RFP* – aTC group was excluded prior to the start of the experiment for fight wounds.

For the antibiotic synergy experiment, the *E. coli E1* strain was grown overnight to stationary phase in LB Lenox Broth (VWR) before cells were washed 2x with PBS and OD_{600} determined by NanoDrop 2000c (Thermo Scientific). Cultures were spun down and resuspended to a calculated 5 x 10^9 CFU/mL (www.agilent.com/store/biocalculators/calcODBacterial.jsp) in heat killed cecal slurry prior to administration. 200 μL of this resuspension was injected into the peritoneal space of each mouse. Actual CFU was determined to be ~4 x 10^9 CFU/mL by plating serial dilutions. Beginning one hour of after infection, mice received one of four treatments in equal volumes administered via IP injection: sterile 0.9% saline, diminazene in sterile 0.9% saline 7 mg/kg daily, tetracycline in sterile 0.9% saline 25 mg/kg every 12 hours, or both diminazene and tetracycline. Survival was monitored over the proceeding 48 hours.

Intranasal inoculation for pneumonia. Intranasal inoculation of *Klebsiella pneumonia* (KP9) was carried out as previously described[32,33]. Briefly, bacteria were grown to stationary phase overnight in LB Lennox Broth (VWR) before washing 2x with PBS and checking OD_{600} NanoDrop 2000c (Thermo Scientific). Cells were diluted to an OD_{600} = 0.8 for use. Actual CFUs were calculated to be ~2.2 x 10^9 CFU/mL by serial dilution. Mice were anesthetized as above with ketamine and xylazine and 40 μL of cells administered intranasally. Mice were kept vertical for ~30-60 seconds to ensure delivery to the lungs prior to recovery from anesthesia. After 16 hours, mice were anesthetized again as above and their tracheas cannulated. Bronchial alveolar lavage with 1 mL of sterile PBS was performed (4 washes with same PBS solution), cells pelleted, and cell free supernatant was frozen at –80 °C for metabolomics analysis. Mice were subsequently sacrificed.

Putrescine and N-acetylputrescine injections

Mice received an intraperitoneal injection with either 100 mg/kg putrescine dihydrochloride (Sigma Aldrich), 50 mg/kg *N*-acetylputrescine hydrochloride (Sigma Aldrich) dissolved in PBS, or PBS as indicated. Area under the curve (AUC) was calculated for each individual mouse as μM*min (nmol*min/mL) and baseline (PBS injected average) AUC was subtracted. Estimated blood volume was calculated as 0.08 mL per g body weight[100,101] and used determine total nmol of metabolite in blood over the course of the experiment. This was then normalized to estimated dry weight (26% of total weight)[102] to determine nmol metabolite per g of dry weight.

Plasma samples

Plasma was collected for each experiment at the time points indicated. For repeat bleeding experiments, the tail vein was accessed and small amounts of blood harvested, in total reaching less than 10% of the total blood volume. At experimental completion, mice were anesthetized with ketamine and xylazine as above and terminally bled prior to sacrifice. In all cases, blood was placed in EDTA-pretreated tubes (Sarsedt) and centrifuged to separate plasma. Plasma was aliquoted and frozen at −80 °C for further analysis.

Bacteria Experiments

Cell Lines

The *Escherichia coli* BW25113 parental strain and *ΔspeG* mutant (CGSC#: 9346, Name: JW1576-1) were obtained from the KEIO collection[42] housed at Yale University (cgsc.biology.yale.edu/KeioList.php). *E. coli* M 1/5 strain is a human isolate that was a generous gift from Professor Ulrich Dobrindt (University of Münster). All remaining cell lines described are clinical patient isolates provided as a generous gift by Dr. Sophia Koo (Brigham and Women's Hospital).

Putrescine derivative production

Indicated cell lines were growth overnight at 37 ºC in M9 minimal media (1x M9 Salts, 0.1 mM $CaCl_2$, 2 mM $MgSO_4$, 0.4% glucose, 0.2% CAS amino acids, pH 7.3-7.4) to stationary phase in 5 mL culture. The following morning cells were pelleted and resuspended in 1 mL fresh M9 minimal media lacking CAS amino acids and

supplemented with either 10 mM putrescine or *N*-acetylputrescine. Cells were then cultured for 5 hours at 37 ºC. Half of the culture was applied to pre-weighed Whatman filter paper, dried overnight at 55 ºC, and then filters re-weighed to determine dry cell mass. CFUs were calculated via serial dilution and plating on LB Lennox Agar. The remaining culture was pelleted and spent media removed and frozen at –80 ºC for subsequent LC–MS analysis. Metabolite amounts were normalized to CFUs or dry mass as indicated.

Complementation

For all complementation studies, a truncated version of the pTrcHis 2A expression vector (ThermoFisher) was utilized, which allowed use of the native *E. coli* K12 *speG* promoter. All promoters were designed with the NEBuilder assembly tool (www.nebuilder.neb.com/#!/). To obtain the native *E. coli* sequence for use, *speG* and its promoter were amplified via PCR from genomic DNA harvested from *E. coli* K12 MG1655. After PCR amplification, this sequence was cloned into the truncated pTrcHis vector using Gibson assembly. After the correct sequence was confirmed with DNA sequencing, this vector was transformed into *E. coli* BW25113 *ΔspeG* using electroporation. This construct containing the *speG* promoter was then used to assemble of the remaining complementation constructs utilized. To generate these constructs, amino acid sequences were obtained from the UniProt database (uniprot.org) and uploaded to the ThermoFisher GeneArt synthesis portal, which generated *E. coli* codon-optimized versions of each gene. After PCR amplification, these sequences were cloned into the modified pTrcHis + *speG* promoter vector using Gibson assembly. As before, the correct sequence was confirmed with DNA sequencing prior to transformation into *E. coli* BW25113 *ΔspeG* using electroporation. All primers and codon optimized gene sequences used are listed in **Table S3–S4**.

To test for polyamine metabolite production, stationary phase cultures were diluted 1:1000 into LB Lennox and grown overnight at 37 ºC. Parental BW25113 was grown without antibiotics, *ΔspeG* with Kanamycin (VWR, 50 µg/mL), and complemented strains with Kananmycin and Ampicillin (Sigma Aldrich, 100 µg/mL). The following morning OD_{600} was measured by plate reader (BioTek Synergy HTX), cells were pelleted, and spent media was frozen at –80 ºC for subsequent analysis.

Growth curves

Stationary phase cultures were diluted 1:100 into either LB Lenox or M9 minimal media with 0.4% glucose and 0.2% CAS-amino acids as indicated. Cultures were performed in either 96 or 384-well plates, maintained at 37 ºC and OD_{600} measured after shaking every 10 minutes for 16 hours by plate reader (BioTek Synergy HTX). For CRISPRi and MIC_{90} experiments, anhydrotetracycline (Cayman Chemical) or diminazene (Selleck Chemicals) respectively were added at the time of dilution. For growth relative to no treatment controls, the area under the curve (AUC) was calculated for each individual biological replicate of the experimental condition and normalized to the average of the no treatment control AUC.

CRISPRi

The inducible CRISPRi system consisting of pdCaS7-bacteria (AddGene #44249) and pgRNA-bacteria (AddGene #44251) was a gift from Stanley Qi [60,103]. Guide sequence targeting *speG* was designed using Millepore Sigma's CRISPR Design Tools. Cloning was performed as described in [60]. Guide sequences for *E. coli* BW25113 and M 1/5 (5'->3') ttaaaggtgattctacacca and for *E. coli* E23 (5'->3') ttaaagctgattctacacca. Doses of the pdCaS7 expression inducer anhydrotetracyline (Cayman Chemical) used were 2 μM for BW25113, 0.5 μM for M 1/5, and 2 μM for E23. For CRISPRi + 10 μM diminazene experiment, 0.25 μM and 1.5 μM concentrations of anhydrotetracyline were used for M 1/5 and E23 respectively. All cultures were grown in media containing Ampicillin (Sigma Aldrich, 100 μg/mL) and chloramphenicol (Sigma Aldrich, 25 μg/mL). For gene expression, membrane permeability, and metabolite production experiments, cells were diluted 1:50 into fresh media supplemented with anhydrotetracycline. Growth curves were diluted 1:100 as discussed above. Transcriptional repression was assessed after 6 hours of induction, growth curves and membrane permeability after 16 hours of induction, and polyamine metabolite production with 6 hours of induction, followed by repeat dilution 1:50 and additional 16 hours of induction.

RT-qPCR

Cells pellets were resuspended in Direct-zol (Zymo) before RNA isolation using the Direct-zol RNA Miniprep Kit (Zymo). RNA quality and concentration was checked using Nano-drop 2000 (Thermo Scientific) with a target

concentration of ~10 ng/µL. RT-qPCR was then performed using Luna Universal One-step RT-qPCR kit (New England Biolabs) following the provided protocol on a BioRad CFX Opus 96 quantitative Real-Time PCR machine. Primers were previously published[104-106] (**Table S5**) and efficiency of all the primers used was confirmed to be 95 ± 5% using a standard curve of template. Melt curves were performed to confirm the absence of primer dimers and the presence of a single amplicon. Samples were normalized to the geometric mean of a panel of endogenous control genes as previously described[107,108].

Intracellular Putrescine Accumulation and Extracellular Production

For CRISPRi experiments, the stationary phase cultures of the indicated cell lines were diluted into 1:50 fresh LB Lennox media ± anhydrotetracycline (0.5 µM for M 1/5 and 2 µM for E23) and cultured for 5-6 hours shaking at 37 ºC, before repeat dilution at 1:50 into fresh LB Lennox media ± anhydrotetracycline and overnight culture for 16 hours shaking at 37 ºC. The following morning, OD_{600} was measured and cells pelleted. Spent media was removed and frozen at –80 ºC for subsequent LC–MS analysis. Cell pellets were harvested as below.

For diminazene experiments, stationary phase cultures of the indicated cell lines were diluted 1:50 into fresh LB Lennox media and cultured for 5-6 hours shaking at 37 ºC, before repeat dilution at 1:50 into fresh LB Lennox media with the indicated concentrations of diminazene and overnight culture for 16 hours shaking at 37 ºC. The following morning, OD_{600} was measured and cells pelleted. Spent media was removed and frozen at –80 ºC for subsequent LC–MS analysis. Cell pellets were harvested as below.

Cell pellets were washed twice with PBS and then resuspended in LC–MS grade water (400 µL per 1 mL culture). Resuspended cells underwent two freeze thaw cycles alternating between liquid nitrogen and heating to 65 ºC. Cell debris was pelleted and 90% of aqueous supernatant removed. LC–MS grade methanol (200 µL per 1 mL culture) was added to the cell debris. Cell debris was re-pelleted and methanol supernatant combined with the previously removed aqueous supernatant. This 2:1 water:methanol mix was centrifuged one additional time and the resulting supernatant was ready for LC–MS analysis (described below).

Antibiotic synergy

Stationary phase cultures of indicated bacterial strains were diluted 1:5000 into M9 minimal media + 0.4% glucose + 0.2% CAS-amino acids containing indicated combinations of diminazene (Cayman Chemical) and vancomycin HCl (Research Products International), ciprofloxacin (Sigma Aldrich), tetracycline (Sigma), or erythromycin (Sigma). Drug concentrations were serially diluted 50% at each increment from the top indicated dose and checkerboard pattern was prepared by Tecan D300e Droplet Dispenser. Cells were cultured shaking overnight at 37 ºC and OD_{600} measured the following morning by plate reader (BioTek Synergy Neo2). Background was subtracted from each well and then each well was normalized to the OD_{600} of the well without drug to calculate relative growth. MIC_{90} for each drug was determined to be the column or row in which there was no growth seen. In cases where growth was seen in every column or row, MIC_{90} was estimated to be 2x the highest concentration of drug. Fractional inhibitory concentration (FIC) was calculated $FIC = FIC_A + FIC_B = (C_A/MIC_A) + (C_B/MIC_B)$, where MIC_A and MIC_B are the MIC_{90}s of drugs A and B alone, respectively, and C_A and C_B are the concentrations of the drugs in combination corresponding to an MIC. We report here the FIC_{min} from multiple repeat experiments. Synergistic interactions were defined as FIC <0.5, additive/indifferent interactions were defined as 0.5≤ FIC ≤4, and antagonistic interactions were defined as FIC >4[67,68].

Determination of vancomycin MIC with CRISPRi

Stationary phase cultures of indicated cell lines were diluted 1:1000 into LB media LB Lennox media ± anhydrotetracycline (0.25 µM for M 1/5 and 1.5 µM for E23) along with vancomycin serially diluted at each increment from the top dose (256 µg/mL) as prepared by Tecan D300e Droplet Dispenser. Cells were cultured shaking overnight at 37 ºC and OD_{600} measured the following morning. Background was subtracted from each well and then each well was normalized to the OD_{600} of the well without vancomycin.

Membrane Permeability

For CRISPRi experiments, the stationary phase cultures of the indicated cell lines were diluted 1:50 into fresh LB Lennox media ± anhydrotetracycline (0.5 µM for M 1/5 and 2 µM for E23) and cultured overnight for 16 hours shaking at 37 ºC. For diminazene experiments, stationary phase cultures of the indicated cell lines were diluted

1:50 into fresh LB Lennox media and cultured for either 3 or 6 hours shaking at 37 ºC. Assessment of inner and outer membrane permeability was adapted previously published protocols[70,71]. Briefly, cells were pelleted and washed 3x with 5 mM HEPES and 5 mM glucose buffer (pH = 7.2) before being resuspended in the same before and OD_{600} measured. Resuspended cells were split and incubated with either 1-*N*-phenylnaphthylamine (NPN, Sigma Aldrich) at a final concentration of 20 μM or propidium iodide (PI, Invitrogen, P3566) at a final concentration of 5 μM in darkness for 30 minutes at room temperature. Fluorescence was measured as follows: NPN λ_{ex} = 340 nm λ_{em} = 420 nm and PI λ_{ex} = 535 nm λ_{em} = 617 nm on a BioTek Synergy Neo2 Plate Reader. Relative fluorescence units (RFUs) were normalized to OD_{600}.

Antibiotic uptake

To assess antibiotic uptake, the stationary phase cultures of the indicated cell lines in were diluted 1:50 into fresh LB Lennox media and cultured with diminazene at the indicated concentrations for 6 hours shaking at 37 ºC. OD_{600} was measured and then cell lines were mixed with 50 μM of indicated antibiotic and cultured for 10 minutes shaking at 37 ºC. Cells were immediately pelleted and then cell pellets were washed twice with PBS before being resuspended in LC–MS grade water (400 μL per 1 mL culture). Resuspended cells underwent two freeze thaw cycles alternating between liquid nitrogen and heating to 65 ºC. Cell debris was pelleted and 90% of aqueous supernatant removed. LC–MS grade methanol (200 μL per 1 mL culture) was added to the cell debris. Cell debris was repelleted and methanol supernatant combined with the previously removed aqueous supernatant. This 2:1 water:methanol mix was centrifuged one additional time and the resulting supernatant used for LC–MS analysis (described below).

In vitro **biochemical experiments**

Enzyme Expression and Purification

SpeG was amplified from *E. coli* K12 MG1655 genomic DNA and *SAT1*, *PA4114, PA1472,* and *PA1377* were ordered as *E. coli* codon optimized sequences (ThermoFisher); all were cloned cloned into pET-28A-inducible expression vectors using Gibson assembly (including an in-frame either N-terminal or C-terminal polyhistidine sequence) (primers in **Table S6**). Identities of the constructs were confirmed with DNA sequencing and then

were transformed into *E. coli* BL21 (DE3) (New England Biolab) for expression. All *E. coli* expression constructs were grown overnight shaking at 37 ºC in Terrific Broth (VWR) supplemented with 5 mM $MgSO_4$ and kanamycin (50µg/ml) and were incubated at 37 °C overnight before dilution at 1:100 into fresh media the next morning. These diluted cultures were grown shaking at 37 °C to an OD_{600} of ~0.6, at which point protein expression was induced by the addition of 200 µM isopropyl β-D-1-thiogalactopyranoside (IPTG, Teknova), followed by culturing shaking overnight at 16 °C. The next morning, *E. coli* were pelleted by centrifugation and then lysed in 20 mM HEPES pH 8.0 buffer containing 30 mM imidazole and 300 mM NaCl and supplemented with 0.5% octyl-β-D-thrioglucopyranoside (Chem-Impex), 0.5 mg/mL lysozyme (Sigma-Aldrich) and SIGFAST protease inhibitor cocktail (Sigma-Aldrich). After lysis and clarification by centrifugation, lysates were incubated for 1hour at 4 °C with His-Pure Cobalt Purification beads (Thermo Fisher Scientific). After incubation, beads were washed with six column volumes of 20 mM HEPES pH 8.0 buffer containing 30 mM imidazole and 300 mM NaCl before elution with one column volume of 20 mM HEPES pH 8.0 containing 300 mM imidazole and 300 mM NaCl. Eluted protein was then buffer exchanged into 20 mM HEPES pH 8.0 with 300 mM NaCl and 10% glycerol for storage at –80 °C before further experiments. Enzyme concentrations were calculated according to Beer's Law with extinction coefficients calculated by Benchling software based on the amino acid sequences.

Enzyme assays

End point Assays. Assay mixtures contained 20 mM HEPES pH 7.5 with 50 mM NaCl with 1 µM enzyme, 50 mM putrescine, and 1 mM acetyl-CoA (CoALA Biosciences), supplemented with 1mM $MgCl_2$ and 1mM Tris-(2-carboxyethyl)phosphine (TCEP, Sigma-Aldrich). Reactions were conducted at room temperature for 1 hour. Experiments were carried out in triplicate and repeated on different days with distinct protein preparations. Quenching/extraction was performed as below.

Determination of enzyme kinetics. For the determination of enzyme kinetics, a continuous spectrophotometric assay was used. Assay conditions were similar to those used in the above end point assays with 20 mM HEPES pH 7.5 with 50 mM NaCl supplemented with 1 mM $MgCl_2$. Enzyme concentrations were varied based on the assay: 50 nM and 100 nM for SpeG with spermidine and putrescine respectively, 100 nM and 500 nM with

SAT1 with spermidine and putrescine respectively, and 500 nM for PA1472 with putrescine. Concentrations of putrescine and spermidine were varied as indicated with 1 mM acetyl-CoA held constant. 100 μM 4,4'-dithiodipyridine (Sigma Aldrich) was added to measure the rate of coenzyme A generation (absorption maxima at 324 nm wavelength). Assays were carried out for 20-30 minutes at room temperature with absorption measured every 30-40 seconds. Each assay was performed in technical duplicates on the day of the experiment and results from distinct enzyme preparations tested on distinct days were averaged to produce the kinetic parameters.

Determination of IC_{50} for diminazene. For the determination of IC_{50}s of diminazene for enzyme inhibition, the continuous enzyme assay from above was adapted with the modification that concentrations of substrate were held constant (near the empirically determined K_{half}s for SpeG, 50 mM putrescine and 600 μM spermidine, and K_m for SAT1, 55 μM spermidine) and the concentration of diminazene was varied as indicated. As above, each assay was performed in technical duplicates on the day of the experiment and results from distinct enzyme preparations tested on distinct days were averaged to produce the kinetic parameters.

Mass spectrometry

Putrescine metabolites. Plasma samples, (spent) media, and end-point enzyme assays were quenched/extracted with one part sample and nine parts extraction mix (74.9% acetonitrile: 24.9% methanol: 0.2% formic acid v/v/v with 2 μg/mL of valine-d_8 and phenylalanine-d_8 from Cambridge Isotopes as an internal standard for quantification). For intracellular putrescine accumulation, cells were extracted via multiple freeze thaw cycles with water and methanol (final 67% water: 33% methanol v/v). Extracted/quenched samples were vortexed and cooled to −20 °C and then centrifuged before LC–MS analysis. MS analyses were conducted using an LC–MS system composed of an Agilent 1290 Infinity II UHPLC (capable of column switching) coupled to an Agilent 6470A Triple Quadrupole LC/MS. The samples were injected into an Infinity Lab Poroshell 120 HILIC column (2.1×100mm×2.7μm) at 25 °C. The column was eluted isocratically at a flow rate of 600 μL min^{-1} with 5% mobile phase A (10mM ammonium formate with 0.1% formic acid in water) for 18 seconds, followed by a linear gradient for 132 seconds to 60% mobile phase B (acetonitrile with 0.1% formic acid). This

was followed by a 3-second gradient to 40% mobile phase B. This was then followed by a 27-second gradient returning to 5% mobile phase A at a flow rate of 1,200 µL/min. This flow rate and ratio was held for an additional 48seconds. Additional column equilibration was carried out on a secondary pump for 117 seconds at 5% mobile phase A and a flow rate of 1,000 µL/min. MS was conducted in positive ion mode using ESI. Data were collected via MRM (**Table S7**). Other MS settings were as follows: heater temp 300 °C, ESI nebulizer 45 psi, spray voltage 3.5 kV and acquisition time 75 ms per spectrum. Raw data from the LC–MS were analyzed using Agilent MassHunter Quantitative Analysis version 10.1 software. For absolute quantification, all samples were normalized to the valine and phenylalanine internal standards and concentrations calculated against a standard curve. Standard curves were generated using putrescine dihydrochloride and *N*-acetylputrescine hydrochloride purchased from Sigma Aldrich, and lysophastidylcholine 16:0 and 18:0 purchased from Avanti Polar Lipids. For all cell culture experiments, metabolite measurements were further normalized to OD_{600}.

Antibiotic uptake. MS analyses were conducted using an LC–MS system composed of an Agilent 1290 Infinity II UHPLC (capable of column switching) coupled to an Agilent 6470A Triple Quadrupole LC/MS. The samples were injected into an Infinity Lab Poroshell 120 C18 column (2.1×50mm×2.7µm) at 30 °C. The column was eluted isocratically at a flow rate of 200 µL/min with 90% mobile phase A (0.1% formic acid in water) for 1 minute, followed by a linear gradient for 4 minutes to 98% mobile phase B (acetonitrile with 0.1% formic acid). This was followed by 1 minute of isocratic elution at 98% mobile phase B, before a 6 second gradient returning to 90% mobile phase A at a new flow rate of 400 µL/min. The column was then eluted isocratically with 90% mobile phase A for 1.4 minutes at a flow rate of 400 µL/min. MS was conducted in positive ion mode using ESI. Data were collected via MRM (**Table S7**). Other MS settings were as follows: heater temp 300 °C, ESI nebulizer 45 psi, spray voltage 3.5 kV and acquisition time 200 ms per spectrum. For all cell culture experiments, measurements were normalized to OD_{600}.

Computational Experiments

Identification of PA1472 and PA1377

The *E. coli* SpeG and *B. subtilis* PaiA and BltD protein sequences were used in a Basic Local Alignment Search

Tool (BLAST) search of the Joint Genome Institute – Integrated Microbial Genomes database[109] of *P. aeruginosa* PAO1 isolates. SpeG as a query identified PA1472 and PA1377 with alignment scores of 7e-10 and 3e-9 respectively. PaiA as a query identified no hits. BltD identified PA4114 and PA1377 with alignment scores of 2e-16 and 4e-8 respectively.

Phylogenetic tree

All sequences from Uniprot (uniprot.org) tagged with EC 2.3.1.57 and spermidine or spermidine were downloaded in FASTA format. Analysis was limited to sequences with between 140 and 200 amino acids. A multiple sequence alignment was generated using MUSCLE[49] v3.8.425 on Geneious Prime 2022.2.1 (Dotmatics) of the 1483 representatives of enzyme groups sharing >80% amino acid sequence identity in the UniProt database (release 2023_2) using EC: 2.3.1.57 AND “spermidine or spermidine” as a query. PA1472 and PA1377 were also included in this analysis. A maximum-likelihood phylogenetic tree was constructed using iQ-TREE2 v2.1.0 with model finder[51,110], which determined VT+R10 as the best model, and visualized using iTOL[50]. Branch supports were calculated from 1001 independent tree iterations.

Protein structures

AlphaFold2[111] was used to generate a predicted homodimeric structures for PA1472 using sequence Q9I3P0_PSEAE downloaded from the UniProt database. Published sequences of *E. coli* SpeG (3WR7) and *H. sapiens* SAT1 (2B5G) were downloaded from the Protein Data Bank (PBD) and used for comparison[44,53]. Alignments were conducted using the dimer structures of each protein and “align” tool in Pymol 2.5.3.

Statistical Analyses

Separate from our human analyses, appropriate statistical tests were performed where indicated. All analyses were carried out using GraphPad Prism 9 (GraphPad Software).

REFERENCES

1 Murray, C. J. *et al.* Global burden of bacterial antimicrobial resistance in 2019: a systematic analysis. *Lancet*, 629-655 (2022).

2 O'Neill, J. Tackling Drug-Resistant Infections Globally: Final Report and Recommendations. *The Review on Antimicrobial Resistance* (2016).

3 Rawson, T. M. *et al.* Bacterial and Fungal Coinfection in Individuals With Coronavirus: A Rapid Review To Support COVID-19 Antimicrobial Prescribing. *Clin Infect Dis* **71**, 2459-2468 (2020). https://doi.org:10.1093/cid/ciaa530

4 Ventola, C. L. The antibiotic resistance crisis: part 1: causes and threats. *P T* **40**, 277-283 (2015).

5 Chen, N. *et al.* Epidemiological and clinical characteristics of 99 cases of 2019 novel coronavirus pneumonia in Wuhan, China: a descriptive study. *Lancet* **395**, 507-513 (2020). https://doi.org:10.1016/S0140-6736(20)30211-7

6 Zhou, F. *et al.* Clinical course and risk factors for mortality of adult inpatients with COVID-19 in Wuhan, China: a retrospective cohort study. *Lancet* **395**, 1054-1062 (2020). https://doi.org:10.1016/S0140-6736(20)30566-3

7 CDC. COVID-19: U.S. Impact on Antimicrobial Resistance, Special Report 2022. *U.S. Department of Health and Human Services, CDC* (2022).

8 Rangel-Frausto, M. S. *et al.* The natural history of the systemic inflammatory response syndrome (SIRS). A prospective study. *JAMA* **273**, 117-123 (1995).

9 Kalantar, K. L. *et al.* Integrated host-microbe plasma metagenomics for sepsis diagnosis in a prospective cohort of critically ill adults. *Nat Microbiol* **7**, 1805-1816 (2022). https://doi.org:10.1038/s41564-022-01237-2

10 Cheng, M. P. *et al.* qSOFA does not predict bacteremia in patients with severe manifestations of sepsis. *J Assoc Med Microbiol Infect Dis Can* **7**, 364-368 (2022). https://doi.org:10.3138/jammi-2022-0006

11 Rhodes, A. *et al.* Surviving Sepsis Campaign: International Guidelines for Management of Sepsis and Septic Shock: 2016. *Intensive Care Med* **43**, 304-377 (2017). https://doi.org:10.1007/s00134-017-4683-6

12 Singer, M. *et al.* The Third International Consensus Definitions for Sepsis and Septic Shock (Sepsis-3). *JAMA* **315**, 801-810 (2016). https://doi.org:10.1001/jama.2016.0287

13 Organization, W. H. Global antimicrobial resistance and use surveillance system (GLASS) report. (2021).

14 Miethke, M. *et al.* Towards the sustainable discovery and development of new antibiotics. *Nat Rev Chem* **5**, 726-749 (2021). https://doi.org:10.1038/s41570-021-00313-1

15 Stokes, J. M., Lopatkin, A. J., Lobritz, M. A. & Collins, J. J. Bacterial Metabolism and Antibiotic Efficacy. *Cell Metab* **30**, 251-259 (2019). https://doi.org:10.1016/j.cmet.2019.06.009

16 Butler, M. S., Henderson, I. R., Capon, R. J. & Blaskovich, M. A. T. Antibiotics in the clinical pipeline as of December 2022. *J Antibiot (Tokyo)* **76**, 431-473 (2023). https://doi.org:10.1038/s41429-023-00629-8

17 Stine, Z. E., Schug, Z. T., Salvino, J. M. & Dang, C. V. Targeting cancer metabolism in the era of precision oncology. *Nat Rev Drug Discov* **21**, 141-162 (2022). https://doi.org:10.1038/s41573-021-00339-6

18 DeBerardinis, R. J. & Keshari, K. R. Metabolic analysis as a driver for discovery, diagnosis, and therapy. *Cell* **185**, 2678-2689 (2022). https://doi.org:10.1016/j.cell.2022.06.029

19 Puskarich, M. A. *et al.* Serum Levels of Branched Chain Amino Acids Predict Duration of Cardiovascular Organ Failure in Septic Shock. *Shock* (2020). https://doi.org:10.1097/SHK.0000000000001687

20 Wang, J., Sun, Y., Teng, S. & Li, K. Prediction of sepsis mortality using metabolite biomarkers in the blood: a meta-analysis of death-related pathways and prospective validation. *BMC Med* **18**, 83 (2020). https://doi.org:10.1186/s12916-020-01546-5

21 Langley, R. J. *et al.* An integrated clinico-metabolomic model improves prediction of death in sepsis. *Sci Transl Med* **5**, 195ra195 (2013). https://doi.org:10.1126/scitranslmed.3005893

22 Liu, Z. *et al.* Nuclear magnetic resonance-based serum metabolomic analysis reveals different disease evolution profiles between septic shock survivors and non-survivors. *Crit Care* **23**, 169 (2019). https://doi.org:10.1186/s13054-019-2456-z

23 Rogers, A. J. *et al.* Metabolomic derangements are associated with mortality in critically ill adult patients. *PLoS One* **9**, e87538 (2014). https://doi.org:10.1371/journal.pone.0087538

24 Knaus, W. A., Draper, E. A., Wagner, D. P. & Zimmerman, J. E. APACHE II: a severity of disease classification system. *Crit Care Med* **13**, 818-829 (1985).

25 Headley, J., Theriault, R. & Smith, T. L. Independent validation of APACHE II severity of illness score for predicting mortality in patients with breast cancer admitted to the intensive care unit. *Cancer* **70**, 497-503 (1992). https://doi.org:10.1002/1097-0142(19920715)70:2<497::aid-cncr2820700220>3.0.co;2-h

26 Dubin, D. T. & Rosenthal, S. M. The acetylation of polyamines in Escherichia coli. *J Biol Chem* **235**, 776-782 (1960).

27 Seiler, N. & Al-Therib, M. J. Putrescine catabolism in mammalian brain. *Biochem J* **144**, 29-35 (1974). https://doi.org:10.1042/bj1440029

28 Cho, W. H. *et al.* Clinical significance of enzymatic lysophosphatidylcholine (LPC) assay data in patients with sepsis. *Eur J Clin Microbiol Infect Dis* **31**, 1805-1810 (2012). https://doi.org:10.1007/s10096-011-1505-6

29 Drobnik, W. *et al.* Plasma ceramide and lysophosphatidylcholine inversely correlate with mortality in sepsis patients. *J Lipid Res* **44**, 754-761 (2003). https://doi.org:10.1194/jlr.M200401-JLR200

30 Starr, M. E. *et al.* A new cecal slurry preparation protocol with improved long-term reproducibility for animal models of sepsis. *PLoS One* **9**, e115705 (2014). https://doi.org:10.1371/journal.pone.0115705

31 Otero-Anton, E. *et al.* Cecal ligation and puncture as a model of sepsis in the rat: influence of the puncture size on mortality, bacteremia, endotoxemia and tumor necrosis factor alpha levels. *Eur Surg Res* **33**, 77-79 (2001). https://doi.org:10.1159/000049698

32 Ng, J. *et al.* Augmenting emergency granulopoiesis with CpG conditioned mesenchymal stromal cells in murine neutropenic sepsis. *Blood Adv* **4**, 4965-4979 (2020). https://doi.org:10.1182/bloodadvances.2020002556

33 Bielen, K. *et al.* Animal models of hospital-acquired pneumonia: current practices and future perspectives. *Ann Transl Med* **5**, 132 (2017). https://doi.org:10.21037/atm.2017.03.72

34 Seiler, N. & al-Therib, M. J. Acetyl-CoA: 1,4-diaminobutane N-acetyltransferase. Occurrence in vertebrate organs and subcellular localization. *Biochim Biophys Acta* **354**, 206-212 (1974). https://doi.org:10.1016/0304-4165(74)90007-5

35 Filippova, E. V. *et al.* A novel polyamine allosteric site of SpeG from Vibrio cholerae is revealed by its dodecameric structure. *J Mol Biol* **427**, 1316-1334 (2015). https://doi.org:10.1016/j.jmb.2015.01.009

36 Fukuchi, J., Kashiwagi, K., Takio, K. & Igarashi, K. Properties and structure of spermidine acetyltransferase in Escherichia coli. *J Biol Chem* **269**, 22581-22585 (1994).

37 Fukuchi, J., Kashiwagi, K., Yamagishi, M., Ishihama, A. & Igarashi, K. Decrease in cell viability due to the accumulation of spermidine in spermidine acetyltransferase-deficient mutant of Escherichia coli. *J Biol Chem* **270**, 18831-18835 (1995). https://doi.org:10.1074/jbc.270.32.18831

38 Igarashi, K. & Kashiwagi, K. Polyamines: mysterious modulators of cellular functions. *Biochem Biophys Res Commun* **271**, 559-564 (2000). https://doi.org:10.1006/bbrc.2000.2601

39 Cohen, S. S. *A guide to the polyamines*. (Oxford University Press, 1998).

40 Miyamoto, S., Kashiwagi, K., Ito, K., Watanabe, S. & Igarashi, K. Estimation of polyamine distribution and polyamine stimulation of protein synthesis in Escherichia coli. *Arch Biochem Biophys* **300**, 63-68 (1993). https://doi.org:10.1006/abbi.1993.1009

41 de Mattos, C. D. *et al.* Polyamines and linear DNA mediate bacterial threat assessment of bacteriophage infection. *Proc Natl Acad Sci U S A* **120**, e2216430120 (2023). https://doi.org:10.1073/pnas.2216430120

42 Baba, T. *et al.* Construction of Escherichia coli K-12 in-frame, single-gene knockout mutants: the Keio collection. *Mol Syst Biol* **2**, 2006 0008 (2006). https://doi.org:10.1038/msb4100050

43 Tabor, C. W. & Tabor, H. Polyamines in microorganisms. *Microbiol Rev* **49**, 81-99 (1985). https://doi.org:10.1128/mr.49.1.81-99.1985

44 Sugiyama, S. *et al.* Molecular mechanism underlying promiscuous polyamine recognition by spermidine acetyltransferase. *Int J Biochem Cell Biol* **76**, 87-97 (2016). https://doi.org:10.1016/j.biocel.2016.05.003

45 Zallot, R., Oberg, N. & Gerlt, J. A. The EFI Web Resource for Genomic Enzymology Tools: Leveraging Protein, Genome, and Metagenome Databases to Discover Novel Enzymes and Metabolic Pathways. *Biochemistry* **58**, 4169-4182 (2019). https://doi.org:10.1021/acs.biochem.9b00735

46 Gerlt, J. A. *et al.* Enzyme Function Initiative-Enzyme Similarity Tool (EFI-EST): A web tool for generating protein sequence similarity networks. *Biochim Biophys Acta* **1854**, 1019-1037 (2015). https://doi.org:10.1016/j.bbapap.2015.04.015

47 Forouhar, F. *et al.* Structural and functional evidence for Bacillus subtilis PaiA as a novel N1-spermidine/spermine acetyltransferase. *J Biol Chem* **280**, 40328-40336 (2005). https://doi.org:10.1074/jbc.M505332200

48 Woolridge, D. P., Martinez, J. D., Stringer, D. E. & Gerner, E. W. Characterization of a novel spermidine/spermine acetyltransferase, BltD, from Bacillus subtilis. *Biochem J* **340 (Pt 3)**, 753-758 (1999).

49 Edgar, R. C. MUSCLE: multiple sequence alignment with high accuracy and high throughput. *Nucleic Acids Res* **32**, 1792-1797 (2004). https://doi.org:10.1093/nar/gkh340

50 Letunic, I. & Bork, P. Interactive Tree Of Life (iTOL) v5: an online tool for phylogenetic tree display and annotation. *Nucleic Acids Res* **49**, W293-W296 (2021). https://doi.org:10.1093/nar/gkab301

51 Minh, B. Q. *et al.* IQ-TREE 2: New Models and Efficient Methods for Phylogenetic Inference in the Genomic Era. *Mol Biol Evol* **37**, 1530-1534 (2020). https://doi.org:10.1093/molbev/msaa015

52 Hegde, S. S., Chandler, J., Vetting, M. W., Yu, M. & Blanchard, J. S. Mechanistic and structural analysis of human spermidine/spermine N1-acetyltransferase. *Biochemistry* **46**, 7187-7195 (2007). https://doi.org:10.1021/bi700256z

53 Bewley, M. C. *et al.* Structures of wild-type and mutant human spermidine/spermine N1-acetyltransferase, a potential therapeutic drug target. *Proc Natl Acad Sci U S A* **103**, 2063-2068 (2006). https://doi.org:10.1073/pnas.0511008103

54 Miller-Fleming, L., Olin-Sandoval, V., Campbell, K. & Ralser, M. Remaining Mysteries of Molecular Biology: The Role of Polyamines in the Cell. *J Mol Biol* **427**, 3389-3406 (2015). https://doi.org:10.1016/j.jmb.2015.06.020

55 Pegg, A. E. Spermidine/spermine-N(1)-acetyltransferase: a key metabolic regulator. *Am J Physiol Endocrinol Metab* **294**, E995-1010 (2008). https://doi.org:10.1152/ajpendo.90217.2008

56 Fang, S. B. *et al.* speG Is Required for Intracellular Replication of Salmonella in Various Human Cells and Affects Its Polyamine Metabolism and Global Transcriptomes. *Front Microbiol* **8**, 2245 (2017). https://doi.org:10.3389/fmicb.2017.02245

57 Thurlow, L. R. *et al.* Functional modularity of the arginine catabolic mobile element contributes to the success of USA300 methicillin-resistant Staphylococcus aureus. *Cell Host Microbe* **13**, 100-107 (2013). https://doi.org:10.1016/j.chom.2012.11.012

58 Planet, P. J. *et al.* Emergence of the epidemic methicillin-resistant Staphylococcus aureus strain USA300 coincides with horizontal transfer of the arginine catabolic mobile element and speG-mediated adaptations for survival on skin. *mBio* **4**, e00889-00813 (2013). https://doi.org:10.1128/mBio.00889-13

59 Barbagallo, M. *et al.* A new piece of the Shigella Pathogenicity puzzle: spermidine accumulation by silencing of the speG gene [corrected]. *PLoS One* **6**, e27226 (2011). https://doi.org:10.1371/journal.pone.0027226

60 Hawkins, J. S., Wong, S., Peters, J. M., Almeida, R. & Qi, L. S. Targeted Transcriptional Repression in Bacteria Using CRISPR Interference (CRISPRi). *Methods Mol Biol* **1311**, 349-362 (2015). https://doi.org:10.1007/978-1-4939-2687-9_23

61 Casero, R. A., Jr., Murray Stewart, T. & Pegg, A. E. Polyamine metabolism and cancer: treatments, challenges and opportunities. *Nat Rev Cancer* **18**, 681-695 (2018). https://doi.org:10.1038/s41568-018-0050-3

62 Casero, R. A., Jr. & Woster, P. M. Terminally alkylated polyamine analogues as chemotherapeutic agents. *J Med Chem* **44**, 1-26 (2001). https://doi.org:10.1021/jm000084m

63 Libby, P. R. & Porter, C. W. Inhibition of enzymes of polyamine back-conversion by pentamidine and berenil. *Biochem Pharmacol* **44**, 830-832 (1992). https://doi.org:10.1016/0006-2952(92)90424-h

64 Joshi, G. S., Spontak, J. S., Klapper, D. G. & Richardson, A. R. Arginine catabolic mobile element encoded speG abrogates the unique hypersensitivity of Staphylococcus aureus to exogenous polyamines. *Mol Microbiol* **82**, 9-20 (2011). https://doi.org:10.1111/j.1365-2958.2011.07809.x

65 Wu, S. Y., Park, G. Y., Kim, S. H., Hulme, J. & An, S. S. Diminazene aceturate: an antibacterial agent for Shiga-toxin-producing Escherichia coli O157:H7. *Drug Des Devel Ther* **10**, 3363-3378 (2016). https://doi.org:10.2147/DDDT.S114832

66 Rios, T. B. *et al.* Repurposing streptomycin and chloramphenicol against bacterial pathogens by combination with diminazene aceturate. *Lett Appl Microbiol* **76** (2023). https://doi.org:10.1093/lambio/ovac009

67 Meletiadis, J., Pournaras, S., Roilides, E. & Walsh, T. J. Defining fractional inhibitory concentration index cutoffs for additive interactions based on self-drug additive combinations, Monte Carlo simulation analysis, and in vitro-in vivo correlation data for antifungal drug combinations against Aspergillus fumigatus. *Antimicrob Agents Chemother* **54**, 602-609 (2010). https://doi.org:10.1128/AAC.00999-09

68 Bonapace, C. R., Bosso, J. A., Friedrich, L. V. & White, R. L. Comparison of methods of interpretation of checkerboard synergy testing. *Diagn Microbiol Infect Dis* **44**, 363-366 (2002). https://doi.org:10.1016/s0732-8893(02)00473-x

69 Stokes, J. M. *et al.* Pentamidine sensitizes Gram-negative pathogens to antibiotics and overcomes acquired colistin resistance. *Nat Microbiol* **2**, 17028 (2017). https://doi.org:10.1038/nmicrobiol.2017.28

70 Halder, S. *et al.* Alteration of Zeta potential and membrane permeability in bacteria: a study with cationic agents. *Springerplus* **4**, 672 (2015). https://doi.org:10.1186/s40064-015-1476-7

71 Ma, B. *et al.* Contemporaneous Measurement of Outer and Inner Membrane Permeability in Gram-negative Bacteria. *Bio Protoc* **10**, e3548 (2020). https://doi.org:10.21769/BioProtoc.3548

72 MacNair, C. R. *et al.* Preclinical Development of Pentamidine Analogs Identifies a Potent and Nontoxic Antibiotic Adjuvant. *ACS Infect Dis* **8**, 768-777 (2022). https://doi.org:10.1021/acsinfecdis.1c00482

73 Reygaert, W. C. An overview of the antimicrobial resistance mechanisms of bacteria. *AIMS Microbiol* **4**, 482-501 (2018). https://doi.org:10.3934/microbiol.2018.3.482

74 Chopra, I. & Roberts, M. Tetracycline antibiotics: mode of action, applications, molecular biology, and epidemiology of bacterial resistance. *Microbiol Mol Biol Rev* **65**, 232-260 ; second page, table of contents (2001). https://doi.org:10.1128/MMBR.65.2.232-260.2001

75 Shariati, A. *et al.* The resistance mechanisms of bacteria against ciprofloxacin and new approaches for enhancing the efficacy of this antibiotic. *Front Public Health* **10**, 1025633 (2022). https://doi.org:10.3389/fpubh.2022.1025633

76 Peregrine, A. S. & Mamman, M. Pharmacology of diminazene: a review. *Acta Trop* **54**, 185-203 (1993). https://doi.org:10.1016/0001-706x(93)90092-p

77 Yayeh, M. *et al.* Comparative experimental studies on Trypanosoma isolates in mice and response to diminazene aceturate and isometamidium chloride treatment. *Heliyon* **4**, e00528 (2018). https://doi.org:10.1016/j.heliyon.2018.e00528

78 de Brito, M. G. *et al.* Therapeutic Effect of Diminazene Aceturate on Parasitic Blood Fluke Schistosoma mansoni Infection. *Antimicrob Agents Chemother* **64** (2020). https://doi.org:10.1128/AAC.01372-20

79 Morris, T. H. Antibiotic therapeutics in laboratory animals. *Lab Anim* **29**, 16-36 (1995). https://doi.org:10.1258/002367795780740393

80 Hoerauf, A. *et al.* Tetracycline therapy targets intracellular bacteria in the filarial nematode Litomosoides sigmodontis and results in filarial infertility. *J Clin Invest* **103**, 11-18 (1999). https://doi.org:10.1172/JCI4768

81 Walesch, S. *et al.* Fighting antibiotic resistance-strategies and (pre)clinical developments to find new antibacterials. *EMBO Rep* **24**, e56033 (2023). https://doi.org:10.15252/embr.202256033

82 Jendoubi, T. Approaches to Integrating Metabolomics and Multi-Omics Data: A Primer. *Metabolites* **11** (2021). https://doi.org:10.3390/metabo11030184

83 Ribeiro da Cunha, B., Fonseca, L. P. & Calado, C. R. C. Antibiotic Discovery: Where Have We Come from, Where Do We Go? *Antibiotics (Basel)* **8** (2019). https://doi.org:10.3390/antibiotics8020045

84 Ordonez, A. A. *et al.* Molecular imaging of bacterial infections: Overcoming the barriers to clinical translation. *Sci Transl Med* **11** (2019). https://doi.org:10.1126/scitranslmed.aax8251

85 Luyt, C. E., Brechot, N., Trouillet, J. L. & Chastre, J. Antibiotic stewardship in the intensive care unit. *Crit Care* **18**, 480 (2014). https://doi.org:10.1186/s13054-014-0480-6

86 Shah, P. & Swiatlo, E. A multifaceted role for polyamines in bacterial pathogens. *Mol Microbiol* **68**, 4-16 (2008). https://doi.org:10.1111/j.1365-2958.2008.06126.x

87 Igarashi, K. & Kashiwagi, K. Effects of polyamines on protein synthesis and growth of Escherichia coli. *J Biol Chem* **293**, 18702-18709 (2018). https://doi.org:10.1074/jbc.TM118.003465

88 Minton, K. W., Tabor, H. & Tabor, C. W. Paraquat toxicity is increased in Escherichia coli defective in the synthesis of polyamines. *Proc Natl Acad Sci U S A* **87**, 2851-2855 (1990). https://doi.org:10.1073/pnas.87.7.2851

89 Michael, A. J. Polyamine function in archaea and bacteria. *J Biol Chem* **293**, 18693-18701 (2018). https://doi.org:10.1074/jbc.TM118.005670

90 Schuster, I. & Bernhardt, R. Interactions of natural polyamines with mammalian proteins. *Biomol Concepts* **2**, 79-94 (2011). https://doi.org:10.1515/bmc.2011.007

91 Schuber, F. Influence of polyamines on membrane functions. *Biochem J* **260**, 1-10 (1989). https://doi.org:10.1042/bj2600001

92 Carper, S. W., Willis, D. G., Manning, K. A. & Gerner, E. W. Spermidine acetylation in response to a variety of stresses in Escherichia coli. *J Biol Chem* **266**, 12439-12441 (1991).

93 Annunziato, G. Strategies to Overcome Antimicrobial Resistance (AMR) Making Use of Non-Essential Target Inhibitors: A Review. *Int J Mol Sci* **20** (2019). https://doi.org:10.3390/ijms20235844

94 Armalyte, J. *et al.* A polyamine acetyltransferase regulates the motility and biofilm formation of Acinetobacter baumannii. *Nat Commun* **14**, 3531 (2023). https://doi.org:10.1038/s41467-023-39316-5

95 Homeida, A. M., El Amin, E. A., Adam, S. E. & Mahmoud, M. M. Toxicity of diminazene aceturate (Berenil) to camels. *J Comp Pathol* **91**, 355-360 (1981). https://doi.org:10.1016/0021-9975(81)90005-0

96 Tsimbalyuk, S. *et al.* Structural and Kinetic Characterization of the SpeG Spermidine/Spermine N-acetyltransferase from Methicillin-Resistant Staphylococcus aureus USA300. *Cells* **12** (2023). https://doi.org:10.3390/cells12141829

97 Dolinay, T. *et al.* Inflammasome-regulated cytokines are critical mediators of acute lung injury. *Am J Respir Crit Care Med* **185**, 1225-1234 (2012). https://doi.org:10.1164/rccm.201201-0003OC

98 Lewis, A. J., Seymour, C. W. & Rosengart, M. R. Current Murine Models of Sepsis. *Surg Infect (Larchmt)* **17**, 385-393 (2016). https://doi.org:10.1089/sur.2016.021

99 Varon, J. *et al.* Surfactant Protein D Influences Mortality During Abdominal Sepsis by Facilitating Escherichia coli Colonization in the Gut. *Crit Care Explor* **4**, e0699 (2022). https://doi.org:10.1097/CCE.0000000000000699

100 Harkness, J. E. & Wagner, J. E. *The biology and medicine of rabbits and rodents*. 3rd edn, (Lea & Febiger, 1989).

101 Mitruka, B. M., Rawnsley, H. M. & Mitruka, B. M. *Clinical biochemical and hematological reference values in normal experimental animals and normal humans*. 2nd edn, (Masson, 1981).

102 Annegers, J. Total body water in rats and in mice. *Proc Soc Exp Biol Med* **87**, 454-456 (1954). https://doi.org:10.3181/00379727-87-21410

103 Qi, L. S. *et al.* Repurposing CRISPR as an RNA-guided platform for sequence-specific control of gene expression. *Cell* **152**, 1173-1183 (2013). https://doi.org:10.1016/j.cell.2013.02.022

104 Campilongo, R. *et al.* Molecular and functional profiling of the polyamine content in enteroinvasive E. coli : looking into the gap between commensal E. coli and harmful Shigella. *PLoS One* **9**, e106589 (2014). https://doi.org:10.1371/journal.pone.0106589

105 Clifford, R. J. *et al.* Detection of bacterial 16S rRNA and identification of four clinically important bacteria by real-time PCR. *PLoS One* **7**, e48558 (2012). https://doi.org:10.1371/journal.pone.0048558

106 Zhou, K. *et al.* Novel reference genes for quantifying transcriptional responses of Escherichia coli to protein overexpression by quantitative PCR. *BMC Mol Biol* **12**, 18 (2011). https://doi.org:10.1186/1471-2199-12-18

107 Vandesompele, J. *et al.* Accurate normalization of real-time quantitative RT-PCR data by geometric averaging of multiple internal control genes. *Genome Biol* **3**, RESEARCH0034 (2002). https://doi.org:10.1186/gb-2002-3-7-research0034

108 Livak, K. J. & Schmittgen, T. D. Analysis of relative gene expression data using real-time quantitative PCR and the 2(-Delta Delta C(T)) Method. *Methods* **25**, 402-408 (2001). https://doi.org:10.1006/meth.2001.1262

109 Chen, I. A. *et al.* The IMG/M data management and analysis system v.7: content updates and new features. *Nucleic Acids Res* **51**, D723-D732 (2023). https://doi.org:10.1093/nar/gkac976

110 Kalyaanamoorthy, S., Minh, B. Q., Wong, T. K. F., von Haeseler, A. & Jermiin, L. S. ModelFinder: fast model selection for accurate phylogenetic estimates. *Nat Methods* **14**, 587-589 (2017). https://doi.org:10.1038/nmeth.4285

111 Jumper, J. *et al.* Highly accurate protein structure prediction with AlphaFold. *Nature* **596**, 583-589 (2021). https://doi.org:10.1038/s41586-021-03819-2

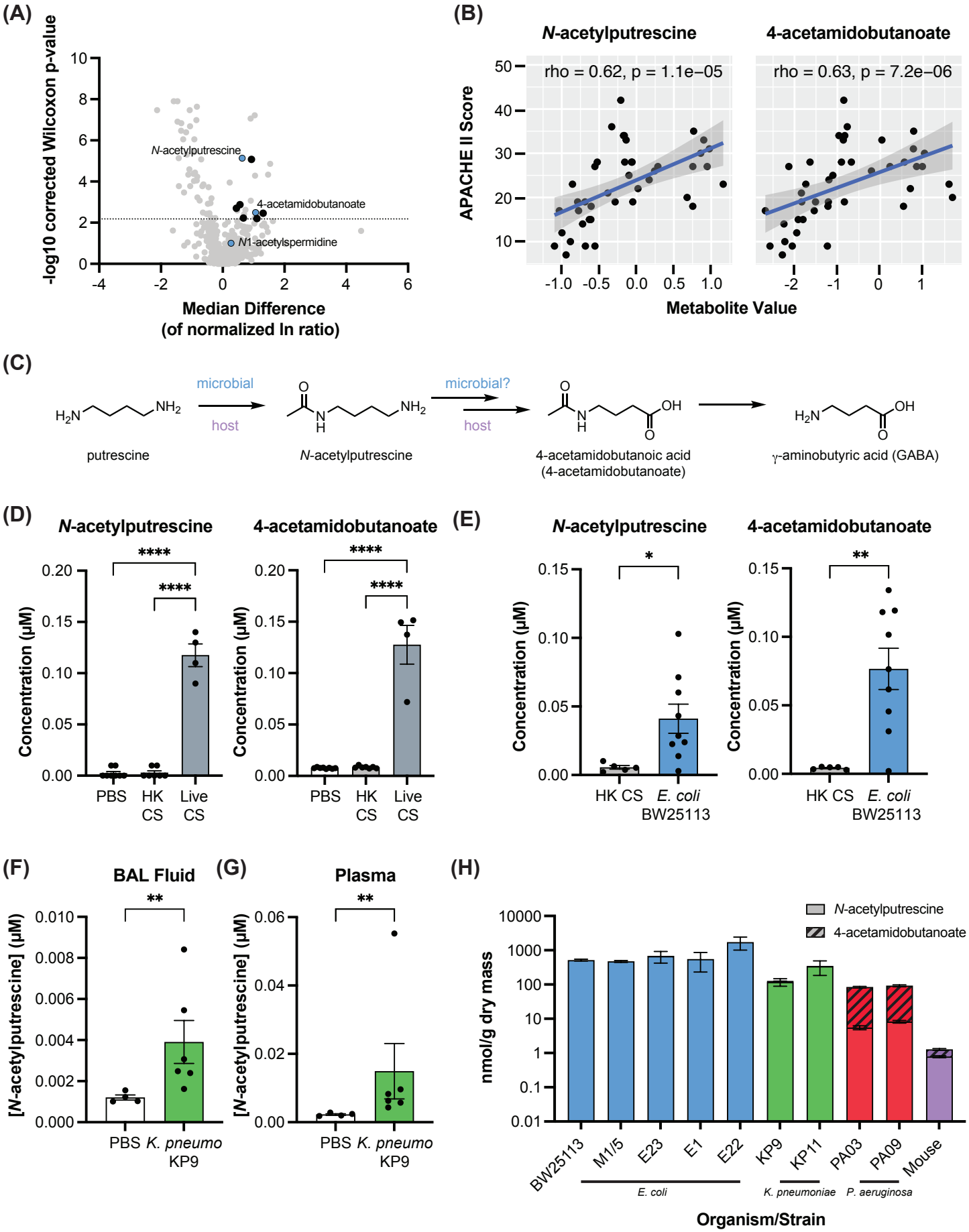

Figure 1

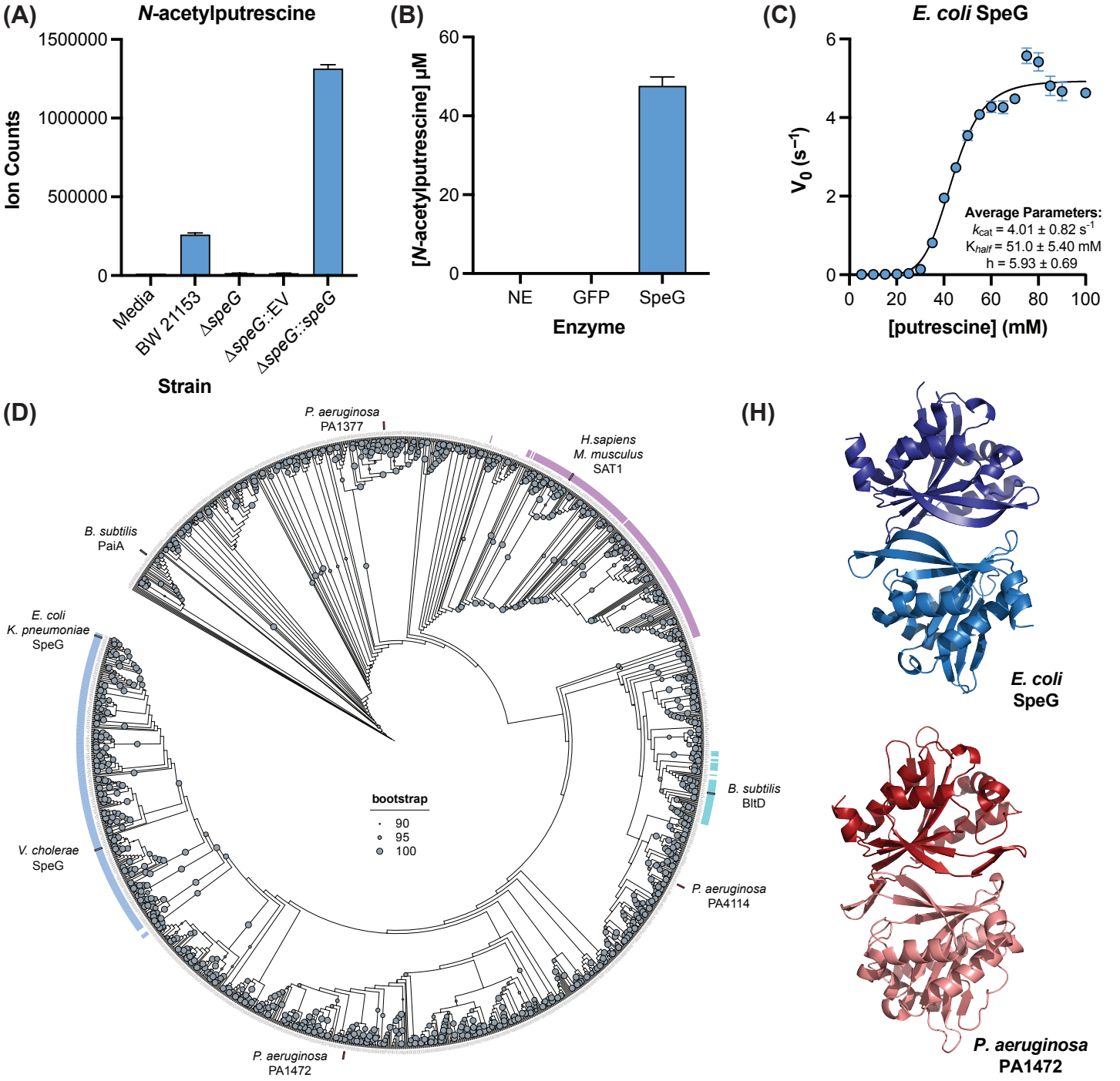

Figure 2

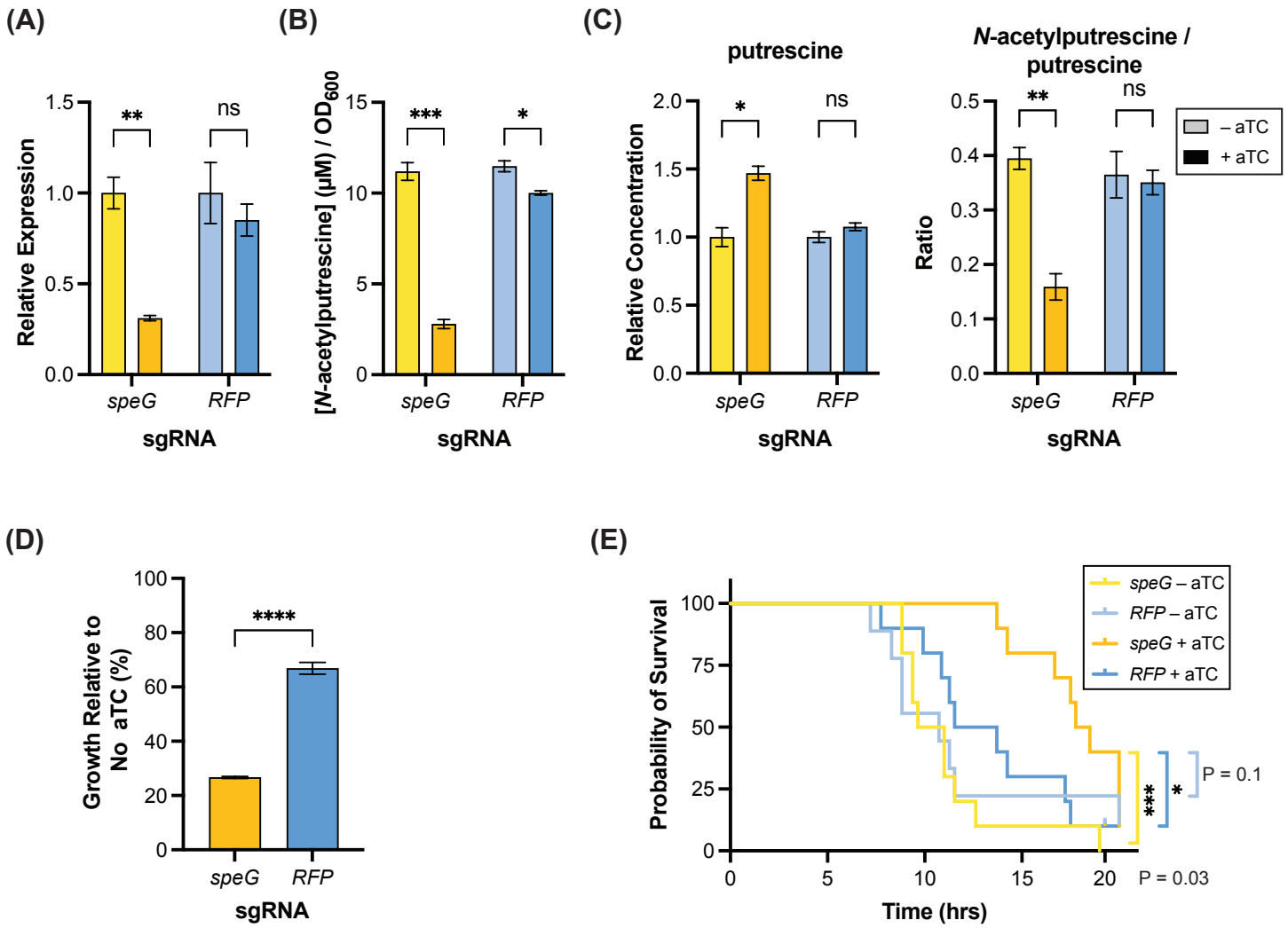

Figure 3

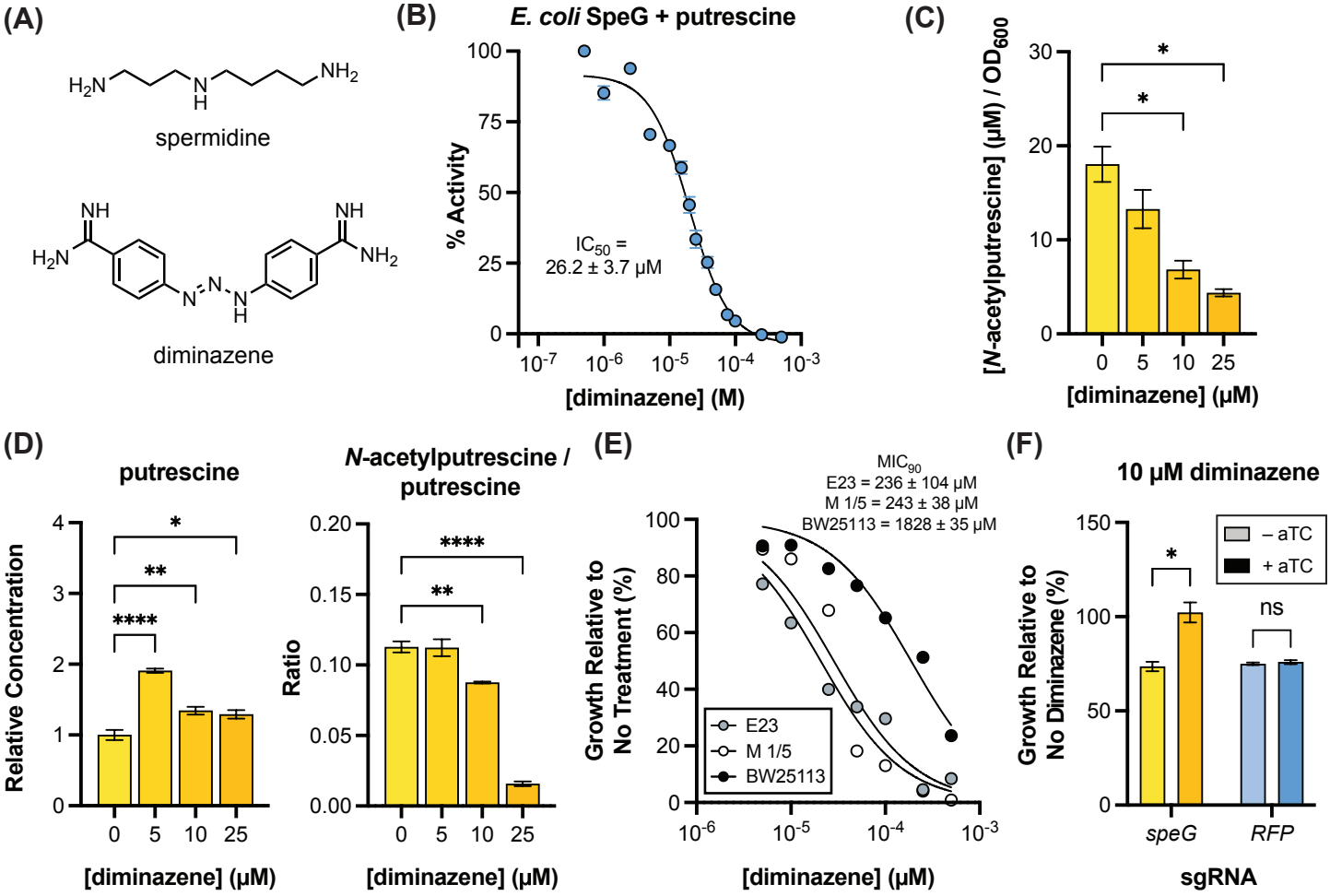

Figure 4

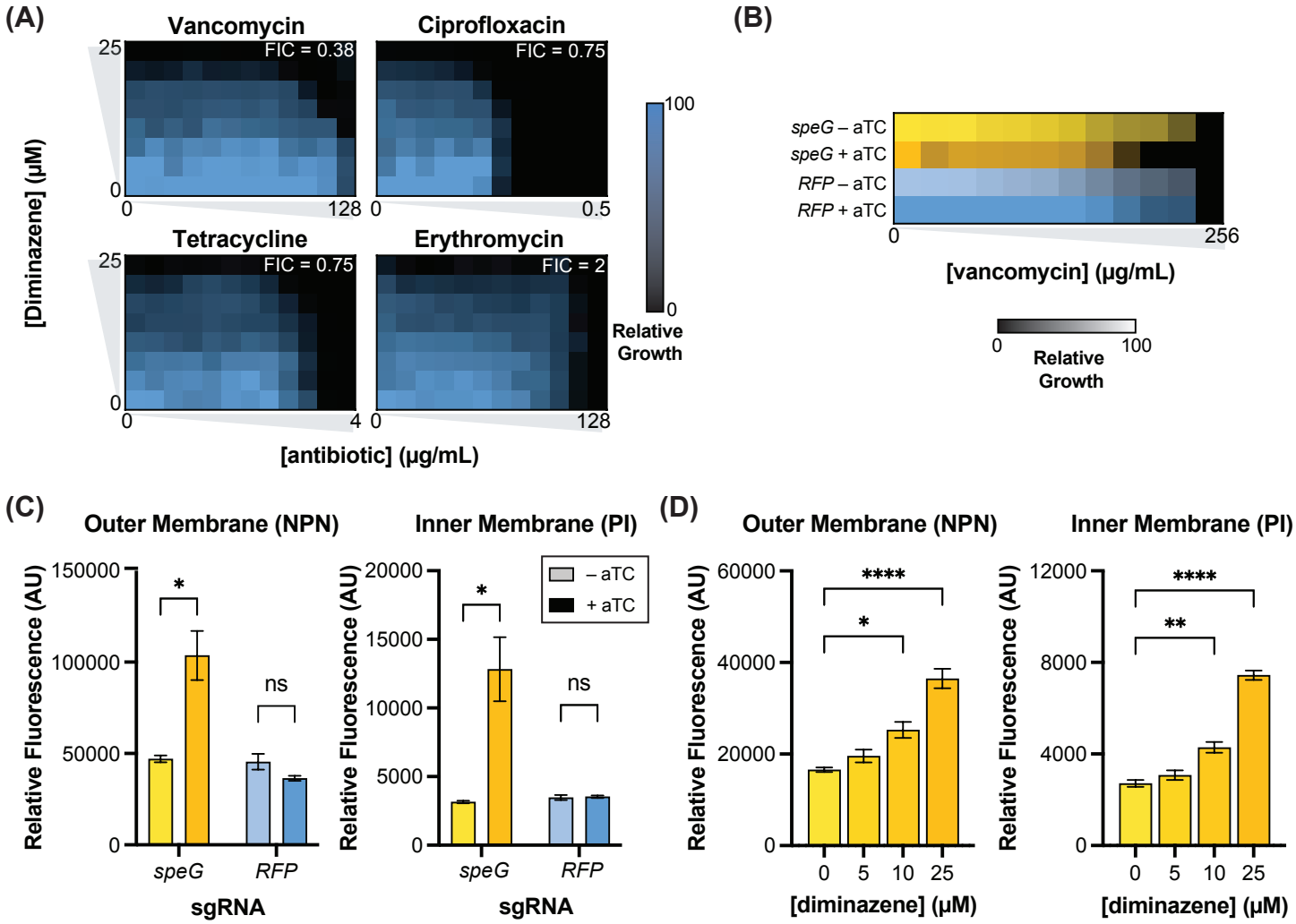

Figure 5

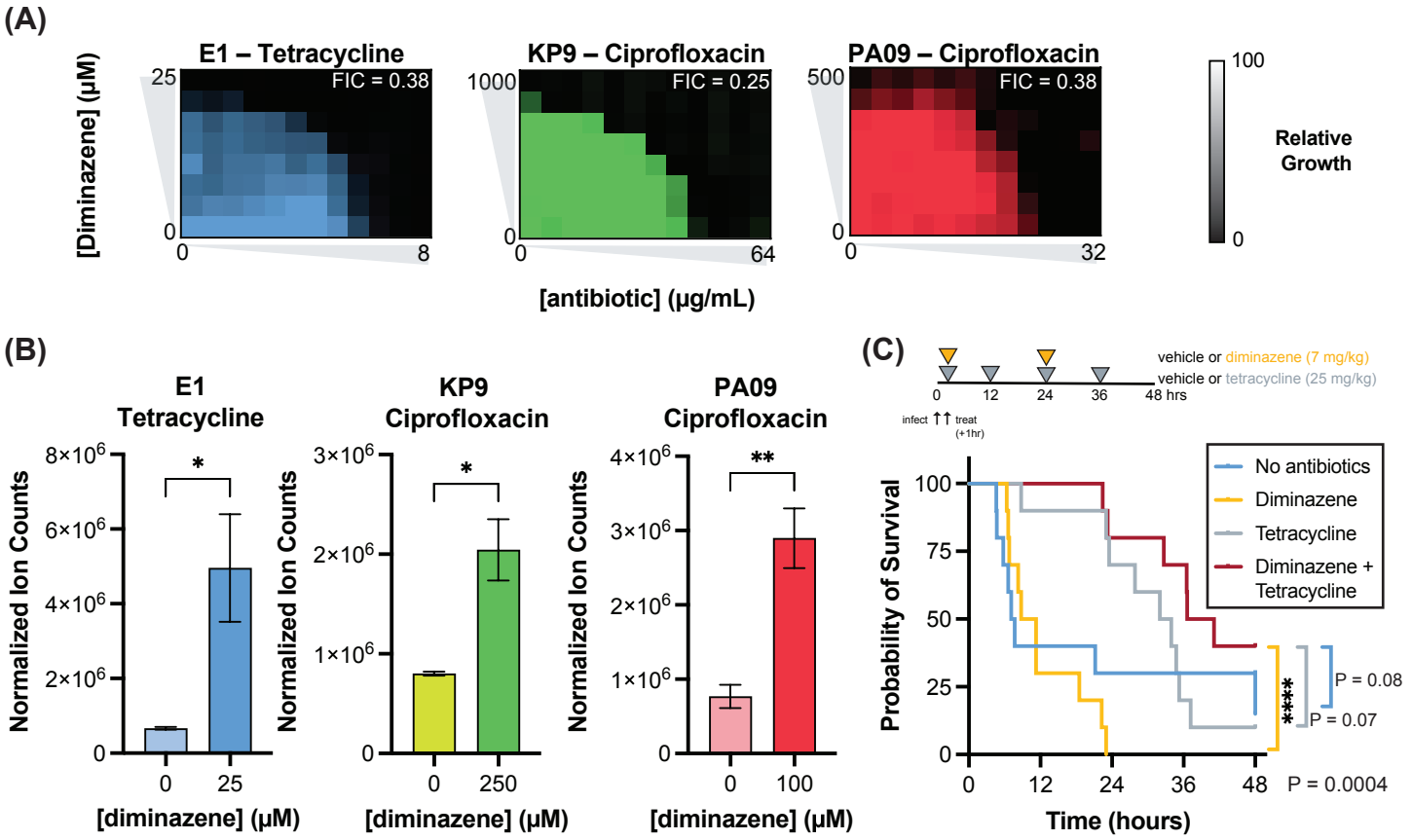

Figure 6

(A)

	Control	GNR Septic Shock
Number of subjects	22	21
% Female	68.2%	42.9%
Median Age	59.5	62
Age Range	22-79	22-93
Bacteremic	0%	100%
Escherichia coli		57.1%
Klebsiella spp		19.0%
Pseudomonas spp		23.8%
Median APACHE II	17	28
APACHE II Range	7-34	18-42
Median SOFA	3	5
SOFA Range	0-11	2-12
In Hospital Mortality	4.5%	19.0%

(B)

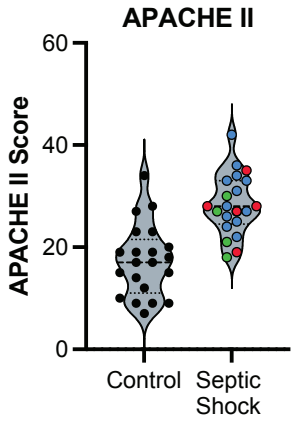

(C)

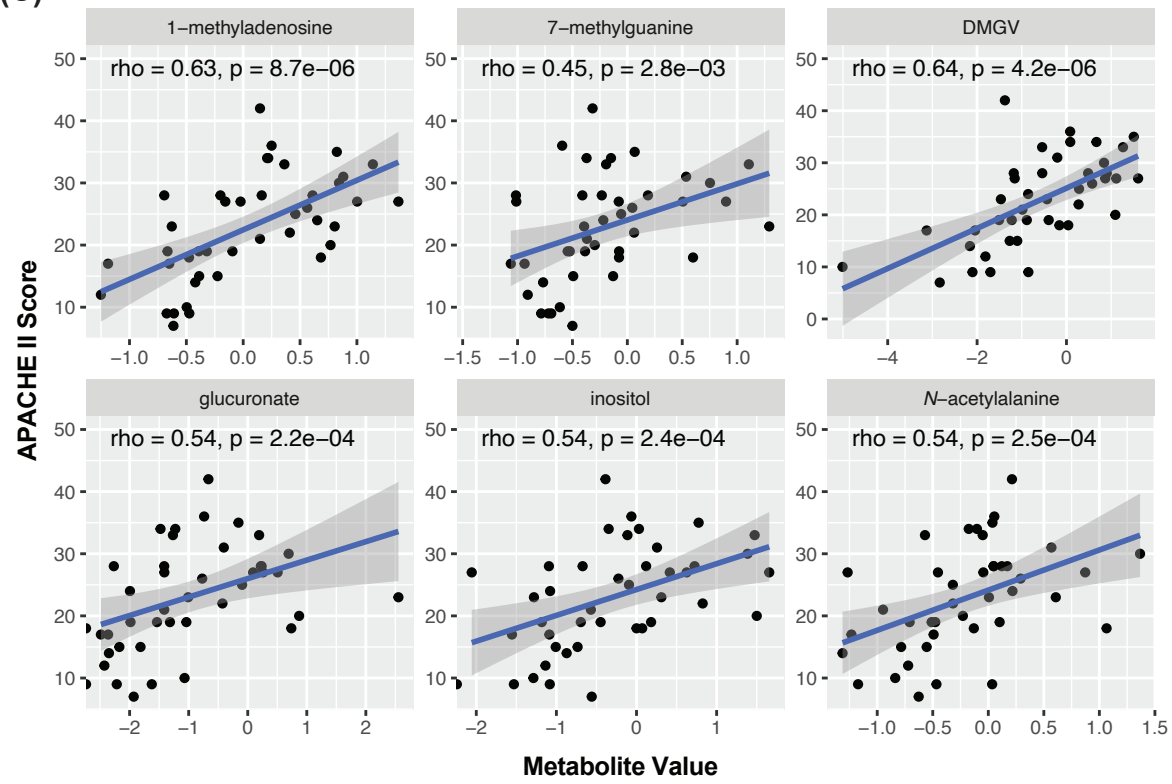

(D)

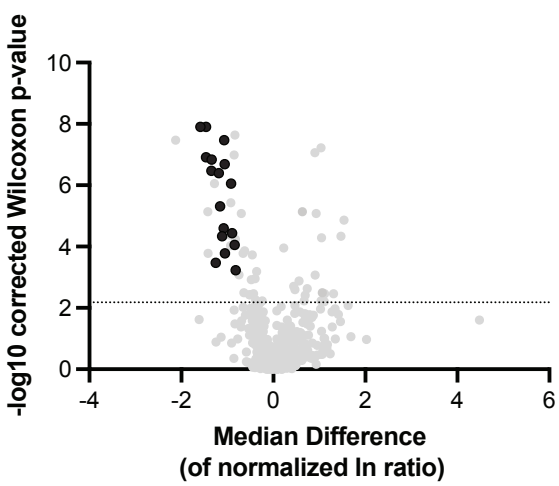

Figure S1

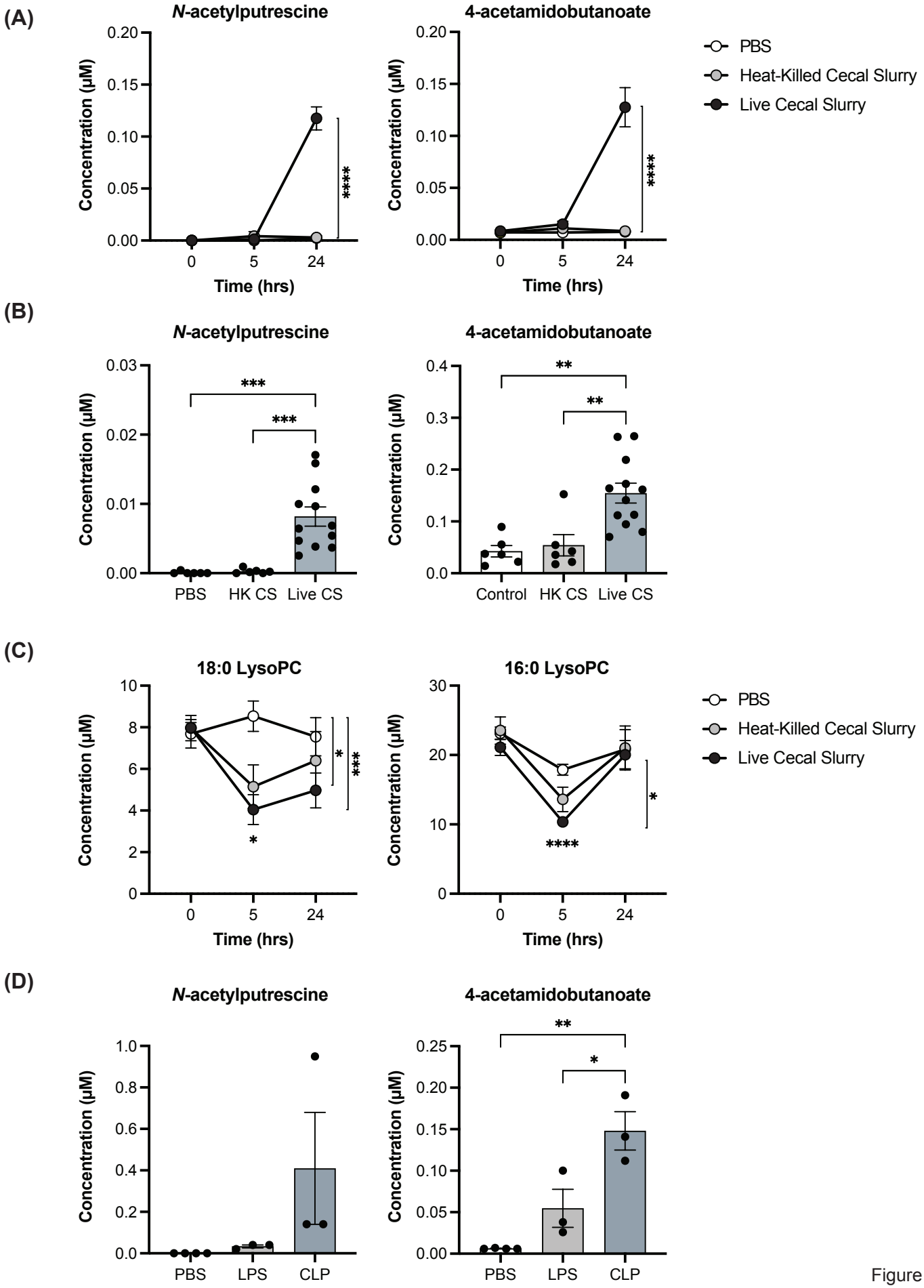

Figure S2

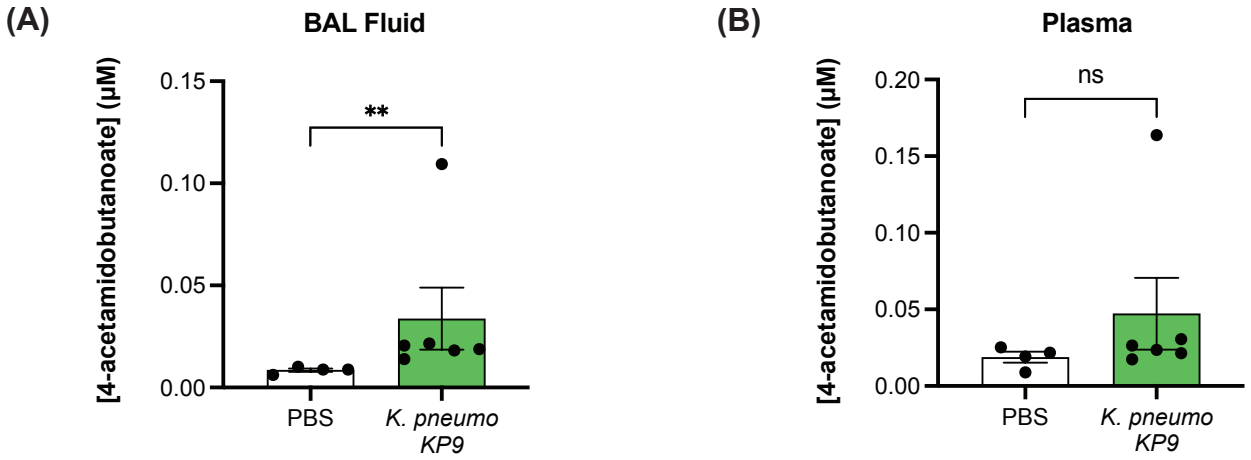

Figure S3

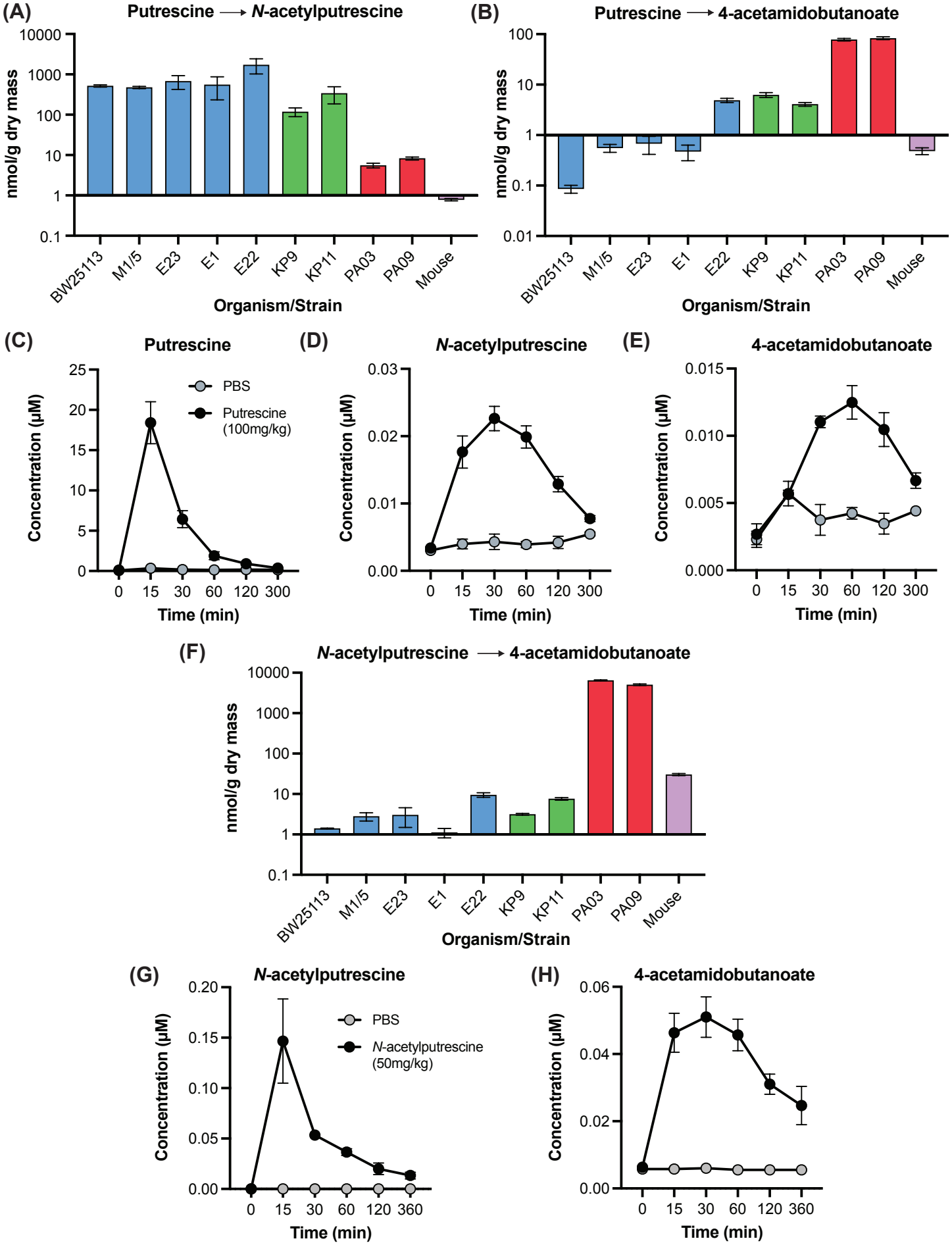

Figure S4

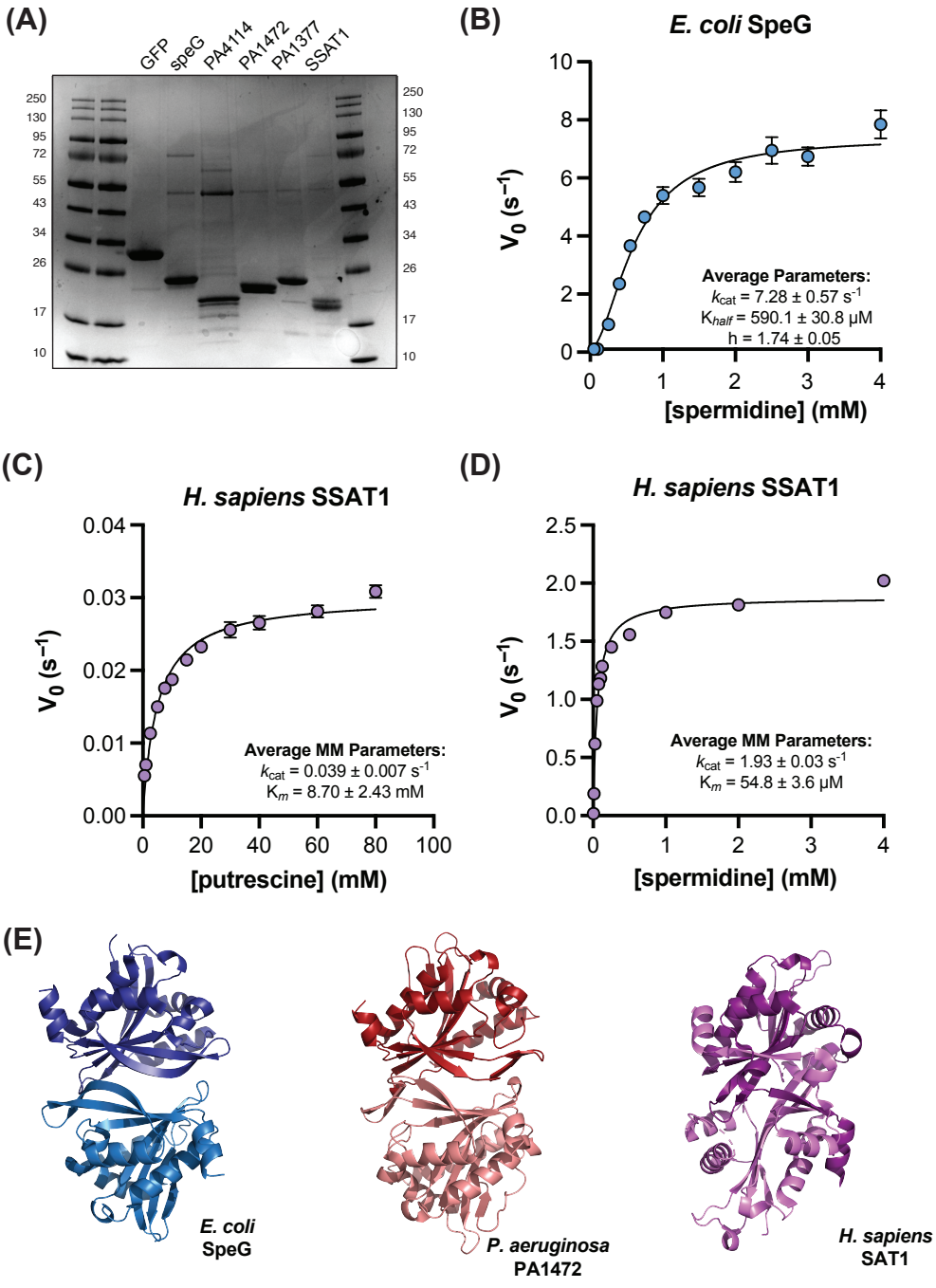

Figure S5

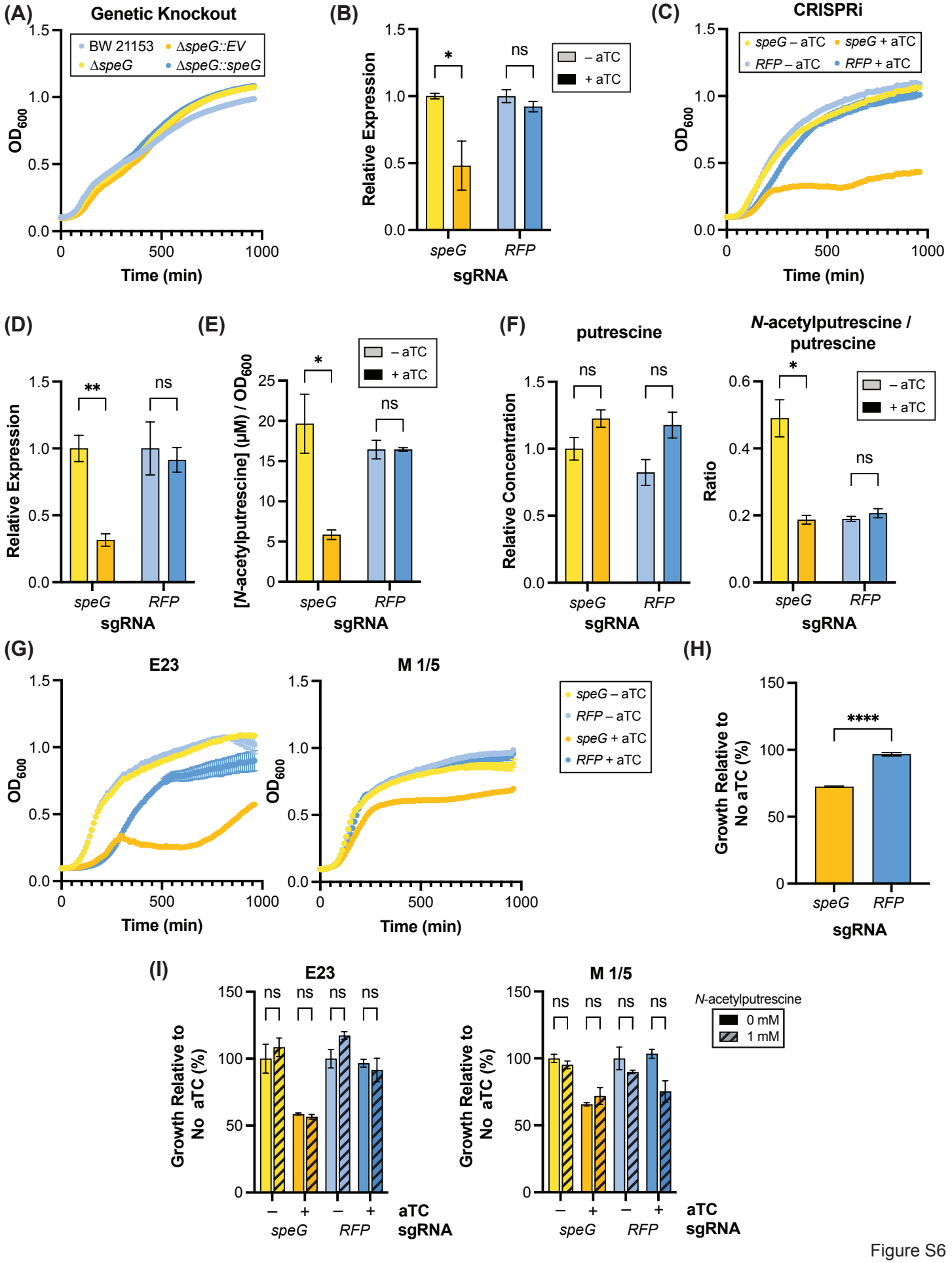

Figure S6

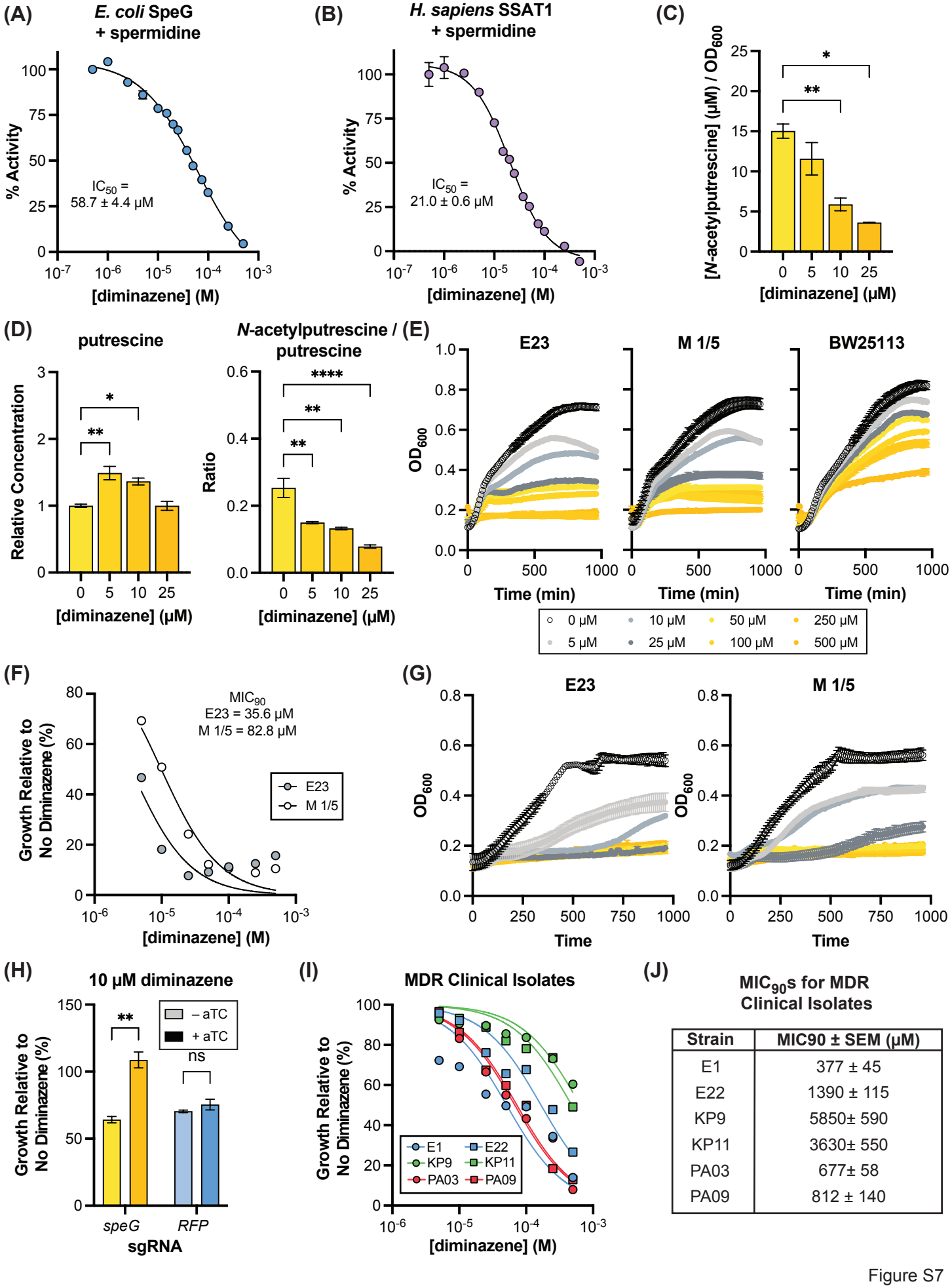

Strain	MIC90 ± SEM (µM)
E1	377 ± 45
E22	1390 ± 115
KP9	5850± 590
KP11	3630± 550
PA03	677± 58
PA09	812 ± 140

Figure S7

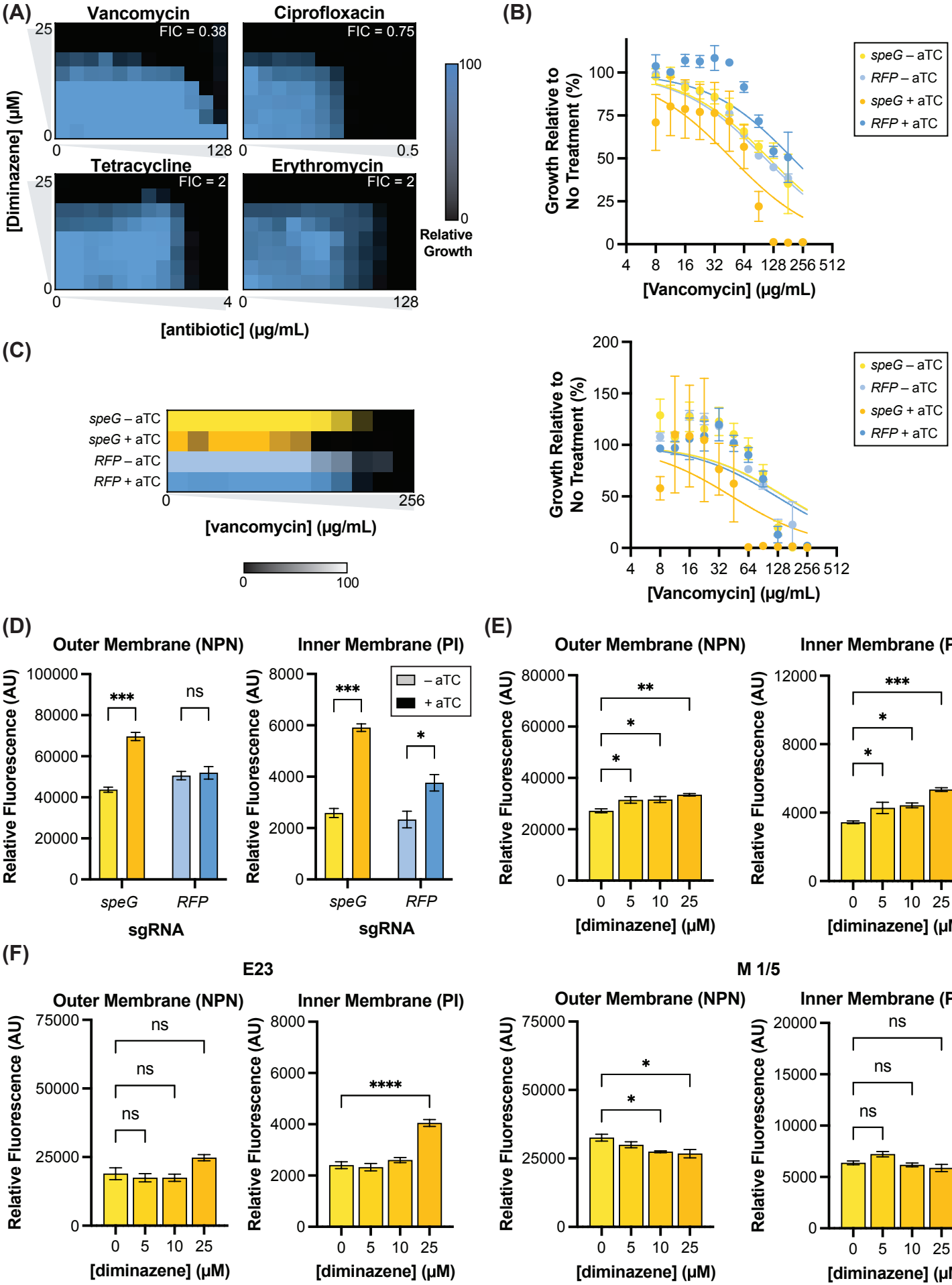

Figure S8

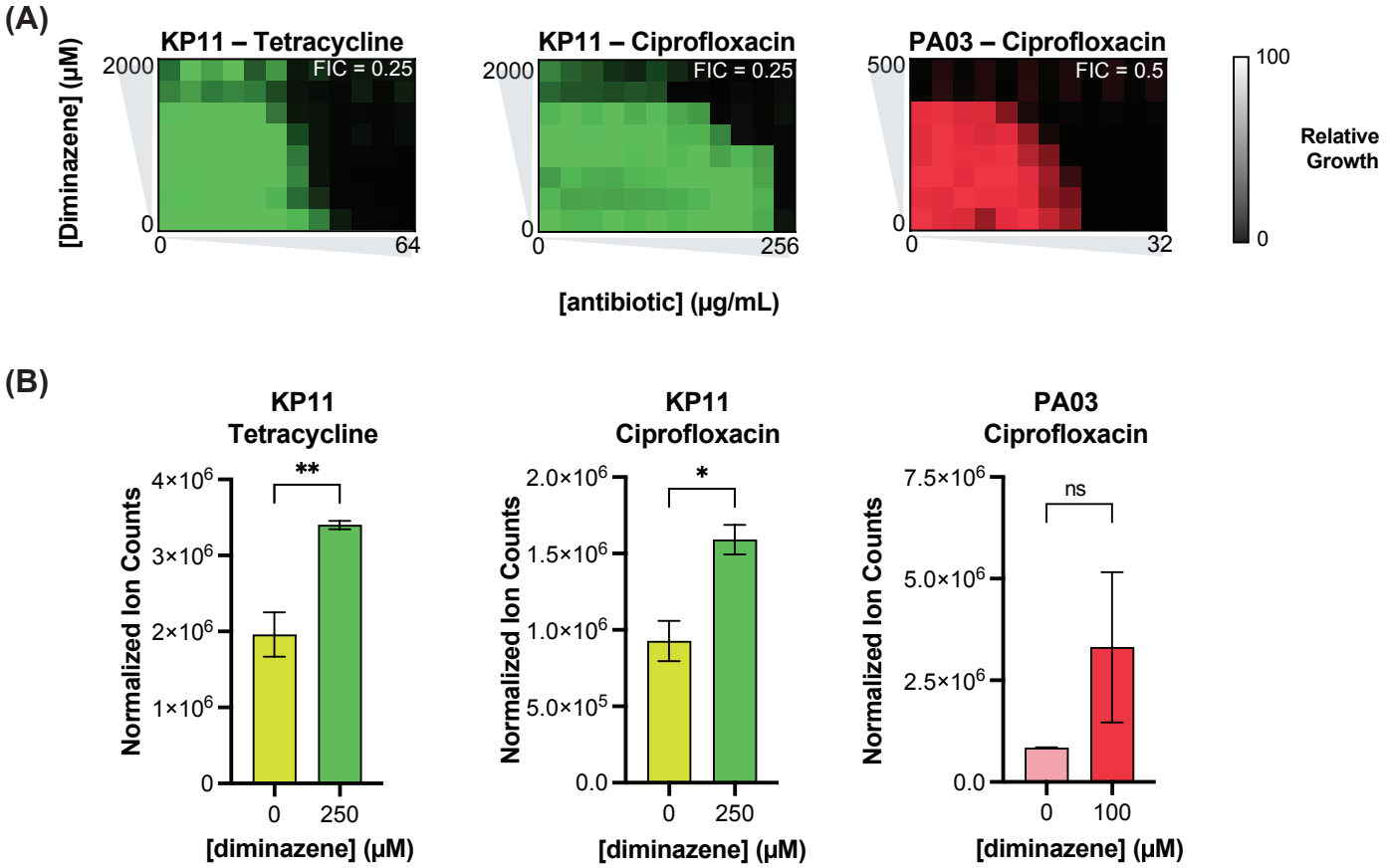

Figure S9

Table S1. Individual patient characteristics

Subject ID	Age	Sex	Group	Diagnosis	Microorganism	Baseline APACHE II	Baseline SOFA	In hosp mortality?
1	64	F	Septic Shock	Septic shock	*Escherichia coli*	28	6	N
2	93	M	Septic Shock	Septic shock	*Pseudomonas species*	28	4	N
3	87	F	Septic Shock	Septic shock	*Klebsiella species*	30	4	N
4	44	F	Septic Shock	Septic shock	*Pseudomonas species*	28	3	Y
5	53	M	Septic Shock	Septic shock	*Escherichia coli*	24	2	N
6	60	M	Septic Shock	Septic shock	*Klebsiella species*	18	5	Y
7	26	M	Control	Crohn's, desensitization		9	0	N
8	73	M	Septic Shock	Septic shock	*Escherichia coli*	36	7	N
9	72	M	Septic Shock	Septic shock	*Escherichia coli*	26	2	N
10	68	F	Control	Aspirin desensitization		9	0	N
11	62	M	Septic Shock	Septic shock	*Escherichia coli*	42	9	Y
12	56	F	Septic Shock	Septic shock	*Pseudomonas species*	27	2	N
13	45	M	Septic Shock	Septic shock	*Pseudomonas species*	35	9	N
14	85	F	Septic Shock	Septic shock	*Escherichia coli*	33	6	N
15	58	M	Septic Shock	Septic shock	*Pseudomonas species*	19	3	N
16	42	F	Septic Shock	Septic shock	*Klebsiella species*	27	4	N
17	57	M	Septic Shock	Septic shock	*Escherichia coli*	27	12	N
18	58	F	Septic Shock	Septic shock	*Escherichia coli*	31	4	Y
19	43	M	Control	Volume overload, possible pneumonia		34	8	N
20	22	F	Septic Shock	Septic shock	*Klebsiella species*	21	4	N
21	84	F	Septic Shock	Septic shock	*Escherichia coli*	34	9	N
22	58	F	Control	Angioedema		15	3	N
23	61	F	Control	ALS		14	3	N
24	57	M	Control	Hyponatremia and alcohol intoxication		23	7	N
25	64	F	Control	Upper GI bleed		10	5	N
26	68	F	Control	Bleeding after interventional radiology procedure		20	3	N
27	71	M	Septic Shock	Septic shock	*Escherichia coli*	25	6	N
28	89	M	Septic Shock	Septic shock	*Escherichia coli*	33	6	N
29	79	M	Control	Mouth bleeding		15	2	N
30	58	M	Control	Status post cardiac arrest		7	3	N
31	57	F	Control	Respiratory failurefrom influenza (cultures negative)		17	1	N
32	66	F	Control	COPD exacerbatoin		27	4	N
33	57	M	Control	Pneumonitis		28	11	Y
34	42	F	Control	Hyponatremia with PCP pneumonia		19	5	N
35	75	F	Control	Tumor impinging on trachea		18	0	N
36	68	F	Control	RF and ILD admitted for lung transplant evaluation		17	2	N
37	22	F	Control	Asthma exacerbation		12	0	N
38	68	F	Control	Respiratory failure from SCLC		19	0	N
39	91	M	Septic Shock	Septic shock	*Escherichia coli*	22	9	N
40	30	F	Control	Influenza B complicated by ARDS		23	10	N

41	31	F	Control	Pancreatitis from hypertriglyerceridemia		9	2	N
42	76	M	Control	Community acquired pneumonia, rule out MERS		19	3	N
43	61	F	Control	Pulmonary hypertension admitted for lung transplant evaluation		not available	not available	N

Table S2. Targeted metabolomics results

Method	Compound_ID	MZ	RT	HMDB ID	HMDB ID Assignment_Certainty (1=match; 2=representative ID)	Metabolite	median_BSI_minus_control	p	fdr
HILIC-pos	QI8150	524.3698	7.75	HMDB0010384	1	C18:0 LPC	-1.465779842	1.25E-08	2.45E-06
HILIC-pos	QI7953	546.3525	7.63	HMDB0010393	2	C20:3 LPC A	-1.585878336	1.25E-08	2.45E-06
HILIC-pos	QI3484	482.3234	5.56	HMDB0011130	1	C18:0 LPE	-0.835464924	2.29E-08	2.49E-06
HILIC-neg	QI4670	518.3207	4.95	redundant ion	1	C16:0 LPC_Na	-1.067776561	3.39E-08	2.49E-06
HILIC-neg	QI3767	538.3864	5.87	HMDB0011520	1	C22:0 LPE	-2.122316174	3.39E-08	2.49E-06
HILIC-pos	QI6079	376.3414	5.99	redundant ion	1	NH4_C18:0 MAG	1.035814026	5.97E-08	3.90E-06
HILIC-neg	QI6116	381.2967	5.99	HMDB0011131	1	C18:0 MAG	0.90437016	8.60E-08	5.06E-06
HILIC-neg	QI6898	482.3226	6.32	HMDB0011130	1	C18:0 LPE A	-0.853688255	1.03E-07	5.50E-06
HILIC-neg	QI10882	480.3434	7.7	HMDB0010407	2	C16:1 LPC plasmalogen	-1.465619462	1.23E-07	6.02E-06
HILIC-pos	QI10902	550.3857	7.69	HMDB0010391	2	C20:1 LPC	-1.34393056	1.46E-07	6.61E-06
HILIC-pos	QI8242	496.3383	7.87	HMDB0010382	1	C16:0 LPC	-1.057566731	2.06E-07	8.65E-06
HILIC-neg	QI10804	546.3532	7.77	HMDB0010393	2	C20:3 LPC B	-1.346927595	3.39E-07	1.33E-05
HILIC-neg	QI10656	508.3748	7.91	HMDB0013122	2	C18:1 LPC plasmalogen	-1.186224252	3.99E-07	1.47E-05
HILIC-neg	QI10708	518.3205	7.88	HMDB0010387	2	C18:3 LPC	-0.921285619	8.75E-07	2.86E-05
HILIC-pos	QI8191	510.3541	7.81	HMDB0011511	1	C20:0 LPE	-1.27881329	8.75E-07	2.86E-05
HILIC-pos	QI11995	454.2914	6.39	HMDB0011503	1	C16:0 LPE	-0.924563917	3.73E-06	9.97E-05
HILIC-neg	QI8185	522.3541	7.8	HMDB0002815	2	C18:1 LPC	-1.159914173	4.90E-06	0.00012
HILIC-pos	QI8326	482.3228	7.93	HMDB0011130	1	C18:0 LPE B	-1.425593273	7.30E-06	0.000165
HILIC-pos	QI10562	131.1176	7.99	HMDB0002064	1	N-acetylputrescine	0.629703917	7.30E-06	0.000165
HILIC-pos	QI10805	282.1186	7.76	HMDB0003331	1	1-methyladenosine	0.932959	8.32E-06	0.000175
HILIC-pos	QI12060	502.2914	6.33	HMDB0011517	1	C20:4 LPE	-0.699823675	8.32E-06	0.000175
HILIC-pos	QI2878	363.2152	2.06	HMDB0000063	1	cortisol	1.537763929	1.39E-05	0.000272
HILIC-pos	QI8229	520.3384	7.85	HMDB0010386	2	C18:2 LPC	-1.081470577	2.55E-05	0.000484
HILIC-pos	QI10789	544.338	7.79	HMDB0010395	1	C20:4 LPC	-0.895143935	3.63E-05	0.000628
C8-pos	QI6985	476.2741	6.41	HMDB0011478	2	C18:3 LPE	-0.949456178	4.14E-05	0.000695
HILIC-pos	QI10836	570.3538	7.73	HMDB0010403	2	C22:5 LPC	-1.114558385	4.58E-05	0.000727
HILIC-pos	QI12518	302.3042	5.91	HMDB0000269	1	sphinganine	1.471267599	4.58E-05	0.000727
HILIC-pos	QI2646	166.0858	2.03	HMDB0034169	1	methyl N-methylanthranilate	1.04796863	5.13E-05	0.000793
HILIC-pos	QI6956	478.2914	6.38	HMDB0011507	2	C18:2 LPE	-0.826538148	5.74E-05	0.000865
HILIC-neg	QI8139	568.3377	7.74	HMDB0010404	1	C22:6 LPC	-0.843392188	8.91E-05	0.00131
HILIC-pos	QI6957	540.4975	6.38	HMDB0006347	1	C26 carnitine	-0.931158025	9.32E-05	0.001337
HILIC-neg	QI4682	339.2499	5.05	HMDB0011565	2	C16:1 MAG	0.227420153	0.00011	0.001476
HILIC-pos	QI9655	258.1092	10.5	HMDB0000086	1	alpha-glycerophosphocholine	-0.627630269	0.000136	0.001743
HILIC-neg	QI10648	494.3229	7.92	HMDB0010383	2	C16:1 LPC	-1.051703275	0.000168	0.002013
HILIC-pos	QI12042	480.307	6.34	HMDB0011506	2	C18:1 LPE	-0.656815586	0.000168	0.002013
HILIC-pos	QI10727	508.3386	7.86	HMDB0011512	2	C20:1 LPE	-1.421031846	0.000168	0.002013
HILIC-pos	QI11461	787.6665	7.14	HMDB0012103	1	C22:0 SM	-0.455937583	0.000186	0.002142
HILIC-neg	QI8415	468.307	8	HMDB0010379	1	C14:0 LPC	-1.253857293	0.000337	0.003811
HILIC-neg	QI10733	542.3208	7.85	HMDB0010397	1	C20:5 LPC	-0.817590431	0.000593	0.00646
HILIC-neg	QI5288	666.617	11.96	redundant ion	2	NH4_C18:2 CE	-0.362999788	0.00065	0.00695
HILIC-neg	TF35	173.08	6.34	HMDB00893	1	suberate	-0.749237917	0.000835	0.008762
HILIC-neg	QI7994	260.1847	7.65	HMDB0000705	1	C6 carnitine	0.906888882	0.000851	0.008783
HILIC-pos	QI2844	796.6194	9.29	HMDB0011252	2	C38:4 PC plasmalogen	-0.398782585	0.001108	0.011229
HILIC-pos	QI12085	526.2916	6.3	HMDB0011526	1	C22:6 LPE	-0.483224358	0.001207	0.012032
HILIC-pos	QI14745	132.0652	3.68	HMDB0000766	1	N-acetylalanine	0.557947108	0.001315	0.012887
HILIC-pos	QI6388	166.0718	5.83	HMDB0000897	1	7-methylguanine	0.443441497	0.001995	0.019228
HILIC-pos	QI7844	274.2003	7.54	HMDB0013238	1	C7 carnitine	0.735840803	0.002345	0.021887
HILIC-pos	QI9949	241.0304	9.12	HMDB0000192	1	cystine	0.467253568	0.00254	0.023336
HILIC-pos	QI14867	146.0807	3.48	HMDB0003681	1	4-acetamidobutanoate	1.061575501	0.003215	0.028639
HILIC-pos	QI6181	692.6326	12.09	redundant ion	2	NH4_C20:3 CE	-0.64352	0.003215	0.028639

HILIC-pos	TF22	101.06	3.41	HMDB00718	2	isovalerate/valerate/methylbutyrate	-0.429125848	0.003458	0.029592
HILIC-pos	QI8362	244.1535	7.96	HMDB0002366	1	C5:1 carnitine	1.111152077	0.003473	0.029592
HILIC-pos	QI8163	202.1181	7.78	HMDB0240212	1	DMGV	1.309129083	0.003473	0.029592
HILIC-pos	TF03	790.632	9.65	HMDB0008036	2	C36:0 PC	-0.516273876	0.003749	0.031045
HILIC-pos	QI4988	670.6487	12.64	redundant ion	1	NH4_C18:0 CE	-0.521732848	0.003749	0.031045
C8-pos	QI32	181.0508	4.07	HMDB00118	1	homovanillate	0.689768689	0.003865	0.031562
HILIC-pos	QI5672	675.604	12.64	HMDB0010368	1	C18:0 CE	-0.386031891	0.005443	0.043843
HILIC-pos	QI7700	288.2158	7.43	HMDB0000791	1	C8 carnitine	1.038089793	0.005853	0.045287
HILIC-pos	TF21	179.06	2.56	HMDB00211	1	inositol	0.671909783	0.005853	0.045287
C8-pos	QI4957	642.6171	12.19	redundant ion	1	NH4_C16:0 CE	-0.241251821	0.005853	0.045287
HILIC-pos	TF15	193.04	4.52	HMDB00127	1	glucuronate	1.108829693	0.006245	0.047691
HILIC-pos	QI3271	815.6988	10.17	HMDB0011697	1	C24:0 SM	-0.286724279	0.006757	0.050935
C8-pos	QI12855	222.0965	5.49	HMDB0000853	1	acetyl-galactosamine	0.46905711	0.008341	0.061009
HILIC-pos	QI4350	768.587	8.99	HMDB0011310	2	C36:4 PC plasmalogen	-0.330391996	0.008341	0.061009
HILIC-pos	QI51	341.1093	2.31	HMDB00258	2	sucrose/lactose/trehalose	1.624089908	0.008404	0.061009
C8-pos	QI1459	647.5566	10.13	HMDB0007158	2	C36:0 DAG	0.168558108	0.008937	0.064083
HILIC-pos	QI49	201.1134	6.28	HMDB00792	1	sebacate	-0.659692923	0.009562	0.066986
HILIC-pos	QI11796	428.3718	6.69	HMDB0000848	1	C18 carnitine	-0.426461916	0.009569	0.066986
C8-pos	QI5857	697.5879	12.09	HMDB0006736	2	C20:3 CE	-0.496469386	0.010202	0.070573
HILIC-pos	QI7534	367.1485	7.18			C-glycosyltryptophan	1.343802653	0.010595	0.072442
HILIC-pos	QI3688	732.5523	8.51	HMDB0007873	2	C32:1 PC	1.025029749	0.010953	0.073184
C8-pos	QI2688	859.5308	8.23	HMDB0009789	2	C36:4 PI	-0.854889025	0.011707	0.077347
HILIC-pos	QI3992	812.6144	9.26	HMDB0008047	2	C38:3 PC	-0.314599779	0.012507	0.079933
HILIC-pos	QI1602	300.289	5.12	HMDB0002100	1	palmitoylethanolamide	0.072358326	0.012507	0.079933
C8-pos	QI10125	204.1224	8.75	HMDB0000201	1	C2 carnitine	0.576333697	0.013353	0.081785
HILIC-pos	QI7531	759.6346	7.18	HMDB0012102	1	C20:0 SM	-0.217913855	0.013353	0.081785
C8-pos	QI2622	887.562	8.73	HMDB0009815	2	C38:4 PI	-0.375143843	0.013353	0.081785
HILIC-pos	QI9301	287.2431	10.45	HMDB0002172	1	diacetylspermine	1.274408059	0.013353	0.081785
HILIC-pos	QI5447	664.6013	11.71	redundant ion	2	NH4_C18:3 CE	-0.372714644	0.014248	0.086368
C8-pos	TF01	782.5694	8.49	HMDB0007983	2	C36:4 PC-A	-0.475689769	0.015194	0.089797
HILIC-pos	QI8812	166.0528	8.69	HMDB0002005	1	methionine sulfoxide	0.464289527	0.015194	0.089797
HILIC-pos	TF14	115	6.54	HMDB00134	2	fumarate/maleate	0.686880599	0.015272	0.089797
C8-pos	QI14	151.0613	1.69	HMDB00508	2	adonitol/arabitol	0.684641333	0.016194	0.09138
HILIC-pos	QI2727	835.5315	8.22	HMDB0009784	2	C34:2 PI	-0.538434218	0.016194	0.09138
HILIC-pos	QI12931	466.3149	5.42	HMDB0000138	1	glycocholate	1.414926874	0.01638	0.09138
	QI15	145.0143	6.97	HMDB00208	1	alpha-ketoglutarate	0.786864159	0.016721	0.09138
HILIC-pos	QI41	133.0143	6.52	HMDB00744	1	malate	0.683857819	0.01723	0.09138
HILIC-pos	QI14753	229.0812	3.67	HMDB0000012	1	2-deoxyuridine	0.708445635	0.01725	0.09138
C8-pos	QI9916	175.1185	9.24	HMDB0000517	1	arginine	-0.609566134	0.01725	0.09138
HILIC-pos	QI11389	316.247	7.25	HMDB0000651	1	C10 carnitine	0.869226623	0.01725	0.09138
HILIC-pos	QI8515	232.1536	8.1	HMDB0002013	1	C4 carnitine	0.684094731	0.01725	0.09138
C8-pos	QI8107	106.0496	7.71	HMDB0000187	1	serine	-0.253943258	0.01725	0.09138
HILIC-pos	QI11761	424.3406	6.77	HMDB0006469	2	C18:2 carnitine	-0.425606415	0.018365	0.096415
HILIC-pos	TF30	165.06	3.41	HMDB00159	1	phenyllactate	0.837591354	0.02058	0.106148
HILIC-pos	QI16	161.0457	6.33	HMDB00640	2	anhydroDglucose/3-hydroxymethylglutarate	0.713384235	0.021816	0.111547
HILIC-pos	QI6062	716.6325	11.91	redundant ion	2	NH4_C22:5 CE	-0.309815065	0.02254	0.114253
HILIC-pos	QI14688	197.0665	3.74	HMDB0011103	1	1,7-dimethyluric acid	-1.615005688	0.023985	0.120541
HILIC-pos	QI16204	152.0701	2.04	HMDB0001859	1	acetaminophen	4.482577704	0.024908	0.122048
HILIC-pos	QI7186	756.5507	6.74	HMDB0008006	2	C34:3 PC	0.300980223	0.024908	0.122048
C8-pos	QI10583	76.0391	7.98	HMDB0000123	1	glycine	-0.31325607	0.024908	0.122048
HILIC-pos	QI2129	671.5718	11.98	HMDB0000610	2	C18:2 CE	-0.176768125	0.02643	0.126347
HILIC-pos	QI10295	176.1025	8.41	HMDB0000904	1	citrulline	-0.459839836	0.02643	0.126347
C8-pos	QI8327	118.061	7.93	HMDB0000128	1	guanidinoacetic acid	-0.693946517	0.02643	0.126347
HILIC-pos	QI5760	268.1031	5.07	HMDB0000050	1	adenosine	1.458114154	0.028029	0.131305
HILIC-pos	QI2685	818.6031	9.31	HMDB0011294	2	C40:7 PC plasmalogen	-0.223697555	0.028029	0.131305
C8-pos	TF05	893.6624	9.98			C54:10 TAG	-0.39011705	0.028137	0.131305
HILIC-pos	TF36	117.02	6.49	HMDB00254	1	succinate	-0.342411975	0.029	0.134267
C8-pos	QI4935	176.0549	4.35	HMDB0000812	1	N-acetylaspartic acid	0.674309067	0.02971	0.134381
C8-pos	QI10992	120.0656	7.64	HMDB0000167	1	threonine	-0.376206677	0.02971	0.134381
HILIC-pos	QI5305	180.0511	4.67			xanthopterin	0.641432572	0.02971	0.134381
HILIC-pos	QI5885	690.6169	11.83	redundant ion	1	NH4_C20:4 CE	-0.233115451	0.031475	0.141276

C8-pos	QI9075	189.1341	9.29	HMDB0000670	1	homoarginine	-0.833485709	0.033326	0.147338
HILIC-pos	QI4699	133.0605	4.19	HMDB0000026	1	N-carbamoyl-beta-alanine	0.731840757	0.033326	0.147338
C8-pos	TF8	132.1016	7.17	HMDB0000172	1	isoleucine	-0.320657251	0.035269	0.154761
HILIC-pos	QI1998	907.7703	12.41	HMDB0005405	2	C54:3 TAG	0.076956835	0.037304	0.161286
HILIC-pos	QI9832	189.1341	9.45	HMDB0029416	1	NMMA	-0.411968155	0.037304	0.161286
C8-pos	TF31	73.03	3.74	HMDB00237	1	propionate	0.351037298	0.038171	0.163827
C8-pos	QI33	103.0401	3.49	HMDB00008	2	alpha-hydroxybutyrate/beta-hydroxybutyrate/hydroxyisobutyrate	0.372374861	0.039437	0.165635
HILIC-pos	QI5291	668.6327	12.28	redundant ion	2	NH4_C18:1 CE	-0.200779933	0.039437	0.165635
C8-pos	QI4781	245.076	4.24	HMDB0000767	1	pseudouridine	0.804284599	0.039437	0.165635
HILIC-pos	QI4359	726.5423	9.08	HMDB0011442	2	C36:4 PE plasmalogen	-0.705130696	0.04167	0.170152
HILIC-pos	QI10042	248.1485	8.93	HMDB0013127	1	C4-OH carnitine	1.278591341	0.04167	0.170152
HILIC-pos	QI2435	957.7852	12.36	HMDB0005458	2	C58:6 TAG	0.178124607	0.04167	0.170152
HILIC-pos	QI3689	172.0711	2.76	HMDB0015052	1	metronidazole	0.335990321	0.04167	0.170152
C8-pos	QI6161	728.557	5.54	HMDB0011441	2	C36:3 PE plasmalogen	-0.54418734	0.046451	0.185803
C8-pos	QI6098	752.5562	5.48	HMDB0011386	2	C38:5 PE plasmalogen	-0.313847326	0.046451	0.185803
C8-pos	QI9146	147.1123	9.47	HMDB0000182	1	lysine	-0.411459311	0.046451	0.185803
C8-pos	QI7239	400.3407	6.8	HMDB0000222	1	C16 carnitine	-0.293120228	0.051674	0.202564
C8-pos	QI9743	265.1108	9.77	HMDB0000235	1	thiamine	-0.397067722	0.051674	0.202564
C8-pos	QI5937	718.6479	12.22	redundant ion	2	NH4_C22:4 CE	-0.443930832	0.056936	0.221709
C8-pos	QI4766	184.06	4.23	HMDB0000017	1	4-pyridoxate	1.048389638	0.05737	0.22193
C8-pos	QI57	243.0622	1.69	HMDB00296	1	uridine	-0.221746483	0.059354	0.226623
HILIC-pos	QI7476	342.2625	7.09	HMDB0013326	2	C12:1 carnitine	0.51616874	0.060403	0.227674
C8-pos	QI8669	276.1432	8.41	HMDB0013130	1	C5-DC carnitine	0.502664845	0.060403	0.227674
C8-pos	QI2704	583.2535	2.04	HMDB0001008	1	biliverdin	0.291064961	0.063566	0.229306
HILIC-pos	QI4588	756.5895	9.13	HMDB0011384	2	C38:3 PE plasmalogen	0.577981392	0.063566	0.229306
C8-pos	QI5859	893.7549	12.22	HMDB0043058	2	C53:3 TAG	0.440825799	0.063566	0.229306
C8-pos	QI5954	921.7867	12.59	HMDB0042466	2	C55:3 TAG	0.230069263	0.063566	0.229306
HILIC-pos	QI7086	114.066	6.55	HMDB0000562	1	creatinine	0.497764445	0.063566	0.229306
C8-pos	QI13004	190.0494	5.35	HMDB0000715	1	kynurenic acid	0.2552805	0.063566	0.229306
C8-pos	QI27	105.0193	3.95	HMDB00139	1	glycerate	0.287457585	0.063932	0.229306
C8-pos	TF10	115.04	3.12	HMDB00019	1	alpha-ketoisovalerate	0.190514893	0.063956	0.229306
C8-pos	QI4220	690.5048	8.51	HMDB0008924	2	C32:1 PE	0.594934327	0.066692	0.235415
C8-pos	QI11738	720.5515	6.79	HMDB0008925	2	C34:0 PE	0.375163824	0.066861	0.235415
HILIC-pos	QI4497	669.5564	11.72	HMDB0010370	2	C18:3 CE	-0.25390599	0.070292	0.240302
C8-pos	QI3630	695.5718	11.83	HMDB0006726	1	C20:4 CE	-0.268763603	0.070292	0.240302
C8-pos	QI3550	734.5678	8.81	HMDB0007871	2	C32:0 PC	0.245284203	0.070292	0.240302
HILIC-pos	QI3987	746.5685	9.38	HMDB0008993	2	C36:1 PE	0.53006069	0.070292	0.240302
HILIC-pos	QI2867	814.6306	9.47	HMDB0008270	2	C38:2 PC	-0.336721176	0.070292	0.240302
C8-pos	QI16664	538.5182	1.9	HMDB0004949	1	C16:0 ceramide (d18:1)	0.32394916	0.073864	0.251051
C8-pos	QI3252	704.5213	8.01	HMDB0007870	2	C30:1 PC	0.763025412	0.077579	0.259543
HILIC-pos	QI5	102.056	2.89	HMDB00650	1	2-aminobutyrate	-0.521073408	0.077686	0.259543
HILIC-pos	QI3826	692.5211	8.09	HMDB0008923	2	C32:0 PE	0.681401382	0.080512	0.263119
HILIC-pos	QI8758	262.1276	8.64	HMDB0013133	1	C3-DC-CH3 carnitine	0.453080615	0.081442	0.263119
HILIC-pos	QI5278	885.6711	11.28	HMDB0001072	1	coenzyme Q10	-0.442026584	0.081442	0.263119
C8-pos	QI4502	760.5835	8.96	HMDB0007972	2	C34:1 PC	0.285929829	0.085456	0.273047
C8-pos	QI3021	781.6306	11.02			C45:3 TAG	1.687522316	0.085908	0.273047
C8-pos	QI4063	167.0559	3.38	HMDB0001886	1	3-methylxanthine	-1.13632508	0.089625	0.280315
C8-pos	QI7252	706.5357	6.81	HMDB0007869	2	C30:0 PC	0.564062173	0.089625	0.280315
C8-pos	QI7202	754.5341	6.77	HMDB0007883	2	C34:4 PC	0.329195796	0.089625	0.280315
C8-pos	QI6840	168.1014	6.26	HMDB0000022	1	3-methoxytyramine	0.38728017	0.093952	0.286238
C8-pos	QI5894	836.5375	8.74	HMDB0010167	2	C40:6 PS	0.174617174	0.093952	0.286238
C8-pos	QI9605	189.1593	11.29	HMDB0001325	1	N6,N6,N6-trimethyllysine	0.253614034	0.093952	0.286238
C8-pos	QI12281	126.0218	6.13	HMDB0000251	1	taurine	0.349291476	0.093952	0.286238
C8-pos	QI5214	693.5564	11.59	HMDB0006731	1	C20:5 CE	-0.402641617	0.098442	0.290875
HILIC-pos	QI12808	764.5194	5.54	HMDB0009102	2	C38:6 PE	0.259579947	0.098442	0.290875
C8-pos	QI21	239.0925	6.56	HMDB61112	1	CMPF	1.115461489	0.098442	0.290875
HILIC-pos	QI10315	132.0764	8.4	HMDB0000064	1	creatine	0.476564637	0.098442	0.290875
C8-pos	QI9252	188.1753	9.93	HMDB0001276	1	N1-acetylspermidine	0.271146654	0.098442	0.290875
HILIC-pos	QI8574	76.0755	8.21	HMDB0000925	1	trimethylamine-N-oxide	1.103914703	0.098442	0.290875
C8-pos	TF11	87.05	3.5	HMDB00039	1	butyrate	-0.192137215	0.102387	0.295717
C8-pos	QI6194	700.5251	5.57	HMDB0011343	2	C34:3 PE plasmalogen	-0.776402897	0.103098	0.295717
C8-pos	TF02	784.5851	8.82	HMDB0008105	2	C36:3 PC	-0.287315957	0.103098	0.295717
C8-pos	QI4231	905.7544	12.14	HMDB0005370	2	C54:4 TAG	0.077111485	0.103098	0.295717
HILIC-pos	QI13598	265.1173	4.72	HMDB0006344	1	phenylacetylglutamine	1.346786406	0.103098	0.295717
C8-pos	QI2416	778.6908	11.15	redundant ion	2	NH4_C45:2 TAG	2.027663395	0.107831	0.300756
C8-pos	QI5841	298.1134	5.16	HMDB0001563	1	1-methylguanosine	0.243826674	0.107924	0.300756
C8-pos	QI5993	617.5105	9.45	HMDB0007102	2	C34:1 DAG	-0.303617633	0.107924	0.300756
C8-pos	QI12864	750.5404	5.48	HMDB0011387	2	C38:6 PE plasmalogen	-0.129868929	0.107924	0.300756
C8-pos	QI12915	312.1291	5.43	HMDB0004824	1	N2,N2-dimethylguanosine	0.474942343	0.107924	0.300756
HILIC-pos	QI5702	714.6167	11.7	redundant ion	1	NH4_C22:6 CE	-0.34958115	0.107924	0.300756
C8-pos	QI5836	719.572	11.7	HMDB0006733	1	C22:6 CE	-0.342099357	0.109258	0.303037
C8-pos	TF1	147.03	6.46	HMDB59655	2	2-hydroxyglutarate	0.380492502	0.112923	0.308833
HILIC-pos	QI2279	647.5724	12.19	HMDB0000885	1	C16:0 CE	-0.139234657	0.112923	0.308833
C8-pos	QI11870	790.5715	6.57	HMDB0011229	2	C38:7 PC plasmalogen	-0.310993496	0.112923	0.308833
C8-pos	QI3858	748.5839	8.99	HMDB0008991	2	C36:0 PE	0.158790664	0.118099	0.321493
HILIC-pos	TF26	71.01	3.62	HMDB06112	1	MDA	0.302781942	0.120002	0.325167
C8-pos	QI5962	166.0718	5.35	HMDB0003282	1	1-methylguanine	0.349673772	0.123456	0.328287

C8-pos	QI12728	716.5201	5.63	HMDB0008928	2	C34:2 PE	0.397986108	0.123456	0.328287
C8-pos	QI8255	246.1692	7.88	HMDB0000688	1	C5 carnitine	0.49285473	0.123456	0.328287
C8-pos	QI5908	853.7234	11.94	HMDB0005377	2	C50:2 TAG	0.350259948	0.123456	0.328287
C8-pos	QI4249	157.0603	3.71	HMDB0000544	1	5-hydroxymethyl-4-methyluracil	0.446475728	0.123945	0.328287
C8-pos	QI8	131.0715	3.22	HMDB00317	2	2-hydroxy-3-methylpentanoate/hydroxyisocaproate	0.209595828	0.128996	0.334172
C8-pos	TF11	166.0857	6.79	HMDB0000159	1	phenylalanine	0.18029857	0.128996	0.334172
HILIC-pos	QI47	191.0563	4	HMDB03072	1	quinate	-1.246886277	0.128996	0.334172
C8-pos	QI6041	721.5877	11.91	HMDB0010375	2	C22:5 CE	-0.222275225	0.129008	0.334172
C8-pos	QI9000	118.086	9.03	HMDB0000043	1	betaine	0.237136711	0.134723	0.344423
C8-pos	QI5933	639.4946	9.01	HMDB0007248	2	C36:4 DAG	-0.372549804	0.134723	0.344423
HILIC-pos	QI6063	614.5853	11.79	redundant ion	1	NH4_C14:0 CE	-0.301618218	0.134723	0.344423
C8-pos	QI5834	619.5411	11.79	HMDB0006725	1	C14:0 CE	-0.454681376	0.137244	0.349348
HILIC-pos	QI6200	851.7075	11.72	HMDB0005433	2	C50:3 TAG	0.208528155	0.140641	0.35041
HILIC-pos	QI15202	195.0873	2.88	HMDB0001847	1	caffeine	-0.907877318	0.140641	0.35041
HILIC-pos	TF10	141.0653	8.94	HMDB0002820	1	methylimidazoleacetic acid	0.845346631	0.140641	0.35041
C8-pos	QI4603	612.5552	9.46	redundant ion	2	NH4_C34:1 DAG	-0.424559315	0.140641	0.35041
HILIC-pos	QI8801	130.0859	8.68			N-methylproline	0.64018701	0.146752	0.364094
HILIC-pos	QI4942	810.5979	9.12	HMDB0008048	2	C38:4 PC	-0.214954055	0.15306	0.376567
HILIC-pos	QI5028	813.6929	11.69	HMDB0042100	2	C47:1 TAG	0.711225113	0.155295	0.380474
HILIC-pos	QI38	212.0025	3.56	HMDB00682	1	indoxylsulfate	1.172608923	0.156048	0.380731
C8-pos	QI7578	731.604	7.25	HMDB0001348	1	C18:0 SM	-0.167116936	0.159568	0.384534
C8-pos	QI15630	258.2055	2.41	HMDB0013272	1	N-lauroylglycine	-0.390586105	0.159568	0.384534
HILIC-pos	QI1658	642.6016	10.13	redundant ion	2	NH4_C36:0 DAG	0.141471009	0.159568	0.384534
C8-pos	QI6293	185.128	5.7	HMDB0061384	1	acisoga	0.425812858	0.166279	0.389531
C8-pos	QI10306	218.138	8.4	HMDB0000824	1	C3 carnitine	0.338398665	0.166279	0.389531
HILIC-pos	QI5177	766.5717	8.95	HMDB0011220	2	C36:5 PC plasmalogen-B	-0.084251637	0.166279	0.389531
C8-pos	QI3641	935.8027	12.77	HMDB0005410	2	C56:3 TAG	0.28560201	0.166279	0.389531
C8-pos	QI7486	150.0578	7.11	HMDB0000696	1	methionine	-0.267756393	0.166279	0.389531
C8-pos	QI9071	144.1013	9.29	HMDB0004827	1	proline-betaine	0.953889876	0.166279	0.389531
C8-pos	TF14	182.0807	6.89	HMDB0000158	1	tyrosine	0.075351601	0.166279	0.389531
C8-pos	QI3123	770.6044	9.38	HMDB0011244	2	C36:3 PC plasmalogen	0.293490888	0.173196	0.396261
C8-pos	QI1852	795.6457	11.09	HMDB0042751	2	C46:3 TAG	1.093037979	0.173196	0.396261
C8-pos	QI5021	903.7387	11.9	HMDB0005385	2	C54:5 TAG	0.209958033	0.173196	0.396261
C8-pos	QI5766	933.7866	12.49	HMDB0005398	2	C56:4 TAG	0.181481731	0.173196	0.396261
C8-pos	QI12530	300.2885	5.89	HMDB0000252	2	sphingosine	0.327422965	0.173196	0.396261
C8-pos	QI11350	703.5722	7.31	HMDB0010169	1	C16:0 SM	-0.111618375	0.18032	0.410963
C8-pos	QI1925	790.6904	11.09	redundant ion	2	NH4_C46:3 TAG	1.142404918	0.195205	0.441464
C8-pos	TF24	89.02	3.63	HMDB00190	1	lactate	0.205488313	0.197008	0.443834
C8-pos	QI11494	344.2782	7.07	HMDB0002250	1	C12 carnitine	0.328541314	0.20297	0.453788
C8-pos	TF4	785.6502	7.13	HMDB0012104	2	C22:1 SM	-0.212888597	0.210952	0.464569
C8-pos	QI2262	847.6765	11.27	HMDB0010471	2	C50:5 TAG	0.47669485	0.210952	0.464569
C8-pos	QI4942	286.1023	4.35	HMDB0005923	1	N4-acetylcytidine	1.161192096	0.210952	0.464569
C8-pos	QI4246	634.5392	9	redundant ion	2	NH4_C36:4 DAG	-0.219704607	0.210952	0.464569
C8-pos	QI34	135.0314	3.01	HMDB00157	1	hypoxanthine	-0.02491433	0.212758	0.466798
C8-pos	QI5568	865.7234	11.87	HMDB0011701	2	C51:3 TAG	0.28986427	0.219155	0.472026
C8-pos	QI4010	881.7545	12.3	HMDB0005369	2	C52:2 TAG	0.074217795	0.219155	0.472026
C8-pos	QI7839	141.0653	7.53	HMDB0002271	1	imidazole propionate	0.354642394	0.219155	0.472026
C8-pos	QI43	188.0566	6.22	HMDB01138	1	N-acetylglutamate	0.454524973	0.219155	0.472026
C8-pos	QI2681	673.5878	12.26	HMDB0000918	2	C18:1 CE	-0.146228133	0.227579	0.484843
C8-pos	QI2108	783.6458	11.15	HMDB0043170	2	C45:2 TAG	1.117285469	0.227579	0.484843
C8-pos	QI8343	134.0445	7.95	HMDB0000191	1	aspartate	0.236384024	0.236227	0.48909
HILIC-pos	QI17242	585.2688	1.72	HMDB0000054	1	bilirubin	0.363916111	0.236227	0.48909
HILIC-pos	QI3260	744.5887	9.25	HMDB0011210	2	C34:2 PC plasmalogen	0.153905913	0.236227	0.48909
HILIC-pos	QI1837	793.6302	10.84	HMDB0042548	2	C46:4 TAG	1.08177309	0.236227	0.48909
C8-pos	QI1789	821.661	11.18	HMDB0042811	2	C48:4 TAG	0.711911049	0.236227	0.48909
C8-pos	QI1793	819.6459	10.93	HMDB0042789	2	C48:5 TAG	0.527385832	0.236227	0.48909
C8-pos	QI4592	610.5394	9.17	redundant ion	2	NH4_C34:2 DAG	-0.315498257	0.236227	0.48909
C8-pos	QI1886	814.6905	10.93	redundant ion	2	NH4_C48:5 TAG	0.517163021	0.236227	0.48909
C8-pos	QI11804	742.5724	6.68	HMDB0011211	2	C34:3 PC plasmalogen	0.257782942	0.2451	0.503912
C8-pos	QI1909	816.7056	11.18	redundant ion	2	NH4_C48:4 TAG	0.745316066	0.2451	0.503912
C8-pos	QI5317	825.692	11.63	HMDB0005376	2	C48:2 TAG	0.270713435	0.254199	0.517195
C8-pos	QI2785	930.8475	12.77	redundant ion	2	NH4_C56:3 TAG	0.260060368	0.254199	0.517195
C8-pos	QI15063	220.1173	3.07	HMDB0000210	1	pantothenate	0.30163363	0.254199	0.517195
C8-pos	QI3892	650.6436	10.29	HMDB0004956	1	C24:0 Ceramide (d18:1)	-0.094814399	0.263526	0.528851
C8-pos	QI5415	837.6926	11.55	HMDB0042103	2	C49:3 TAG	0.503644849	0.263526	0.528851
C8-pos	QI4461	638.571	9.59	redundant ion	2	NH4_C36:2 DAG	-0.26091071	0.263526	0.528851
C8-pos	QI2288	842.7213	11.26	redundant ion	2	NH4_C50:5 TAG	0.474649849	0.263526	0.528851
C8-pos	QI5676	764.5462	8.4	HMDB0012356	2	C34:0 PS	0.313357641	0.273082	0.544312
C8-pos	QI3963	636.555	9.3	redundant ion	2	NH4_C36:3 DAG	-0.360704294	0.273082	0.544312
C8-pos	QI6	144.1031	2.41			2-aminoheptanoate	-0.58436367	0.27499	0.546264
C8-pos	QI2502	837.5477	8.55	HMDB0009783	2	C34:1 PI	-0.237682794	0.282867	0.547124
C8-pos	QI3288	811.6768	11.48	HMDB0042076	2	C47:2 TAG	0.645818016	0.282867	0.547124
C8-pos	QI5018	827.7077	11.87	HMDB0005359	2	C48:1 TAG	0.573833134	0.282867	0.547124
C8-pos	QI2515	823.6761	11.41	HMDB0005432	2	C48:3 TAG	0.723354773	0.282867	0.547124
C8-pos	QI5355	875.707	11.58	HMDB0005380	2	C52:5 TAG	0.158533506	0.282867	0.547124
C8-pos	QI4998	450.32	4.38	HMDB0000631	2	glycodeoxycholate/glycochenodeoxycholate	0.382305837	0.282867	0.547124
C8-pos	QI4510	688.6012	11.59	redundant ion	1	NH4_C20:5 CE	-0.14766464	0.282867	0.547124
C8-pos	QI14576	153.0402	3.85	HMDB0000292	1	xanthine	0.241343797	0.282867	0.547124
C8-pos	QI7	117.0558	3.24	HMDB00407	2	2-hydroxy-3-methylbutyrate/hydroxyisovalerate	0.213846218	0.292882	0.557329
C8-pos	QI5653	643.5262	9.59	HMDB0007218	2	C36:2 DAG	-0.156999311	0.292882	0.557329
C8-pos	QI3746	801.6933	11.78	HMDB0010411	2	C46:0 TAG	0.617153367	0.292882	0.557329
C8-pos	TF9	132.1016	7.04	HMDB0000687	1	leucine	-0.203489949	0.292882	0.557329
C8-pos	QI9291	175.1436	10.35	HMDB0013287	1	N6,N6-dimethyllysine	0.171881249	0.292882	0.557329
C8-pos	QI54	125.0357	1.29	HMDB00262	1	thymine	0.25492894	0.29992	0.56764
C8-pos	QI11764	730.5358	6.77	HMDB0007874	2	C32:2 PC	0.329684945	0.303128	0.56764
C8-pos	QI1983	929.754	12.11	HMDB0005456	2	C56:6 TAG	-0.079208366	0.303128	0.56764
C8-pos	QI4688	927.739	11.91	HMDB0005462	2	C56:7 TAG	-0.035361094	0.303128	0.56764

C8-pos	QI10278	189.1229	8.44	HMDB0000206	1	N6-acetyllysine	0.203877269	0.303128	0.56764
C8-pos	QI6124	792.5512	5.5	HMDB0009012	2	C40:6 PE	0.099526359	0.313604	0.576247
C8-pos	QI6077	776.5563	5.46	HMDB0011394	2	C40:7 PE plasmalogen	-0.178554653	0.313604	0.576247
C8-pos	QI5155	883.7708	12.57	HMDB0005367	2	C52:1 TAG	0.230898217	0.313604	0.576247
C8-pos	QI2039	788.6751	10.83	redundant ion	2	NH4_C46:4 TAG	1.235931478	0.314632	0.576335
C8-pos	QI7334	74.0711	6.88	HMDB0001522	1	methylguanidine	1.034648036	0.3238	0.584953
C8-pos	QI2924	762.599	9.25	HMDB0007970	2	C34:0 PC	-0.061714453	0.324311	0.584953
C8-pos	QI2378	871.6767	11.25	HMDB0010517	2	C52:7 TAG	0.225700885	0.324311	0.584953
C8-pos	QI5515	909.7866	12.67	HMDB0005403	2	C54:2 TAG	0.084572648	0.324311	0.584953
C8-pos	QI1988	792.7061	11.33	redundant ion	2	NH4_C46:2 TAG	1.064345447	0.324311	0.584953
C8-pos	QI13	145.0507	6.35	HMDB00448	2	adipate/methylglutarate	0.103048342	0.335248	0.595546
C8-pos	QI5986	869.7555	12.37	HMDB0042104	2	C51:1 TAG	0.274307962	0.335248	0.595546
C8-pos	QI3295	838.7845	12.25	redundant ion	2	NH4_C49:0 TAG	0.766985546	0.335248	0.595546
C8-pos	QI2839	928.8312	12.48	redundant ion	2	NH4_C56:4 TAG	0.200794642	0.335248	0.595546
C8-pos	QI8335	133.0605	7.94	HMDB0000168	1	asparagine	-0.268195044	0.346415	0.59559
C8-pos	TF5	786.5964	6.68	HMDB0008039	2	C36:2 PC	-0.132975814	0.346415	0.59559
HILIC-pos	QI5253	829.7234	12.1	HMDB0005356	2	C48:0 TAG	0.203790145	0.346415	0.59559
C8-pos	QI5572	855.739	12.21	HMDB0005360	2	C50:1 TAG	0.363526455	0.346415	0.59559
HILIC-pos	QI3553	849.6917	11.5	HMDB0005435	2	C50:4 TAG	0.388705106	0.346415	0.59559
HILIC-pos	QI10051	162.1118	8.89	HMDB0000062	1	carnitine	0.084794442	0.346415	0.59559
HILIC-pos	QI1896	764.6751	10.99	redundant ion	2	NH4_C44:2 TAG	0.954749133	0.346415	0.59559
HILIC-pos	QI3960	810.7526	11.92	redundant ion	2	NH4_C47:0 TAG	0.757343529	0.346415	0.59559
C8-pos	QI2440	866.7221	11.25	redundant ion	2	NH4_C52:7 TAG	0.314416928	0.346415	0.59559
HILIC-pos	TF12	203.1498	9.74	HMDB0003334	1	SDMA	0.075693089	0.346415	0.59559
C8-pos	QI50	181.0719	1.85	HMDB00247	1	sorbitol	0.5524388	0.354275	0.596014
HILIC-pos	QI2724	383.3302	7.08	HMDB0003896	1	7-Dehydrodesmosterol	-0.025475399	0.357811	0.596014
HILIC-neg	QI17441	615.4956	1.64	HMDB0007103	2	C34:2 DAG_Na	0.084587755	0.357811	0.596014
HILIC-pos	QI4666	826.5341	8.32	HMDB0008511	2	C40:10 PC	-0.062428422	0.357811	0.596014
HILIC-neg	QI1767	769.6302	11	HMDB0042279	2	C44:2 TAG	0.852271477	0.357811	0.596014
C8-pos	QI2070	845.6612	11.14	HMDB0010497	2	C50:6 TAG	0.36853613	0.357811	0.596014
HILIC-pos	QI3330	822.7527	11.87	redundant ion	2	NH4_C48:1 TAG	0.588806413	0.357811	0.596014
HILIC-pos	QI2407	844.7368	11.5	redundant ion	2	NH4_C50:4 TAG	0.503423197	0.357811	0.596014
HILIC-pos	QI2150	840.7064	11.14	redundant ion	2	NH4_C50:6 TAG	0.42905104	0.357811	0.596014
HILIC-pos	QI2245	898.7837	11.89	redundant ion	2	NH4_C54:5 TAG	0.255503621	0.357811	0.596014
HILIC-pos	QI10416	116.0704	8.17	HMDB0000162	1	proline	-0.336721353	0.357811	0.596014
HILIC-pos	QI4867	848.7684	11.96	redundant ion	2	NH4_C50:2 TAG	0.426803668	0.369436	0.613639
HILIC-pos	QI2527	813.6831	9.8	HMDB0012107	2	C24:1 SM	-0.068954932	0.381288	0.624505
HILIC-pos	QI1891	766.6906	11.25	redundant ion	2	NH4_C44:1 TAG	0.839269448	0.381288	0.624505
HILIC-pos	QI2080	794.7214	11.55	redundant ion	2	NH4_C46:1 TAG	0.785462686	0.381288	0.624505
HILIC-pos	QI4678	888.7994	12.22	redundant ion	2	NH4_C53:3 TAG	0.203735118	0.381288	0.624505
HILIC-pos	QI5201	139.0497	4.58	HMDB0000301	1	urocanic acid	0.063851412	0.381288	0.624505
HILIC-neg	QI10071	146.117	8.84	HMDB0001161	1	butyrobetaine	0.309844328	0.393366	0.631964
HILIC-neg	QI5245	782.5671	8.68	HMDB0008138	2	C36:4 PC-B	-0.152962878	0.393366	0.631964
HILIC-neg	QI4080	766.5722	8.71	HMDB0011221	2	C36:5 PC plasmalogen-A	-0.061876917	0.393366	0.631964
HILIC-pos	QI3659	834.5983	9.06	HMDB0008057	2	C40:6 PC	-0.007465011	0.393366	0.631964
HILIC-neg	QI1841	771.6459	11.25	HMDB0042301	2	C44:1 TAG	0.683968661	0.393366	0.631964
HILIC-pos	QI8633	104.1066	8.34	HMDB0000097	1	choline	-0.044819345	0.393366	0.631964
HILIC-pos	QI4971	169.0351	4.37	HMDB0000289	1	urate	0.153268182	0.393366	0.631964
HILIC-pos	QI6197	702.5414	5.58	HMDB0008952	2	C34:2 PE plasmalogen	-0.260289244	0.405667	0.632712
HILIC-neg	QI5579	641.5103	9.3	HMDB0007219	2	C36:3 DAG	-0.205580731	0.405667	0.632712
HILIC-pos	QI6177	740.5203	5.56	HMDB0008937	2	C36:4 PE	0.009727055	0.405667	0.632712
HILIC-pos	QI1916	797.6614	11.33	HMDB0010419	2	C46:2 TAG	0.904941699	0.405667	0.632712
HILIC-pos	QI5852	839.7093	11.77	HMDB0011706	2	C49:2 TAG	0.205528196	0.405667	0.632712
HILIC-pos	QI2445	895.6784	11.22	HMDB0010498	2	C54:9 TAG	0.399233419	0.405667	0.632712
HILIC-pos	QI5800	177.1017	5.12	HMDB0001046	1	cotinine	0.083994206	0.405667	0.632712
HILIC-pos	TF7	104.0703	7.7	HMDB0000112	1	GABA	-0.220420703	0.405667	0.632712
HILIC-pos	QI2483	820.7366	11.63	redundant ion	2	NH4_C48:2 TAG	0.657148994	0.405667	0.632712
HILIC-pos	QI5267	924.7991	12.11	redundant ion	2	NH4_C56:6 TAG	-0.120622785	0.405667	0.632712
HILIC-pos	QI15305	196.06	2.72			4-hydroxyhippurate	0.308933651	0.40819	0.634962
HILIC-neg	QI7708	675.5408	7.43	HMDB0012097	1	C14:0 SM	-0.144745727	0.418192	0.637038
HILIC-pos	QI6206	744.5518	5.59	HMDB0008994	2	C36:2 PE	0.111975827	0.418192	0.637038
HILIC-pos	QI2519	799.6766	11.55	HMDB0010412	2	C46:1 TAG	0.617355172	0.418192	0.637038

HILIC-pos	QI10292	190.1181	8.41	HMDB0000679	1	homocitrulline	0.373795085	0.418192	0.637038
HILIC-neg	QI9230	276.1545	9.81	HMDB0004207	1	L-alpha-glutamyl-L-lysine	-0.302891874	0.418192	0.637038
HILIC-pos	QI2199	818.721	11.41	redundant ion	2	NH4_C48:3 TAG	0.796805656	0.418192	0.637038
HILIC-neg	QI2668	832.7367	11.56	redundant ion	2	NH4_C49:3 TAG	0.66127683	0.418192	0.637038
HILIC-neg	QI5048	285.0818	4.42	HMDB0000299	1	xanthosine	0.197635258	0.418192	0.637038
HILIC-pos	QI9	159.0664	6.33	HMDB00555	2	3-methyladipate/pimelate	-0.082697408	0.427241	0.649141
HILIC-neg	QI11873	792.5873	6.57	HMDB0011319	2	C38:6 PC plasmalogen	-0.065050857	0.430936	0.653068
HILIC-pos	QI24	179.0563	2.05	HMDB00122	2	fructose/glucose/galactose	0.003211419	0.440192	0.65581
HILIC-neg	QI37	204.0667	4.1	HMDB00671	1	indolelactate	-0.041375664	0.440192	0.65581
HILIC-pos	QI2544	911.8027	12.96	HMDB0005395	2	C54:1 TAG	0.50511769	0.443899	0.65581
HILIC-pos	QI4550	947.7084	11.39	HMDB0010531	2	C58:11 TAG	-0.256656067	0.443899	0.65581
HILIC-neg	QI2572	955.7708	12.12	HMDB0005471	2	C58:7 TAG	0.037301844	0.443899	0.65581
HILIC-pos	QI4511	662.5707	9.45	redundant ion	2	NH4_C38:4 DAG	-0.086916623	0.443899	0.65581
HILIC-pos	QI2397	806.7215	11.48	redundant ion	2	NH4_C47:2 TAG	0.838301892	0.443899	0.65581
HILIC-neg	QI2576	286.1427	2	HMDB0029377	1	piperine	-0.85718687	0.443899	0.65581
HILIC-neg	QI4008	584.5239	9.04	redundant ion	2	NH4_C32:1 DAG	-0.378792327	0.457076	0.66856
HILIC-neg	QI3226	846.7521	11.71	redundant ion	2	NH4_C50:3 TAG	0.348528396	0.457076	0.66856
HILIC-neg	QI2497	906.8477	12.96	redundant ion	2	NH4_C54:1 TAG	0.566250884	0.457076	0.66856
HILIC-pos	QI5086	738.5423	9.18	HMDB0011214	2	C34:5 PC plasmalogen	-0.004684545	0.463428	0.676167
HILIC-pos	QI3721	806.5671	8.61	HMDB0007991	2	C38:6 PC	-0.180744585	0.470467	0.678026
HILIC-pos	QI5389	953.755	12	HMDB0005413	2	C58:8 TAG	0.120250668	0.470467	0.678026
HILIC-pos	QI15177	247.1069	2.91	HMDB0013713	1	N-acetyltryptophan	0.254953762	0.470467	0.678026
HILIC-pos	QI10366	217.1289	8.26	HMDB0004620	1	N-alpha-acetylarginine	0.001377609	0.470467	0.678026
HILIC-pos	QI11782	426.3562	6.72	HMDB0005065	2	C18:1 carnitine	-0.196796712	0.484067	0.687515
HILIC-pos	QI5120	591.4948	9.34	HMDB0007098	2	C32:0 DAG	-0.162328121	0.484067	0.687515
HILIC-pos	QI9897	156.0763	9.26	HMDB0000177	1	histidine	-0.135831411	0.484067	0.687515
HILIC-pos	QI4196	608.5237	8.86	redundant ion	2	NH4_C34:3 DAG	-0.215918099	0.484067	0.687515
HILIC-neg	QI2654	878.8159	12.57	redundant ion	2	NH4_C52:1 TAG	0.273727923	0.484067	0.687515
HILIC-pos	QI9095	133.0969	9.36	HMDB0000214	1	ornithine	-0.163862554	0.484067	0.687515
HILIC-pos	QI2230	785.6616	11.39	HMDB0042099	2	C45:1 TAG	0.539888162	0.497872	0.702036
HILIC-pos	QI2319	796.7371	11.78	redundant ion	2	NH4_C46:0 TAG	0.486956177	0.497872	0.702036
HILIC-pos	QI2812	916.8311	12.57	redundant ion	2	NH4_C55:3 TAG	0.161457926	0.497872	0.702036
HILIC-pos	TF2	196.06	2.69	HMDB0013678	1	3-hydroxyhippurate	0.62146448	0.511881	0.709873
HILIC-pos	QI2135	648.6269	1.85	HMDB0004953	2	C24:1 ceramide (d18:1)	0.081008027	0.511881	0.709873
HILIC-pos	QI2835	746.6042	9.24	HMDB0011208	2	C34:1 PC plasmalogen-A	0.00025907	0.511881	0.709873
HILIC-pos	QI6133	615.4948	9.18	HMDB0007103	2	C34:2 DAG	-0.358519872	0.511881	0.709873
C8-pos	QI3036	871.771	12.62	HMDB0031106	2	C51:0 TAG	0.359754862	0.511881	0.709873
HILIC-pos	QI5306	951.7393	11.76	HMDB0005463	2	C58:9 TAG	-0.084310927	0.511881	0.709873
HILIC-pos	QI2533	866.8161	12.64	redundant ion	2	NH4_C51:0 TAG	0.33323123	0.511881	0.709873
HILIC-pos	TF13	135.03	4	HMDB00613	2	erythronate/threonate	0.182288804	0.522428	0.717726
HILIC-pos	QI14783	159.0508	3.63	HMDB0000462	1	allantoin	-0.206658926	0.526088	0.717726
HILIC-pos	QI3857	622.6126	9.87	HMDB0004952	1	C22:0 Ceramide (d18:1)	0.03664275	0.526088	0.717726
HILIC-pos	QI2715	772.6198	9.39	HMDB0011243	2	C36:2 PC plasmalogen	-0.128702776	0.526088	0.717726
HILIC-pos	QI8469	110.0267	8.06	HMDB0000965	1	hypotaurine	-0.083293361	0.526088	0.717726
HILIC-pos	QI2627	808.7373	11.7	redundant ion	2	NH4_C47:1 TAG	0.428855951	0.526088	0.717726
C8-pos	QI2187	870.7523	11.58	redundant ion	2	NH4_C52:5 TAG	0.328804906	0.526088	0.717726
C8-pos	QI3417	923.8029	12.86	HMDB0042226	2	C55:2 TAG	0.14727364	0.540491	0.72725
C8-pos	QI3602	180.065	2.64	HMDB0000714	1	hippurate	0.487989633	0.540491	0.72725
C8-pos	QI3975	902.8155	12.39	redundant ion	2	NH4_C54:3 TAG	0.057535828	0.540491	0.72725
C8-pos	TF15	118.0861	7.48	HMDB0000883	1	valine	-0.244522618	0.540491	0.72725
C8-pos	QI17449	617.5116	1.64	HMDB0007102	2	C34:1 DAG_Na	0.051753748	0.555083	0.738437
C8-pos	QI6094	895.7711	12.49	HMDB0042196	2	C53:2 TAG	0.078585681	0.555083	0.738437
C8-pos	QI4368	864.7999	12.36	redundant ion	2	NH4_C51:1 TAG	0.358019282	0.555083	0.738437
C8-pos	QI2798	942.7534	11.39	redundant ion	2	NH4_C58:11 TAG	-0.393117869	0.555083	0.738437
C8-pos	QI4813	952.8307	12.36	redundant ion	2	NH4_C58:6 TAG	0.011240944	0.555083	0.738437
C8-pos	QI5454	973.7236	11.52	HMDB0005478	2	C60:12 TAG	-0.583504377	0.565366	0.741325
C8-pos	TF6	173.01	8.46	HMDB00072	2	aconitate	0.112408105	0.566382	0.741325
C8-pos	QI6138	768.551	5.52	HMDB0009003	2	C38:4 PE	0.083372833	0.569862	0.741325
C8-pos	QI5749	193.0967	5.06	HMDB0001390	1	hydroxycotinine	0.099763854	0.569862	0.741325
C8-pos	QI4200	586.5397	9.34	redundant ion	2	NH4_C32:0 DAG	-0.273057304	0.569862	0.741325
C8-pos	QI2450	852.8003	12.46	redundant ion	2	NH4_C50:0 TAG	0.502410939	0.569862	0.741325

C8-pos	QI3058	904.8316	12.67	redundant ion	2	NH4_C54:2 TAG	0.018121308	0.569862	0.741325
C8-pos	TF13	205.0966	6.59	HMDB0000929	1	tryptophan	-0.105197316	0.569862	0.741325
C8-pos	QI20	191.0199	8.42	HMDB00094	2	citrate/isocitrate	0.002466544	0.581404	0.752463
C8-pos	TF3	203.1498	9.83	HMDB0001539	1	ADMA	0.035497501	0.584822	0.752463
C8-pos	QI2250	808.5184	8.03	HMDB0012362	2	C38:6 PS	0.100701211	0.584822	0.752463
C8-pos	QI3745	857.7555	12.47	HMDB0005357	2	C50:0 TAG	0.413351779	0.584822	0.752463
C8-pos	QI6203	640.6014	11.89	redundant ion	2	NH4_C16:1 CE	-0.063753021	0.584822	0.752463
C8-pos	TF25	103	6.72	HMDB00691	1	malonate	0.013240778	0.596576	0.761935
C8-pos	QI5953	589.4792	9.03	HMDB0007099	2	C32:1 DAG	-0.550697978	0.599959	0.761935
C8-pos	QI4347	766.537	8.82	HMDB0009069	2	C38:5 PE	-0.091786321	0.599959	0.761935
C8-pos	QI1579	879.7386	12.05	HMDB0005384	2	C52:3 TAG	0.005527574	0.599959	0.761935
C8-pos	QI2065	782.7212	11.61	redundant ion	2	NH4_C45:0 TAG	0.393894082	0.599959	0.761935
C8-pos	QI4188	834.7524	11.78	redundant ion	2	NH4_C49:2 TAG	0.262348237	0.599959	0.761935
C8-pos	QI5123	877.723	11.79	HMDB0005363	2	C52:4 TAG	0.00141954	0.615267	0.776345
C8-pos	QI2501	937.8184	13.05	HMDB0005404	2	C56:2 TAG	-0.008164584	0.615267	0.776345
C8-pos	QI4590	860.768	11.87	redundant ion	2	NH4_C51:3 TAG	0.162495682	0.615267	0.776345
C8-pos	TF40	111.02	1.62	HMDB00300	1	uracil	-0.021455619	0.627521	0.787421
C8-pos	QI5571	587.4637	8.73	HMDB0007128	2	C32:2 DAG	-0.473599385	0.627993	0.787421
C8-pos	QI2944	873.6922	11.36	HMDB0005436	2	C52:6 TAG	0.253128658	0.630741	0.787421
C8-pos	QI2453	868.737	11.37	redundant ion	2	NH4_C52:6 TAG	0.290283392	0.630741	0.787421
C8-pos	QI2752	918.8474	12.86	redundant ion	2	NH4_C55:2 TAG	0.264543088	0.630741	0.787421
C8-pos	QI12856	748.5244	5.49	HMDB0011420	2	C38:7 PE plasmalogen	-0.078045332	0.646375	0.803527
C8-pos	QI3100	824.7685	12.11	redundant ion	2	NH4_C48:0 TAG	0.468981077	0.646375	0.803527
C8-pos	QI48	166.0147	7	HMDB00232	1	quinolinate	0.131441181	0.651201	0.807819
C8-pos	TF1	104.0703	7.83	HMDB0001906	1	2-aminoisobutyric acid	-0.122559142	0.662164	0.809464
C8-pos	QI5239	645.5419	9.89	HMDB0007216	2	C36:1 DAG	-0.087392582	0.662164	0.809464
C8-pos	QI6111	665.5102	9.29	HMDB0007199	2	C38:5 DAG	0.093691858	0.662164	0.809464
C8-pos	QI3207	925.7231	11.67	HMDB0005392	2	C56:8 TAG	-0.14487298	0.662164	0.809464
C8-pos	QI9739	161.1279	9.78	HMDB0002038	1	N6-methyllysine	0.196865245	0.662164	0.809464
C8-pos	QI4323	850.7842	12.2	redundant ion	2	NH4_C50:1 TAG	0.337642955	0.662164	0.809464
C8-pos	QI3666	900.7996	12.14	redundant ion	2	NH4_C54:4 TAG	0.016615262	0.662164	0.809464
C8-pos	QI1958	773.6612	11.46	HMDB0042063	2	C44:0 TAG	0.432325082	0.678101	0.825514
C8-pos	QI10511	130.0859	8.05	HMDB0000716	1	pipecolic acid	0.130151034	0.678101	0.825514
C8-pos	QI44	88.9881	6.97	HMDB02329	1	oxalate	0.151876046	0.683283	0.830104
C8-pos	QI11339	701.5565	7.32	HMDB0029216	2	C16:1 SM	-0.016752696	0.694181	0.83472
C8-pos	QI3512	788.6149	9.38	HMDB0008038	2	C36:1 PC	-0.046353001	0.694181	0.83472
C8-pos	QI13298	269.0871	4.95	HMDB0000195	1	inosine	-0.287521693	0.694181	0.83472
C8-pos	QI2306	780.7059	11.4	redundant ion	2	NH4_C45:1 TAG	0.930249396	0.694181	0.83472
C8-pos	QI2476	932.8633	13.05	redundant ion	2	NH4_C56:2 TAG	0.00669309	0.694181	0.83472
C8-pos	QI16938	254.0585	1.82	HMDB0015150	1	sulfamethoxazole	0.159493815	0.710082	0.843865
C8-pos	QI2182	885.7871	12.85	HMDB0005365	2	C52:0 TAG	0.371904207	0.710397	0.843865
C8-pos	QI11355	302.2314	7.3	HMDB0013288	1	C9 carnitine	0.491611165	0.710397	0.843865
C8-pos	QI10631	132.0652	7.94	HMDB0000725	1	hydroxyproline	-0.03754203	0.710397	0.843865
C8-pos	QI4385	640.5867	9.89	redundant ion	2	NH4_C36:1 DAG	-0.035739382	0.710397	0.843865
C8-pos	QI4399	123.0554	3.87	HMDB0001406	1	niacinamide	0.08906339	0.710397	0.843865
C8-pos	QI16336	151.0749	2.02	HMDB0059824	1	4-hydroxy-3-methylacetophenone	-0.127345203	0.726742	0.851243
C8-pos	QI5777	613.4789	8.86	HMDB0007132	2	C34:3 DAG	0.011125409	0.726742	0.851243
C8-pos	QI4877	614.571	9.77	redundant ion	2	NH4_C34:0 DAG	-0.00253333	0.726742	0.851243
C8-pos	QI1810	768.7059	11.46	redundant ion	2	NH4_C44:0 TAG	0.359903742	0.726742	0.851243
C8-pos	QI3024	944.7676	11.55	redundant ion	2	NH4_C58:10 TAG	-0.139362666	0.726742	0.851243
C8-pos	QI5205	758.5676	8.66	HMDB0007973	2	C34:2 PC	0.017707579	0.74321	0.863651
C8-pos	QI4135	732.5881	9.28	HMDB0009016	2	C36:1 PE plasmalogen	0.205226753	0.74321	0.863651
C8-pos	QI5084	926.8151	12.36	redundant ion	2	NH4_C56:5 TAG	0.040609346	0.74321	0.863651
C8-pos	QI7366	370.2937	6.92	HMDB0002014	2	C14:1 carnitine	0.1276805	0.759794	0.871276
C8-pos	QI4319	645.5566	11.89	HMDB0000658	2	C16:1 CE	-0.104968585	0.759794	0.871276
C8-pos	QI6078	112.0502	5.46	HMDB0000630	1	cytosine	0.229550789	0.759794	0.871276
C8-pos	QI8483	130.0496	8.09			glutamine_fragment1	-0.131583814	0.759794	0.871276
C8-pos	QI4909	876.7997	12.3	redundant ion	2	NH4_C52:2 TAG	0.014718198	0.759794	0.871276
C8-pos	QI2705	968.768	11.53	redundant ion	2	NH4_C60:12 TAG	-0.452929448	0.759794	0.871276
C8-pos	QI1931	759.6463	11.3	HMDB0042062	2	C43:0 TAG	0.263719002	0.760144	0.871276
C8-pos	QI4905	796.5242	9.02			C42:11 PE plasmalogen	0.073585265	0.776487	0.886553
C8-pos	QI2151	880.8317	12.85	redundant ion	2	NH4_C52:0 TAG	0.48095674	0.776487	0.886553
C8-pos	QI5380	841.7254	12.02	HMDB0011705	2	C49:1 TAG	0.087630866	0.780156	0.889015
C8-pos	QI11653	774.5612	6.86			C36:2 PS plasmalogen	-0.016553791	0.793282	0.897019
C8-pos	QI12839	724.5252	5.5	HMDB0011410	2	C36:5 PE plasmalogen	0.121839867	0.793282	0.897019
C8-pos	QI10480	147.0759	8.09	HMDB0000641	1	glutamine	-0.109305431	0.793282	0.897019
C8-pos	TF9	129.06	3.07	HMDB00491	2	alpha-keto-beta-methylvalerate/alpha-ketoisocaproate	-0.354285293	0.810172	0.902237
C8-pos	QI4221	867.7388	12.12	HMDB0005362	2	C51:2 TAG	0.035888762	0.810172	0.902237
C8-pos	QI1804	899.7075	11.44	HMDB0005447	2	C54:7 TAG	0.066778782	0.810172	0.902237
C8-pos	QI10262	175.1072	8.47	HMDB0003357	1	N-acetylornithine	-0.010447668	0.810172	0.902237
C8-pos	QI3446	890.8159	12.47	redundant ion	2	NH4_C53:2 TAG	0.070970491	0.810172	0.902237
C8-pos	QI4986	950.8141	12.12	redundant ion	2	NH4_C58:7 TAG	-0.042725904	0.810172	0.902237
C8-pos	QI4874	948.7994	12	redundant ion	2	NH4_C58:8 TAG	-0.146828193	0.810172	0.902237
C8-pos	QI8922	138.0544	8.94	HMDB0000875	1	trigonelline	-0.185159977	0.810172	0.902237
C8-pos	QI7587	729.5882	7.26	HMDB0012101	2	C18:1 SM	-0.04751712	0.827148	0.914216
C8-pos	QI3030	921.693	11.26	HMDB0010513	2	C56:10 TAG	0.142588575	0.827148	0.914216
C8-pos	QI6838	112.0502	6.26			cytosine_isomer2	0.106471861	0.827148	0.914216
C8-pos	QI2	181.0369	4.37	HMDB03099	1	1-methylurate	-0.444536416	0.844204	0.926105
C8-pos	QI3543	742.5357	8.8	HMDB0009060	2	C36:3 PE	-0.022177842	0.844204	0.926105
C8-pos	QI5094	323.2187	4.59	HMDB0011562	2	C14:1 MAG	-0.0790279	0.861332	0.934434
C8-pos	QI2746	746.6046	9.53	HMDB0011239	2	C34:1 PC plasmalogen-B	-0.055066272	0.861332	0.934434
C8-pos	QI3068	931.7705	12.36	HMDB0005406	2	C56:5 TAG	0.109818035	0.861332	0.934434
C8-pos	QI4746	660.5551	9.28	redundant ion	2	NH4_C38:5 DAG	-0.089113374	0.861332	0.934434
C8-pos	QI4484	874.784	12.05	redundant ion	2	NH4_C52:3 TAG	-0.063539498	0.861332	0.934434
C8-pos	QI2644	918.7531	11.41	redundant ion	2	NH4_C56:9 TAG	0.005676388	0.861332	0.934434
HILIC-pos	QI5031	153.0653	4.41	HMDB0004193	1	N1-methyl-2-pyridone-5-carboxamide	-0.25456174	0.878524	0.949582
HILIC-pos	QI4174	946.782	11.77	redundant ion	2	NH4_C58:9 TAG	-0.155352428	0.878524	0.949582
HILIC-pos	QI6866	207.1487	6.29	HMDB0060656	1	N-ethylglycinexylidide	-0.397766713	0.880785	0.950278
HILIC-neg	QI2545	901.7223	11.66	HMDB0005391	2	C54:6 TAG	-0.058781308	0.895773	0.954193
C8-pos	QI2005	939.834	13.39	HMDB0005396	2	C56:1 TAG	0.285661107	0.895773	0.954193
HILIC-pos	TF6	143.081	8.99			ectoine	-0.12324026	0.895773	0.954193
HILIC-pos	QI4806	862.784	12.13	redundant ion	2	NH4_C51:2 TAG	0.147494536	0.895773	0.954193
HILIC-pos	QI2575	916.7363	11.2	redundant ion	2	NH4_C56:10 TAG	-0.025750175	0.895773	0.954193

HILIC-neg	QI5050	922.7833	11.91	redundant ion	2	NH4_C56:7 TAG	-0.134458819	0.895773	0.954193
HILIC-pos	QI1	168.078	3.24	HMDB00001	1	1-methylhistidine	0.389488066	0.912198	0.957014
HILIC-pos	QI3418	774.635	9.67	HMDB0011241	2	C36:1 PC plasmalogen	-0.006114388	0.91307	0.957014
HILIC-pos	QI6086	667.526	9.44	HMDB0007170	2	C38:4 DAG	-0.010678977	0.91307	0.957014
HILIC-pos	QI1482	897.6925	11.22	HMDB0010518	2	C54:8 TAG	0.07073756	0.91307	0.957014
HILIC-neg	QI5828	949.7236	11.54	HMDB0005476	2	C58:10 TAG	-0.044354555	0.91307	0.957014
HILIC-pos	QI1710	740.675	11.14	redundant ion	2	NH4_C42:0 TAG	-0.044706059	0.91307	0.957014
HILIC-neg	QI1917	934.8786	13.37	redundant ion	2	NH4_C56:1 TAG	0.297172367	0.91307	0.957014
HILIC-neg	QI3152	920.7676	11.68	redundant ion	2	NH4_C56:8 TAG	-0.118615575	0.91307	0.957014
HILIC-pos	QI4	160.0616	4.96	HMDB00510	1	2-aminoadipate	-0.014454646	0.930407	0.969999
HILIC-pos	QI8243	90.0547	7.87	HMDB0000161	1	alanine	-0.033080054	0.930407	0.969999
HILIC-neg	QI3245	872.7677	11.79	redundant ion	2	NH4_C52:4 TAG	0.114013104	0.930407	0.969999
HILIC-pos	QI42	129.0195	6.41	HMDB00749	1	mesaconate/itaconate	0.092487577	0.947245	0.972588
HILIC-neg	QI4198	730.5733	9.66	HMDB0009082	2	C36:2 PE plasmalogen	-0.007979764	0.947777	0.972588
HILIC-pos	QI11853	766.5715	6.59	HMDB0011220	2	C36:5 PC plasmalogen	0.030740326	0.947777	0.972588
HILIC-pos	QI1654	745.6303	11.14	HMDB0072780	2	C42:0 TAG	-0.168472449	0.947777	0.972588
HILIC-neg	QI5346	923.7079	11.41	HMDB0005448	2	C56:9 TAG	-0.01991344	0.947777	0.972588
HILIC-neg	QI3286	369.3507	7.57	HMDB0000067	1	cholesterol	0.108772104	0.947777	0.972588
HILIC-neg	QI13016	284.098	5.33	HMDB0000133	1	guanosine	-0.282604811	0.947777	0.972588
HILIC-pos	QI1619	896.7677	11.66	redundant ion	2	NH4_C54:6 TAG	0.090712056	0.947777	0.972588
HILIC-pos	QI1637	892.7373	11.22	redundant ion	2	NH4_C54:8 TAG	0.401609477	0.947777	0.972588
HILIC-pos	QI7367	372.3094	6.92	HMDB0005066	1	C14 carnitine	0.195595678	0.965171	0.986992
HILIC-pos	QI5750	619.5264	9.72	HMDB0007100	2	C34:0 DAG	0.066961953	0.965171	0.986992
HILIC-neg	TF04	326.3054	6.13	HMDB0002088	1	N-Oleoylethanolamine	0.084602648	0.98006	0.99442
HILIC-pos	QI9242	170.0919	9.9	HMDB0000479	1	3-methylhistidine	0.074587749	0.982581	0.99442
HILIC-pos	QI7415	368.2781	6.98	HMDB0013331	2	C14:2 carnitine	-0.091072346	0.982581	0.99442
HILIC-pos	QI10223	104.0703	8.59	HMDB0000092	1	dimethylglycine	0.063010247	0.982581	0.99442
HILIC-pos	QI8039	148.0599	7.67	HMDB0000148	1	glutamate	-0.024826238	0.982581	0.99442
HILIC-neg	QI4378	836.7686	12.03	redundant ion	2	NH4_C49:1 TAG	0.187105134	0.982581	0.99442
HILIC-pos	QI3890	582.5083	8.72	redundant ion	2	NH4_C32:2 DAG	-0.146886507	0.990981	1
HILIC-neg	QI2791	798.5634	7.56			C36:4 hydroxy-PC	0.071663778	1	1
HILIC-pos	QI3045	772.5825	8.88	HMDB0008942	2	C38:2 PE	-0.138529197	1	1
HILIC-pos	TF06	401.3777	7.59	HMDB0002869	1	campesterol	0.073949626	1	1
HILIC-pos	QI1744	227.1999	1.73	HMDB0002000	1	myristoleic acid	-0.00244373	1	1
HILIC-pos	QI1521	894.7517	11.44	redundant ion	2	NH4_C54:7 TAG	0.168262371	1	1
HILIC-pos	QI8782	152.038	8.66	HMDB0029432	1	S-methyl-L-cysteine-S-oxide	-0.067421389	1	1

Table S3. Codon optimized sequences for *E. coli* (5' -> 3')

speG	atgccaagcgcccacagtgttaagctacgcccgctggagcgtgaagatttacgctatgtacatcaactcgacaataacgccagtgtgatgcgttactggtttgaggaaccctacgaagccttt gttgaactctctgatctgtatgataagcatattcacgatcagagcgaacggcgctttgtggtggaatgtgacggcgaaaaagccggtctggtggagctggtggaaattaaccatgttcatcgcc gcgcagaatttcagataattatctccccggagtatcaggggaaaggtctggcaacccgtgccgccaaattagcaatggactatggctttaccgttctcaatctctataagctgtatctgatcgttg ataaagagaatgaaaaagcgattcacatttaccgcaagcttggcttttcggttgaaggtgaattgatgcacgagttctttattaatggtcaatatcgtaatgccattcgcatgtgtatattccagcat cagtatctggcagagcacaaaacaccgggtcagactctcctgaagccgaccgcacaatag
PA4114	atgattgaactgcgtaccattacacgtgatgattgggaaacctgtattgatctgaaagttgcacgtcatcaggcacattttgttgcaagcaatctgtatagcctggcacagagccgttttctgcctg gttttcgtgcagttggtattcatcatggtggtcgtatggttggttttgcactgtatggtccggatgcagatgatggtcattattggctgtatcgtctgatgattgatcgtcgctatcaaggtaaaggtcat ggtcgtgcagcactgcagcgtattattgcaagcgttcgtcgtacccgtcgtcgtagcgatcgcctgatggttgcatatgccgttgataatgatgttgcccgtcagctgtaccgtgatgcaggtttt gttgaacaaggtctggcaccgtggggtgaaaccatggcatgtctgatgctgccggaaccgagccatcgtagcggtaaagttgccggtgcaccaggtggtcgcgcagcccatggtgttccg gcataa
PA1472	atgaactttgtttttccgcatccgctggatacaccgcgtctgcgtctgcgcacctttcgtgaagaagatgcagcaccgctgtttgcaatgatgagcgatccggaagttatgcgttattggaatacc cctccgtggaccacaccggcacaggcacgtgaagcaattctgcgtgatagccaggcactggttgatggtgaatatctgaatctggcaattgaacgtcgtgaagatggtcagctgctgggtag ctgtattctgtttcattttgaaaaaggtagccgtcgtgcagaactgggttattgtctggcacgtgcagcacaaggtcgtggttatatgggtgaagcactgcgtcgtctgctggcatttgcatttgatg aaattgatctgaatcgtctggaagcagaaatcgatccgcgtaatcgtccgagcgcagcaagcctggaacgtctgggttttcgtcaagaaggcctgctggcacagcgttggattgttagcggtg aagttagcgatagcgcactgtatggactgctggcagaacattggcgtaatcgctaa
PA1377	atgaccgcagaaagcccgaccattcgtctggaacgttatagcgaacgtcatgttgaaggtctgaccgcactgtataatgatccggcagttgcacgtcaggttctgcagatgccgtatcagagc gttgaacagcgtcgtaaacgtctgcatgatagcgcagatgatgatcgtctgctgattctggttgcactgcatcagggtgatgttattggtagcgcaagcctggaacagcatccgcgtattcgtcg tagccatagcggtagcattggtatgggtgttgcagttgcatggcaaggtaaaggtgttggtagccgtctgctgggtgaactgctggatattgcagataattggatgaatctgcgtcgtgttgaact gaccgtttataccgataatgcaccggcactggcactgtatcgtaaatttggttttgaaaccgaaggtgagatgcgtgattatgcagttcgtgatggtcgttttgttgatgtttatagcatggcacgtct gcgtcgcgtggaaggtcgtgttggtgaataa
SAT1	atggccaaatttgttattcgtccggcaaccgcagcagattgtagcgatattctgcgtctgattaaagaactggccaaatacgagtatatggaagaacaggttatcctgaccgaaaaagatctgct ggaagatggttttggtgaacatccgttttatcattgtctggttgcagaagttccgaaagaacattggacaccggaaggtcatagcattgttggttttgccatgtactatttcacctatgatccgtggat tggcaaactgctgtatctggaagatttctttgtgatgagcgattatcgcggttttggtattggttccgaaattctgaaaaatctgagccaggttgcaatgcgttgtcgttgtagcagcatgcattttctg gtggccgaatggaatgaaccgagcattaatttctataaacgtcgtggtgcaagcgatctgagcagcgaagaaggttggcgtctgtttaaaatcgataaagaatacctgctgaaaatggccacc gaagaatag

Table S4. Primers used for complementation cloning

	Forward (5' -> 3')	**Reverse (5' -> 3')**
pTrcHis	ccgtagcgccgatggtag	ggagaaaataccgcatcaggc
speG promoter + speG	cctgatgcggtattttctccaaaatagtaacgttgttttaatcatctttgtc	cactaccatcggcgctacggctattgtgcggtcggcttc
pTrcHis + speG promoter	ccgtagcgccgatggtag	aacgtgtccttacattccttaaatcaataac
PA4114	aaggaatgtaaggacacgttatgattgaactgcgtacc	cactaccatcggcgctacggttatgccggaacaccatg
PA1472	aaggaatgtaaggacacgttatgaactttgtttttccgc	cactaccatcggcgctacggttagcgattacgccaatg
PA1377	aaggaatgtaaggacacgttatgaccgcagaaagcccg	cactaccatcggcgctacggttattcaccaacacgaccttcc
SSAT1	aaggaatgtaaggacacgttatggccaaatttgttattcgtc	cactaccatcggcgctacggctattcttcggtggccattttc

Table S5. qRT-PCR primers

		Forward (5'-> 3')	**Reverse (5'->3')**
speG (rg)[103]	target	AACGCCAGTGTGATGCGTTA	CAGAGAGTTCAACAAAGGCTTCGT
nusA[103]	control	TGAAGCCGCACGTTATGAAG	TCAACGTAATTCGCCCAGGTT
16S[104]	control	ACTCCTACGGGAGGCAGCAGT	TATTACCGCGGCTGCTGGC
cysG[105]	control	TTGTCGGCGGTGGTGATGTC	ATGCGGTGAACTGTGGAATAAACG
idnT[105]	control	CTGTTTAGCGAAGAGGAGATGC	ACAAACGGCGGCGATAGC
hcaT[105]	control	GCTGCTCGGCTTTCTCATCC	CCAACCACGCTGACCAACC

Table S6. Primers used for complementation cloning

	Forward (5' -> 3')	**Reverse (5' -> 3')**
pTrcHis	ccgtagcgccgatggtag	ggagaaaataccgcatcaggc
speG promoter + speG	cctgatgcggtattttctccaaaatagtaacgttgttttaatcatctttgtc	cactaccatcggcgctacggctattgtgcggtcggcttc
pTrcHis + speG promoter	ccgtagcgccgatggtag	aacgtgtccttacattccttaaatcaataac
PA4114	aaggaatgtaaggacacgttatgattgaactgcgtacc	cactaccatcggcgctacggttatgccggaacaccatg
PA1472	aaggaatgtaaggacacgttatgaactttgtttttccgc	cactaccatcggcgctacggttagcgattacgccaatg
PA1377	aaggaatgtaaggacacgttatgaccgcagaaagcccg	cactaccatcggcgctacggttattcaccaacacgaccttcc
SSAT1	aaggaatgtaaggacacgttatggccaaatttgttattcgtc	cactaccatcggcgctacggctattcttcggtggccattttc

Table S7. Multiple reaction monitoring (MRM) transitions

Metabolite	**Transition**
putrescine	89.0 -> 72.0
val-d8	126.1 -> 79.1
N-acetylputrescine	131.1 -> 72.0
4-acetamidobutanoate	146.1 -> 86.0
phe-d8	174.2 -> 112.6
LysoPC16	496.3 -> 184.0
LysoPC18	524.4 -> 184.0
ciprofloxacin	332.1 -> 231.0
tetracycline	445.2 -> 410.2